EFFECTS ON RADIORESISTANCE BY THE TUMOR MICROENVIRONMENT

A Dissertation

by

PANKAJ M PATEL

Submitted to the Office of Graduate and Professional Studies of
Texas A&M University
in partial fulfillment of the requirements for the degree of

DOCTOR OF PHILOSOPHY

Chair of Committee,	Gamal Akabani
Committee Members,	John R. Ford
	Michael A. Deveau
	John W. Poston, Sr.
Head of Department,	Yassin A. Hassan

May 2018

Major Subject: Nuclear Engineering

ABSTRACT

One of the primary reasons *in vitro* therapeutic models lack high levels of efficacy is the inability to accurately model the natural tumor environment. These models only incorporate homogenous tumor cells and lack the complex nature of the tumor microenvironment. The extracellular matrix (ECM) found in tumors provides the structure and growth factors needed to undergo phenotypical changes such as Epithelial Mesenchymal Transition (EMT). EMT provides tumor cells with stem-cell-like characteristics and a resistance to treatment. Tumor spheroids coated in Matrigel® provide a three-dimensional testing modality that mimics radiation responses seen in clinical models. Interactions between tumor cell lines (SJSA osteosarcoma and SKBR3 breast cancer) and the laminin-rich ECM in three-dimensional culture provide a tumor niche that increases growth rate and more accurately represents treatment response. Radiation treatment given in fractionations showed changes in E cadherin expressions and NF-κB expression. This testing modality helps identify biomarkers associated with increased resistance to treatment. Creating a testing environment that allows *in vitro* therapeutic modeling to accurately represent *in vivo* tumor environments increases the efficacy of such studies.

DEDICATION

I would like to dedicate this dissertation to Rakesh Bharat Patel whose ultimate sacrifice lead me on the path that I am on now.

ACKNOWLEDGEMENTS

I would like to thank my committee chair, Dr. Akabani, and my committee members, Dr. Deveau, Dr. Ford, and Dr. Poston, for their guidance and support throughout the course of this research. I would also like to thank Dr. Cosgriff-Hernandez for her guidance which helped shape this dissertation. I would like to thank the Department of Nuclear Engineering and the Texas Institute of Preclinical Studies for allowing me to conduct research in their facilities. A great amount of appreciation and gratitude goes to the Wooley lab, they picked up the slack when things became difficult. I would like to thank Justin Smolen, Sarosh Khan, and Dr. Andrew Hillhouse for their contributions of knowledge and resources. I would also like to thank the radiation oncology team at the Texas A&M Veterinary school for their assistance and resources.

A big thank you goes to all my friends and family who have supported me in my journey, who have helped carry me through the most difficult of times and celebrate the best of times. No amount of gratitude will ever suffice for my mother, father, and sister whose encouragement, support, and unwavering faith have gotten me thus far. Special thanks to Sejal Mistry, for her patience and love. Without her, the light at the end would remain forever so. Lastly, I would like to thank Maharaj and Swami. Without them by my side, none of this would have been possible.

CONTRIBUTORS AND FUNDING SOURCES

This work was supported by a dissertation committee consisting of Professors Gamal Akabani, John R. Ford, and John W. Poston, Sr of the Department of Nuclear Engineering and Professor Michael A. Deveau of the Department of Veterinary Medicine.

The cell work and imaging was done with assistance from Justin Smolden and Sarosh Khan of the Wooley Group. The radiation treatment was conducted in part by Linda Knight of the College of Veterinary Medicine & Biomedical Sciences. The ELISA and EIA were conducted using materials provided by Dr. Hillhouse of Department of Veterinary Medicine. The analyses depicted in Chapter IV were conducted in part by Sejal Mistry of the Department of Psychology.

Funding for the purchase of the ELISA and EIA was made possible by the Department of Nuclear Engineering. No outside contributions were received for the research and compilation of this dissertation. All other work conducted for the dissertation was completed and funded by the student independently.

NOMENCLATURE

AJCC	American Joint Committee on Cancer
AML	Acute Myeloid Lymphoma
BaP	Benzo[a]pyrene
BM	Basement Membrane
CAD	Computer-Aided Design
CD	Clusters of Differentiation
ECM	Extracellular Matrix
EHS	Engelbreth-Holm-Swarm
EIA	Enzyme Immunoassay
ELISA	Enzyme Linked Immunosorbent Assay
EMT	Epithelial-Mesenchymal Transition
ESA	Epithelial Specific Antigen
ESRP	Epithelial Splicing Regulatory Protein
GBM	Glioblastoma
GTP	Guanosine Triphosphate
HNSCC	Head and Neck Squamous Cell Carcinoma
IGF-1	Insulin-like Growth Factor 1
IL	Interleukin Factor
IR	Ionizing Radiaiton
MAP	Mitogen-Activated Protein
MCF-7	Michigan Cancer Foundation-7

MM	Multiple Myeloma
MOCA	4,4'-Methylenebis(2-chloroaniline)
NNK	Nicotine-derived Nitrosamine Ketone
ODC	Ornithine Decarboxylase
PCL	Polycaprolactone
PD	Programed cell Death
PD-L	Programed cell Death Ligand
PGA	Poly(glycolic acid)
PI3-Kinase	Phosphoinositide 3-Kinase
PLA	Polylactic acid
PLGA	Poly(lactic-co-glycolic acid)
PTEN	Phosphatase and Tensin Homolog
Rb	Retinoblastoma
RBM47	RNA Binding Motif protein 47
SRSF1	Serine/arginine-Rich Splicing Factor 1
TGF-α	Tumor Growth Factor Alpha
TGF-β	Tumor Growth Factor Beta
TCM	Poly(trimethylene carbonate)
TMZ	Temozolomide

TABLE OF CONTENTS

Page

LIST OF FIGURES

Page

LIST OF TABLES

Page

CHAPTER I

MECHANISMS AND TREATMENT PARADIGMS OF CANCER

Over the past four decades cancer has been one of the most troubling diseases known to man. Each step in discovery unfolded a new level of complexity and with it a new challenge for scientists to overcome. Knowledge gained by studying the mechanisms, progression, and pathology of cancer revealed the complex multi-variable nature of a single cancerous cell and its environment. Each new piece of information lead to advancements in diagnostics and therapeutics. As knowledge of cancer and its mechanisms progress, the treatments in which we apply become significantly more complex (De Palma & Hanahan, 2012).

1.1. Multistage Carcinogenesis

The multistage carcinogenesis model is an outline of the processes that dictate initial mutation all the way to metastasis. The model breaks down carcinogenesis into four distinct stages: (1) tumor initiation based on oncogenic transformations, (2) tumor promotion based on specific cancer cell pathways, (3) malignant conversion based on specific micro-environmental factors, and (4) tumor progression based on cell kinesis, detachment, invasion, migration resulting in circulating tumor cells, tissue homing, and capillary exit and colonization resulting in metastases. Tumors are initiated by mutations created by carcinogens that have led to DNA methylation in areas that typically promote

tumor suppression (Jones & Baylin, 2002). A carcinogen is a complex term composed of two distinct components, initiators and promoters. In order for an oncogenic transformation to take place, an initiation must be followed by a series of promoter events. Initiators react with DNA in an irreversible manner. Tumor promotion requires the accumulation of events to select for mutations of a malignant phenotype. Promoters typically have irreversible effects as long as an initiation event has occurred. Inflammation soon follows, creating a notable sign of malignancy. Inflammation leads to an increase in genetic factors such as ODC, TGF-α, TGF-β, interleukins, and other cytokines. Without sufficient promotion, initiation events are likely to regress back to more normal function. Complete carcinogens are compounds that have the ability to cause both initiation and promotion. Examples of known complete carcinogens are BaP, aflatoxins, MOCA, NNK, asbestos, and radiation. Tumor promotion produces hyperplasia. For cancer to fully form, cellular changes must be made in order to reflect the malignant phenotype. The number of cells that are exposed to a mutation, the increased probability of a malignant conversion (Weston A, 2003). The malignant phenotype corresponds with traditional processes, associated with carcinogenesis on a cellular level. The malignant phenotype starts to alter various cellular processes such as up-regulation of oncogenes, down-regulation of tumor suppressor genes, immunosuppression, cellular immortality, and the beginnings of tumor invasion. Figure 1 shows the acquired capabilities of cells under the malignant phenotype. These are also known as the Hallmarks of Cancer (Hanahan & Weinberg, 2011).

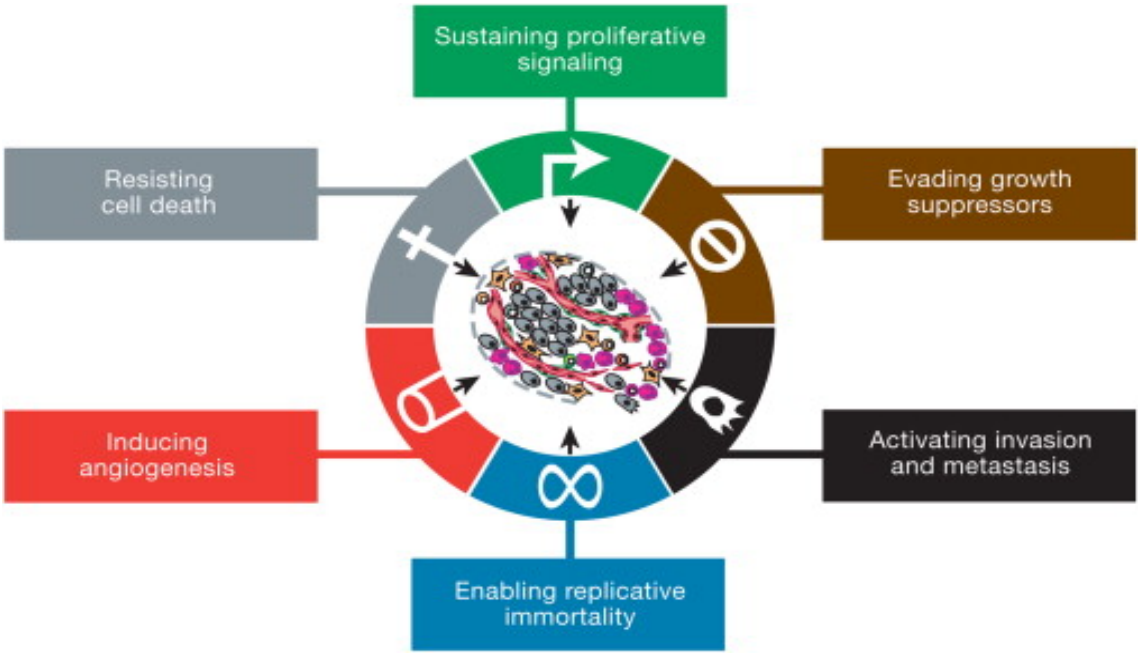

Figure 1. There are six features that are recognized as the Hallmarks of Cancer. Each individual element contributes to the progression of cancer. Reprinted from (Hanahan & Weinberg, 2011).

Transition into the final period of the multistage carcinogenetic model occurs when there is a drastic increase in the aggressive characteristics of these malignant cells. The end result of this transition yields metastatic tumors which are invasions outside the original tumor site. At this stage in carcinogenesis, due to the high number of mutations, treatment plans are mostly palliative or incredibly aggressive with lower chances of success.

1.2. Six Hallmarks of Cancer Biology

1.2.1. Sustaining Proliferative Signaling

Cancer cells have robust methodologies for continuous proliferation. These cells alter a wide variety of signaling pathways and control negative feedback loops within these pathways. The genes associated with high cellular proliferation are known as oncogenes. Cancer cells alter and upregulate oncogenes to sustain high levels of proliferation. For the past twenty years oncogenes have been a pivotal part of targeted therapies by preventing proliferative pathways from hyperactivity. One of the most notable and frequent mutations is the *ras* gene. The *ras* mutation occurs in about 30% of all human tumors (Fernandez-Medarde & Santos, 2011). A mutation in the *ras* gene affects the MAP kinase pathway and provides a drastic increase in cellular proliferation within a variety of cell types. Another well-known pathway, that becomes overly active within cancerous cells, is the PI3-kinase pathway. Mutations within the PI3-kinase pathway cause a variety of cellular ramifications including high cellular proliferation and anti-apoptotic regulation (Liu et al., 2013). Figure 2 shows the various downstream factors that are effected by both *ras* and PI3-Kinase pathways.

Cellular mechanisms have the ability to continuously regulate pathways through a variety of negative feedback loops. Recent studies have highlighted the ability of cancer cells to mutate feedback loops within a system. Mutations within Ras GTPase, an enzyme responsible for shutting down the *ras* pathway, have shown to increase the proliferative efforts of cancer cells. Another example of feedback mutation involves

PTEN phosphatase, which is active in the PI3-kinase pathway. PTEN phosphatase deactivates PIP3, a downstream by-product of an overactive PI3-kinase pathway. Understanding these negative feedback loops are essential for advanced therapeutics that are designed to shutdown specific proliferative pathways (Hielscher & Gerecht, 2015).

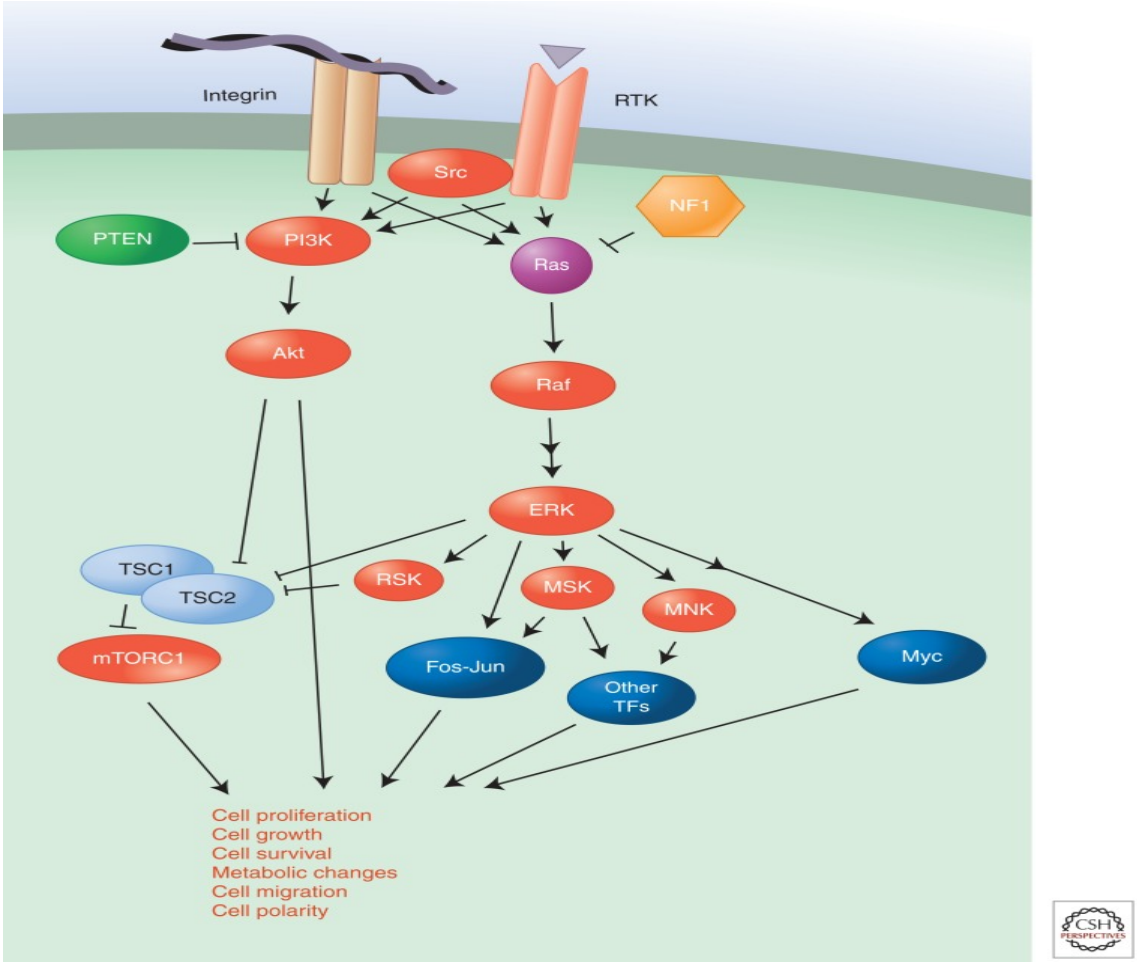

Figure 2. The Ras/raf pathway and PI3-kinase pathway both have a long line of downstream mediators that lead to increase cellular proliferation within a variety of cancer cell types. Reprinted from (Hielscher & Gerecht, 2015).

1.2.2. Evading Growth Suppressors

Another notable genetic discovery that goes hand in hand with oncogenes are tumor suppressor genes. The human body has the ability to detect and eradicate many small mutations that could lead to malignancies. These processes ensure that random mutations and small amounts of change within the DNA do not become cancerous. These processes are dictated by genes known as tumor suppressor genes. Tumor suppressor genes play a main role in the control of the cell cycle. Alterations within the DNA can be accommodated by terminating the cell cycle and commencing repair mechanisms for the damaged DNA. The first notable tumor suppressor gene discovery was that of the Rb protein. Mutations in the gene that account for the Rb protein can lead to a variety of cellular issues on which cancer cells are dependent. The Rb protein is responsible for the G1 checkpoint within the cell cycle. Functionally, the Rb protein suppresses the transcription of the genes needed for the S-phase of the cell cycle to proceed. Without functional Rb proteins, the G1 checkpoint is completely ignored and cellular damage may remain unrepaired during replication (Giacinti & Giordano, 2006).

One of the most important cellular pathways in radiation response deals with p53. The protein that is considered the guardian of the genome. This protein is responsible for the mechanisms that decide the fate of a cell directing it to divide or start the apoptotic pathway (Gottlieb & Oren, 1996). Similar to the importance of the *ras* pathway, mutations in the p53 pathway have been linked to over 50% of tumors (Hollstein, Sidransky, Vogelstein, & Harris, 1991). Both p53 and Rb proteins are easy targets for

tumor cells to take advantage of; this is because they play a large role in in cellular homeostasis. Evading growth suppressors is one of the key parts in cancer progression due to the natural ability of the cell to correct for abnormalities within our DNA.

1.2.3. Resisting Cell Death

Cellular death is a means by which the body rids cells that are unusable and no longer functioning. Three main methods for cellular death within humans includes apoptosis, necrosis, and autophagy. Cancerous cells do an impeccable job of turning these processes off and prolonging survival even when many normal cellular functions have been lost. Apoptotic mechanisms are in place within cells in order to eliminate damaged cells. The p53 pathway described above can designate a cell for apoptosis if cellular damage is too high to repair. Once that process has started, cells are typically bound to their fates. With this being said, cancer cells can alter both extrinsic and intrinsic pathways associated with apoptosis. The intrinsic pathway deals with pro-apoptotic proteins such as Bax and Bak and anti-apoptotic proteins such as Bcl-2. Anti-apoptotic proteins are upregulated and designed to block cytochrome C from being released by mitochondria and prevent the chain of events that leads to apoptosis (Wong, 2011). The extrinsic pathway deals more with receptor-based mutations and prevents external signaling from starting an apoptotic cascade. Autophagy is another cellular response in the presence of stress. Unlike apoptosis, autophagy doesn't render the cell useless because it breaks down cellular components to be used by surrounding cells. However studies have been shown that over-stressed cells, such as those subjected to vast amounts

of chemotherapy or radiation therapy, have the ability to use autophagy pathways to shrink and stay dormant (White & DiPaola, 2009). This can eventually lead to problems further in time if cellular activity and proliferation ever recommence. Lastly, tumors have vast regions of necrotic tissue that can lead to cancer progression. Unlike cells that have undergone autophagy or apoptosis, necrotic cells can still function to help recruit inflammatory cells and release regulatory factors (Lotfi, Kaltenmeier, Lotze, & Bergmann, 2016). Inflammatory cells can assist the progression of a tumor by advancing angiogenesis. While some cells within a tumor are subject to death, a population of cancerous cells have a way of either avoiding or utilizing pathways associated with death as a mechanism for cancer progression.

1.2.4. Inducing Angiogenesis

Originally tumors were thought to enable pro-angiogenic factors later on in their life span. As the tumor developed the need for increased amounts of nutrients seemed necessary in order to survive (Z. Huang & Bao, 2004). Studies have shown that angiogenic factors are required early on in the life span of the tumor, but it is not entirely clear as to why. Tumors activate an "angiogenic switch" that starts to form new vasculature within and around the tumor (Hanahan & Folkman, 1996). However, this vasculature is far from normal. The strength of the walls and the functionality is much different than the normal vessels seen within the body. Tumor vasculature has excessive branching, a leaky nature, and enlarged vessels (McDonald & Baluk, 2005). The differences in vasculature between normal and malignant tumor tissues are shown in

Figure 3 (Vaupel, 2004). The major structural and functional irregularities of tumor vessels are (a) missing differentiation, (b) large diameter, (c) convoluted vessels, (d) aberrant branching, (e) paucity of pericytes, (f) increased vascular permeability and plasma leakage, (g) unstable direction of flow and flow stasis, and (h) formation of RBC aggregates.

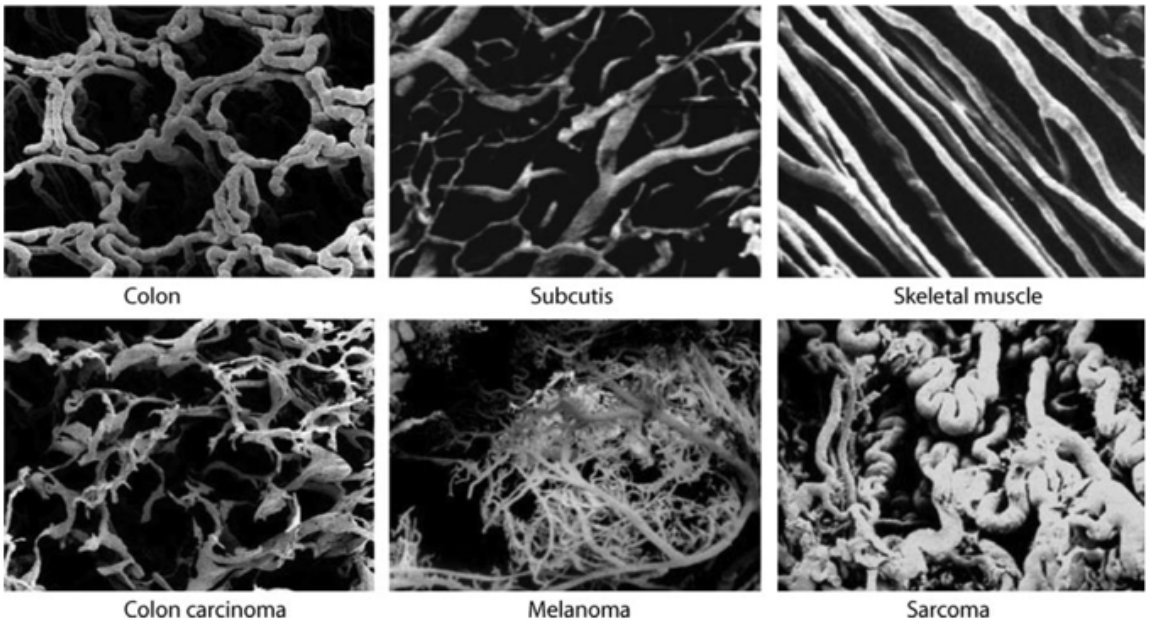

Figure 3. Differences in vasculature between normal and malignant tumor tissue for colon, subcutis, and skeletal muscle. Adapted from (Vaupel, 2004).

All of these characteristics are key components in the sustained growth that tumors experience. Tumors typically utilize factors such as VEGF, TSP-1, and FGF to influence their surrounding environment. Tumors also recruit cells into their created environment

so that they can flip the angiogenic switch. Recent studies have shown that tumors recruit specific cell types such as macrophages, neutrophil, and myeloid progenitor cells before triggering the angiogenic switch (Ferrara, 2010). Not all cancer types are the same; a few cancers contain low amounts of vasculature such as pancreatic ductal adenocarcinomas (Olive et al., 2009). Conversely, there are tumors containing copious amounts of growth factors that induce angiogenesis and are highly vascularized such as infantile hemangioma (Sepulveda & Buchanan, 2014; van der Zee et al., 2010). A variety of cells and growth factors all contribute to the angiogenic phenomenon seen in most tumors. Figure 4 shows the complex nature of a tumor microenvironment including the vasculature and growth factors that contribute toward advance stages of tumorigenesis (Korkaya, Liu, & Wicha, 2011). Tumors depend on the increased nutrition that angiogenesis provides. Without sustained angiogenesis, many resistant properties of the tumor would likely fade away.

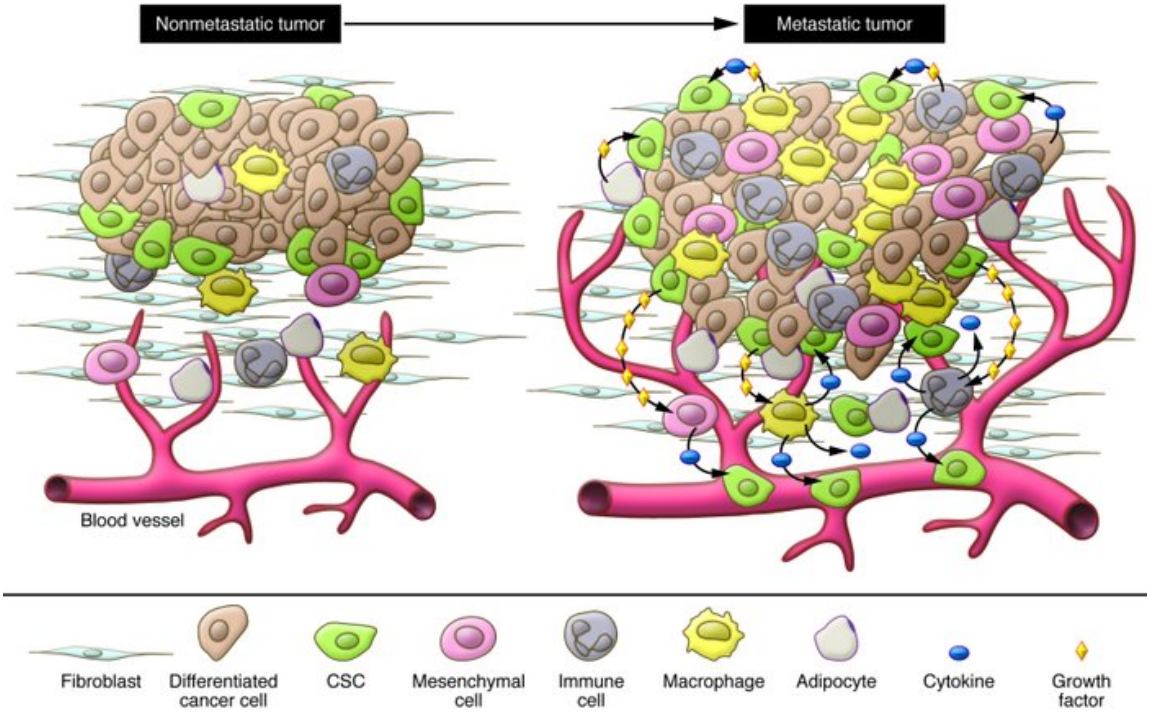

Figure 4. Tumors recruit various cell types and growth factors to increase angiogenesis and eventually begin to travel elsewhere within the body. The larger the tumor becomes, the more complex its microenvironment becomes. Reprinted from (Korkaya et al., 2011).

1.2.5. Cellular Immortality

Cellular aging is one of the most studied topics in recent history. It has direct applicability to many health-related topics and a strong correlation with cancer cells. The process of cellular aging in cells is inversely related to cancer survival. The main process associated with aging within cells is the shortening of telomeres during replication. Chromosomes have telomeres to protect DNA from degradation and fusion with other chromosomes during replication. Once the limited number of telomere sequences have been lost in normal cells, the cell goes through senescence or apoptosis.

However, in cancer cells, the upregulation of a protein known as telomerase allows for the extension of lost telomeric sequence. Cancer cells that have upregulated their telomerase activity are considered "immortalized cells." Immortalized cells have the ability to continuously replicate without the standard loss of their telomeres during each division. Cancer cell lines used for research purposes have drastically high telomerase activity and are viable for many passages without hindering the dependability of the cell line (Hanahan & Weinberg, 2011). Recent studies have questioned the time point in which cancer cells utilize telomerase activity. Premalignant phenotypes have lower telomerase activity in order to increase the probability of genetic mutations to occur during replication. Once the malignant phenotype has been established, cancer cells increase their telomerase activity to provide stability and protection from fates such as senescence and apoptosis (Raynaud et al., 2010).

1.2.6. Activating Invasion and Metastasis

Therapeutic advancements have equipped oncologists with the means to fight cancer very well at early stages. As screening and diagnostic methods improve, the likelihood for survival of those affected with cancer increases. If tumors go unnoticed and are allowed to progress, then treatment and survival becomes increasingly difficult. By the time a tumor progresses to a metastatic site, many cellular processes have been activated and the environment of the original tissue has been drastically altered. For a tumor to start migrating toward other areas within the body, many phenotypical changes must occur. Metastasis from the primary tumor can be characterized into a series of four steps.

The first step is commonly known as the Epithelial-Mesenchymal Transition, EMT. Similar to the "angiogenic switch" this complex change in phenotype requires heavy interaction with the extracellular matrix and a variety of cells. The first notable change occurs with the loss of E-cadherin between adjacent cells. E-cadherin is a binding protein that allows cell to cell adhesion. To down regulate E-cadherin expression, cells start to upregulate transcription factors such as SNAIL, ZEB, SLUG, and TWIST (Serrano-Gomez, Maziveyi, & Alahari, 2016). These transcription factors bind to E-cadherin promoters and deactivate them. After the loss of adhesion, cells are no longer bound to each other and have increased motility allowing for migration to occur. Tumor cells may physical change their shape allowing for the ease of movement within and beyond their primary site. Figure 5 shows the physical changes that primary tumor cells demonstrate during EMT (Pradella, Naro, Sette, & Ghigna, 2017). With the loss of adherent junctions, cancer cells also excrete matrix-degrading enzymes (Hanahan & Weinberg, 2011). Local invasion of the adjacent normal tissue starts with the secretion of IL-4 by cancer cells. IL-4 secretion induces the recruitment of macrophages located around the tumor to start assisting in the extracellular matrix degradation process. Macrophages start to secrete metalloproteinases (MMPs) and cysteine cathepsin proteases which break down the surrounding extracellular matrix creating room to move, invade, and migrate (Joyce & Pollard, 2009; Palermo & Joyce, 2008).

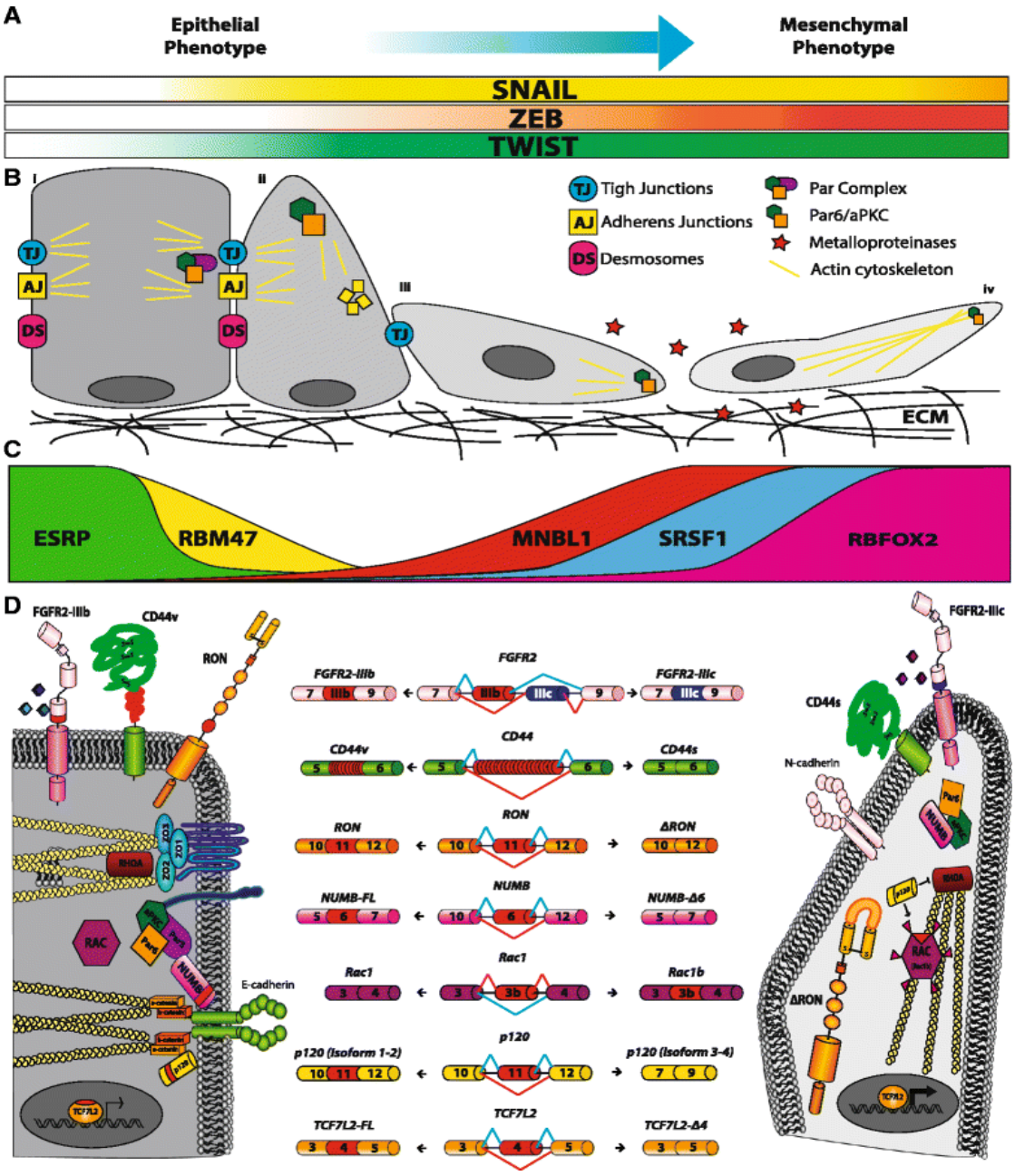

Figure 5. EMT calls for a variety of transcriptional factors that eventually alter cellular adhesion junctions allowing for physical change to occur. A) Shows the regulation of specific transcriptional factors during EMT (SNAIL, ZEB, TWIST). B) The physical changes can be seen as the cell wraps into an amoeboid like structure with there is a loss of the adhesion junctions as EMT progresses. C) Shows the regulation of proteins associated with EMT (ESRP, RBM47, MNBL1, SRSF1, RBFOX2). D) Depiction of how all the factors listed above lead to phenotypical alterations in surface proteins over the transition. Reprinted from (Pradella et al., 2017).

The next phase in the metastatic process, intravasation, is the ability of cells to enter the bloodstream and lymphatic vessels. As tumor cells gain the ability to travel in the initial invasion process, they typically migrate toward blood vessels. Cells attempt to cross the endothelial barrier at a relatively high rate however, only about 0.01% of cells that cross the barrier form secondary tumors (Chiang, Cabrera, & Segall, 2016). Once cells have crossed the endothelial barrier, they are considered circulating tumor cells. These circulating tumor cells have many factors working against them. These factors include the sheer stress caused by blood flow rates and the increased immunological components present within the bloodstream or lymphatic vessels. Once in the bloodstream, circulating tumor cells are often dormant for long periods of time. There are a variety of factors that may contribute toward dormancy. It is likely that the ability of cells to escape circulation and establish secondary tumors is incredibly low. Not much is known about the extravasation of cancer cells from the bloodstream. Cancer cells may exit circulation at random however, they lack the ability to start proliferation in all environments. Studies have shown that these metastatic cells interact poorly with foreign microenvironments (G. P. Gupta et al., 2005). Over time the metastatic cells change and alter their surrounding while recruiting additional cell types required for full metastatic sites to develop (Barkan, Green, & Chambers, 2010). Alternatively, there have been cases that have shown a connection to the primary tumor and the release of suppression factors into the bloodstream. This releases is visible in cases where metastatic sites appeared only after the primary tumor was resected (Retsky, Demicheli, Hrushesky,

Baum, & Gukas, 2008). Regardless of how circulating cells exit the bloodstream, a unique set of parameters must come together for tumor cells to survive in a foreign environment. Similar to the initial proliferation stage, secondary tumors must recruit a variety of growth factors and supplementary cells to survive.

1.3. Treatment Modalities

1.3.1. Surgery

Surgery continues to be the primary strategy for tumor control in solid cancer. Surgical treatment aims to remove the entire tumor, debulk the tumor, or ease cancer symptoms. There are several types of surgeries used depending of the type of tumor and clinical presentation of the patient. Wide local excision is the most common type, followed by organ conserving or minimally invasive surgery. In wide local excision approaches, a large cut is made to remove the tumor and a small margin of normal tissue with or without lymph node dissection. For the case of minimally invasive surgical procedures, a few small cuts are made. This reduces postoperative pain, speeds recovery, and results in less loss of form and function. A laparoscope is inserted into one of the small cuts for direct observation inside the body with a camera. Surgical tools are inserted through the remaining cuts to remove tumor and minimal amounts of healthy tissue. Surgery can be combined with other surgical strategies such as cryosurgery, lasers, hyperthermia, and photodynamic therapy. It is here that the TNM classification becomes relevant. TNM is based on tumor size (T), lymph node involvement (N), and metastases (M). As an example, the TNM classification for breast cancer is given in Table 1. The American

Joint Committee on Cancer (AJCC) and the International Union of Cancer Control presents the AJCC Cancer Staging Manual, which is the gold standard to help the cancer patient management team determine the correct stage for patients and for establishing the best and most appropriate care plan (*AJCC cancer staging manual*, 2016).

Table 1. TNM Staging for Breast Cancer.

T	**T1** Size < 2 cm	**T2** Size 2-5 cm	**T3** Size > 5 cm	**T4** Tumor extends to skin or chest wall
N	**N0** No lymph node involvement	**N1** Metastases to ipsilateral movable axillary LNs	**N2** Metastases to ipsilateral fixed axillary or IM LNs	**N3** Metastases to intraclavicular supraclavicular LN or to axillary IM LNs
M	**M0** No distant metastases	**M1** Distant metastases		

1.3.2. Chemotherapy

The most widely used strategy for the treatment of cancer continues to be chemotherapy. However, chemotherapy is not specific as it is driven by diffusion processes at the cellular level and attacks normal and cancerous cells. Chemotherapy is used for curative intent or as a palliative treatment to reduce the symptoms of terminal cancer. It is used in conjunction with radiation and surgery to attain higher treatment efficacy. There are seven basic classes of chemotherapy based on mechanism of action. These are (1)

alkylating agents such as Cytoxan that chemically affect DNA (Cycle specific: All), (2) antimetabolites, such as 5-FU and Gemzar that substitute the normal blocks (Cycle specific: S), (3) anthracyclines such as Adriamycin inducing DNA damage and inhibit topoisomerase (Cycle specific: All), (4) anti-tumor antibiotics such as Bleomycin that induce severe DNA damage (Cycle specific: All), (5) topoisomerase inhibitors such as Irinotecan that produce DNA complexes and topoisomerase together (Cycle specific: S, G2), (6) vinca alkaloids such as vincristine that binds to tubulin and interferes with mitosis (Cycle specific: M), and (7) taxanes such as Taxol and Taxotere that prevent microtubule from dissociating (Cycle specific: M).

1.3.3. Cancer Immunotherapy

Cancer immunotherapy has made significant advances in the treatment of cancer. Cancer immunotherapy is commonly divided into two distinct strategies. These include targeting the tumor directly and activation of the immune system against cancer cells. Direct tumor targeting requires direct "contact" with tumor cells and derivatives of tumor tissue. Direct tumor targeting can be carried out by using (a) naked monoclonal antibodies, such as trastuzumab, and inhibitors, such as imatinib (Gleevec©), which disrupts specific biological pathways for tumor growth, (b) radiolabeled monoclonal antibodies using full antibodies or their fragments, such as ^{131}I-labeled anti-CD20 MAb (BEXXAR©), ^{90}Y-labeled rituximab (Zevalin©) for the treatment of NHL, and ^{223}RaCl (Xofygo©) for the treatment of castration-resistance metastatic prostate cancer, (c) antibody-drug conjugates (ADC), which combine the specificity of a monoclonal

antibody for the delivery of a highly potent cytotoxic agent, and (d) immunotoxins using engineered oncolytic viruses, such as those using adenovirus, retrovirus, and measles. Strategies that activate the immune system use (a) vaccines using oncolytic viruses, (b) immune checkpoint inhibitors or antagonists, (c) co-stimulatory agonists and co-inhibitory antagonists (Peggs, Quezada, & Allison, 2009), and (d) cellular therapies using chimeric antigen receptor. Immune checkpoint inhibitors and antagonist target the programmed cell death protein receptor (PD-1, also known as CD279), which is expressed on the surface of many cancer cells, or programed cell death ligand (PD-L1 and PD-L2, also known as CD279 and CD273 respectively) which are commonly expressed in surface T-cells. Cellular therapies using chimeric antigen receptor are designed using T-cells from the same patient and modified using adoptive cell transfer and re-injected into the patient to seek and attacked tumor cells (Prasad, 2018).

1.3.4. Radiation Therapy

A fundamental treatment modality of cancer is radiotherapy, which is used concomitantly with chemotherapy and surgery. Currently, surgery and radiation therapy are the most optimal strategies to rid cancer from patients suffering from well localized, solid cancers. The time scale effects of radiation in biological tissue are divided into a physical phase, chemical phase, and biological process. During the physical phase, radiation interaction occurs between 10^{-18} and 10^{-14} s. During the chemical phase, there are physicochemical processes in which affected atoms and molecules react with other atoms and molecules and ionization and excitation lead to breakage of chemical bonds

and production of free radicals. Free radical reactions are complete within approximately 1 ms of radiation exposure. Afterwards, there is a competition between species via scavenging and fixation reactions. The biological phase is the most complex process in radiobiology, where the vast majority of the lesions produced by radiation are repaired. The cells that have acquired irrecoverable damage will attempt to proceed down pathways associated with cellular death. However, these cells may divide before dying. In most cases radiation effects are quite different between normal and tumor tissues. The killing of normal stem cells and loss of differentiated normal cells causes the manifestation of normal-tissue damage during the weeks and months after radiation exposure. Radiotherapy effects have been studied using classical radiobiology, which is macroscopic in nature and did not explain late responding tissues. Focus was placed on dose fractionation, phenomenological repair in terms of sub-lethal and potentially lethal damage, and using the linear-quadratic model (LQ Model). On the other hand, modern radiotherapy is now being studied using a systems-radiobiology approach. This approach takes into consideration the molecular pathways and networks, and use –omics approaches, such as genomics, proteomics, and metabolomics. This includes those of the tumor microenvironment to enhance the therapeutic effects of radiotherapy. In addition, it accounts for the spatiotemporal pathophysiology of tumors, including radiation hormesis, angiogenesis, hypoxia, and growth factors (Sanders, 2017).

1.4. Radioresistance

The classical approach to the radiobiology of cancer is based on the 6 R's. These are (1) repair of DNA damage, (2) redistribution of cells in the cell cycle, (3) repopulation, (4) re-oxygenation of hypoxic tumor regions, (5) Radiosensitivity, and (6) Remote cellular effects. In classical radiobiology, the rate of failure will be determined by the 6 R's of radiobiology. However, today there is compelling evidence that many solid cancers are organized hierarchically and contain a small group of cells commonly referred as cancer stem cells (CSCs). These cells exhibit stem-cell properties and have been found to be inherently resistant to conventional radiation therapy and chemotherapy (Moncharmont et al., 2012; Pajonk, Vlashi, & McBride, 2010; Vlashi, McBride, & Pajonk, 2009). These CSCs have the ability to renew indefinitely, drive invasion, and metastases. The CSCs have an enhanced repair mechanism of DNA, it has been shown that for high-grade gliomas, CSCs have a greater activation of DNA damage checkpoint in response to radiation, and repaired radiation-induced damage (Bao et al., 2006). The mechanisms for radiation resistance are based on (a) quiescence propensity of CSC, (b) enhanced repair of DNA, (c) upregulated cell cycle control mechanism, (d) hypoxia, reactive oxygen species and enhanced radical scavenging, (e) interactions with stroma cells and the microenvironment (Moncharmont et al., 2012). The CD markers used to identify CSCs in various solid cancer is given in Table 2.

Table 2. Common cell surface markers used to identify and enrich CSC in various solid tumors [a)] In breast and ovarian tumors CD24low/−, whereas in the pancreas CD24+ both in combination with CD44+ (Allan, 2011).

CSC marker and enrichment technique	Tumor type
$CD44^{+}$	Breast, Prostate, Colon, HNSCC, Pancreas, Ovarian
$CD24^{a}$	Breast, Ovarian, Pancreas
$CD133^{+}$	Breast, Brain, Prostate, Colon, Liver, Ovarian
ESA^{+}	Breast, Pancreas
EpCAM	Colon
$CD49f^{+}$	Breast
Side population (SP)	Breast, Brain, Lung, Ovarian, Skin
ALDH+	Breast, AML, MM
$CD34^{+}$	AML, Lung
$DLL1^{high}$ $DNER^{high}$	Breast
CD271	Skin

1.4.1. Radioresistance: NF-κB Pathway

A variety of biological pathways influence the ability of cells to be radioresistant. A large number of radioresistant cells are considered to be cancer stem cells or cells that have acquired stem-like characteristics. The main pathways associated with radioresistance are PI3K, *ras,* GLUT-1, and p53. All of these pathways have well known downstream effects which lead to cell survival such as alterations in the NF-κB protein levels. NF-κB is a protein that has been linked to tumor resistance in both chemotherapy and radiation therapy (C. Y. Wang, Cusack, Liu, & Baldwin, 1999).

NF-κB is mainly found within the cytoplasm of cells, in its latent inactive form through binding through an inhibitor. Once cellular stress signals are active, downstream effects

lead to the ubiquitination of IκB. IκB is the key protein in activation of NF-κB. Once NF-κB is free of IκB it can translocate to the nucleus. NF-κB is a pleiotropic mediator of specific gene regulation involving various biological activities, it is responsible for the upregulation of genes associated with the suppression of apoptosis and necrosis, immune, inflammatory, and cell growth responses (Orlowski & Baldwin, 2002; Xia, Shen, & Verma, 2014).

IR has shown to increase NF-κB binding to DNA and increase survival mechanisms within cancer cells (Brach et al., 1991). Figure 6 shows cellular responses after IR impacts the cell. PIP3 is only one of the many possible upstream pathway that relates IR to NF-κB levels. There have been multiple upstream effectors that contribute to increased NF-κB levels. These factors include cytokines, ERK pathway, ATM, HER-2 activation, and many more (Li & Sethi, 2010). All of these factors activate NF-κB and release a variety of radioresistant responses. Studies have shown activation of the ERK pathway from low levels of radiation. Tumor cells responded with anti-apoptotic mechanisms, these responses correlate ERK interactions with NF-κB (T. Wang et al., 2005). Cytokines released by immune cells after ionized radiation (IR) interact with surface receptors on tumor cells which activate NF-κB (Blonska, You, Geleziunas, & Lin, 2004). One such cytokine is TNF-α which is released by T cells and macrophages after IR. TNF-α leads to activation of NF-κB by interactions with NIK. NIK is involved with the inactivation of IκB which activates NF-κB (S. Y. Lee, Lee, & Choi, 1997).

Activation of NF-κB leads to a variety of outcomes that benefit tumor cells and cause resistance to treatment. NF-κB is an important aspect for tumor survival and development after treatment, inhibitors of NF-κB have shown promise in increasing radio-sensitivity and chemo-sensitivity within a variety of cancers (Li & Sethi, 2010).

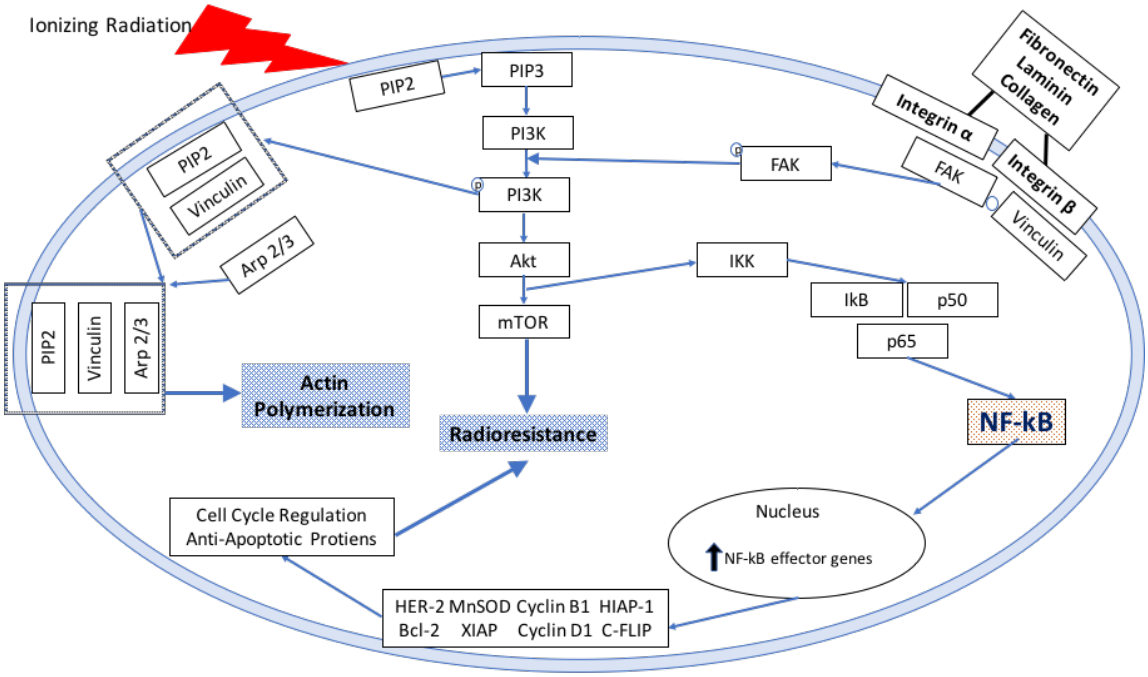

Figure 6. Radiation and ECM effects on tumor cells. Radiation increases NF-κB binding to DNA which releases a variety of pro-survival signals. ECM effects on tumor cells increase actin polymerization which is necessary for invadopodia growth.

1.4.2. Radioresistant E-Cadherin Pathway

E cadherin loss in tumor cells is a notable sign of oncogenic progression. The three main survival attributes that link loss of E cadherin to oncogenic progression are cell motility, invasiveness, and resistance to treatment (Yang et al., 2006). These three tumor attributes also go hand in hand with the EMT phenotype. The EMT phenotype is established late within primary tumor progression. Tumor cells undergo EMT in order to invoke more aggressive and invasive properties (Kang & Pantel, 2013). These changes are necessary for tumor cells to break away from the primary tumor and journey off to metastatic sites (Thiery, Acloque, Huang, & Nieto, 2009). Thus, EMT is highly associated with the loss of adherent junctions on tumor cells such as E cadherin (Kalluri & Weinberg, 2009). EMT promoting factor SNAIL alters tumor morphology by down regulating E cadherin levels which can be seen in Figure 5. Loss of E cadherin facilitates these morphological changes by reducing cell to cell adhesion (Theys et al., 2011). Once adhesion is lost tumor cells increase factors that assist with ECM degradation, such as invadopodia, to help migrate toward blood vessels (Bonnans, Chou, & Werb, 2014; Paz, Pathak, & Yang, 2014).

Radiation plays an important role in the EMT process. The EMT phenotype is associated with radioresistance and chemoresistance (Kyjacova et al., 2015). Breast cancer cells with lower E cadherin content display greater radioresistant properties that cells with higher E cadherin levels (Theys et al., 2011). E cadherin levels are therefore inversely related to treatment resistance. E cadherin loss due to EMT promoters such as SNAIL

have been documented to provide resistance to chemo and radiation treatments (Behrens, Mareel, Van Roy, & Birchmeier, 1989; Singh & Settleman, 2010). SNAIL plays a role in E cadherin mediated radioresistance. Radiation upregulates SNAIL activity which positively affects radioresistant pathways such as PI3k and Erk1 (Vega et al., 2004). Radiation would therefore cause resistance to treatment inducing EMT within tumor cells. Downregulation of E cadherin can enhance radioresistant properties of tumor cells and progress oncogenesis by EMT.

CHAPTER II

CANCER MODELING

Most research in cancer therapeutics is dedicated towards better understanding cancer and its environment. This knowledge leads to increases in effectiveness of therapy modalities. Despite the vast number of projects, dedicated toward improving therapeutics, progress remains fairly slow. This is primarily due to the success rate that studies have when transitioning from animal models to clinical trials. Animal models have been essential tools for testing the side effects and efficacy of drugs prior to human trials. Despite their importance only about 8% of animal studies actually bear successful translation into clinical trials (Mak, Evaniew, & Ghert, 2014). Although they have many advantages, animal models end up costly and inaccurate. The average timeline and success rate for drug discovery is approximately 10-15 years with a success rate under 1%. The time and cost spent on a single drug makes it critical that every phase of testing be as accurate as possible. Typically, drug discovery starts with extensive cell culture testing prior to a preclinical phase. The preclinical stage is generally the stage in which animal studies begin. Improving the accuracy prior to the preclinical stage is a strategy that is constantly being explored. One of the main focuses for researchers is the transition from 2D to 3D cell culture systems. Three-dimensional systems have always shown more aggressive and resistance tumor models than their two-dimensional counter-parts. Increase in resistance is due to increased surface interaction of one cell to

a variety of others. Three-dimensional models have recently tried to incorporate components found within natural tumor microenvironments in order to increase efficacy of studies. Not all components of the tumor microenvironment are easily incorporated into tumor models. However, therapeutic studies involving the ECM have shown great progress in recent years. As the importance of the ECM continues to be explored, three-dimensional modeling continues to improve on the incorporation of these variables (P. Lu, Weaver, & Werb, 2012).

2.1. Tumor Microenvironment

The tumor microenvironment has been overlooked as an incredibly important aspect of oncogenesis. Previously tumors were seen as a collection of homogenous cells that continued to proliferate at high levels. In the past few decades scientists have discovered that tumors are much more complex. Not only do tumors require a heterogeneous mix of cells in order to survive, they also need many non-cellular components in order to progress through oncogenesis.

2.1.1. Angiogenic Cells

Inducing angiogenesis is one the major hallmarks associated with cancer. Tumors go through significant changes and activate processes that lead to the activation of the "angiogenic switch". The angiogenic switch starts the formation of new vasculature required for tumor growth. Endothelial cells help tumor cells construct new vasculature by increasing the amount of growth factors that help induce angiogenesis (Loupakis et

al., 2010). Pericytes work alongside endothelial cells to help create and sustain blood flow. Pericytes are used as a supportive structure which help account for the hydrostatic pressure created by blood flow (Hanahan & Weinberg, 2011). Angiogenic cells are an essential part of the tumor microenvironment by aiding in the creation of new vasculature needed for tumor survival.

2.1.2. Leukocytes

Immune cells within the body play an important role in tumor progression. Contrary to expectations, leukocytes make up a majority of the stromal cells around a tumor (de Visser & Coussens, 2006). The most prominent cell types include: macrophages, granulocytes, natural killer cells, CTLs, and B-cells (De Palma & Hanahan, 2012; Hanahan & Weinberg, 2011). Pro-inflammatory cells are the most utilized cell in tumor progression. Inflammatory cells such a macrophages and granulocytes provide restructuring of the ECM while increasing cell motility (Allavena, Sica, Solinas, Porta, & Mantovani, 2008; Kandalaft, Motz, Duraiswamy, & Coukos, 2011). These cells also provide protection from the adaptive immune system. The adaptive immune system is present in a delicate balance between harmful and beneficial. Adaptive immune cells such as B-cells and CTLs can attack tumor cells by the administration of immunotherapeutics. But they also play a large role in recruitment of inflammatory cells (Hanahan & Weinberg, 2011; Ruffell, DeNardo, Affara, & Coussens, 2010). Inflammatory cells play a large role in cancer progression. Inflammatory cells secrete copious amounts of necessary oncogenic factors such as MMPs, proteases, VEGF, EGF,

FGF2, chemokines, and cytokines (Joyce & Pollard, 2009; Pahler et al., 2008). Inflammatory cells have been shown to help tumors evade the adaptive immune system cells by expressing certain cell markers that neutralize CTLs and natural killer cells (Bunt, Clements, Hanson, Sinha, & Ostrand-Rosenberg, 2009; Qian & Pollard, 2010). Leukocytes play an interesting role in cancer progression and have become a popular therapeutic target for many cancer sub-types.

2.1.3. Fibroblasts

Cancer-associated fibroblasts, (CAFs) are one of the most influential cell types aside from primary tumor cells (Kalluri & Zeisberg, 2006). CAFs assist tumor cells by synthesizing ECM, releasing growth factors necessary for angiogenesis, recruiting macrophages, and enhancing tumor growth (Erez, Truitt, Olson, Arron, & Hanahan, 2010). CAFs are responsible for the formation of the desmoplastic stroma. Presence of the desmoplastic stroma is associated with the level of invasiveness present within a variety of tumor subtypes. Desmoplastic stroma plays a role in the transition between invasive cells and normal tissue (Egeblad, Nakasone, & Werb, 2010). CAFs are responsible for many aspects of tumor progression and survival. CAFs provide resistance to specific anti-VEGF chemotherapeutics (Orimo et al., 2005). Overall, CAFs have a pivotal role in oncogenic progression and survival.

2.1.4. Cancer Stem Cells

Stem cells are cells within a normal tissue which are undifferentiated and have the ability to create a variety of cell types. In recent years tumors have been found to possess a cell type which can mimic the properties of normal stem cells. These tumor cells have the ability to proliferate new tumors when injected into *in vivo* hosts (Cho & Clarke, 2008). These cells are known as cancer stem cells. Cancer stem cells were first found in hematological cancers as a source of constant cancer cell proliferation (Dick, Bhatia, Gan, Kapp, & Wang, 1997). Cancer stem cells are found in almost all tumor types, however, their exact origin in the oncogenic process remains unknown (Hanahan & Weinberg, 2011).

Cancer stem cells possess traits similar to those of cells going through EMT. Studies theorize that differentiated cells may gain stem like characteristics by going through EMT (Singh & Settleman, 2010). Cancer stem cells are resistant to therapy just like many cells that go through EMT (Deonarain, Kousparou, & Epenetos, 2009). Cancer stem cells have been treated with specific drugs that induce differentiation as a possible treatment option (P. B. Gupta et al., 2009).

Cancer stem cells have been seen as the underlying reason for cancer reoccurrence after treatment (Buck et al., 2007; Phillips, Petrie, Creighton, & Garcia, 2010). Not only do cancer cells impact reoccurrence rate they also play a pivotal role in cancer metastasis

(Hermann et al., 2007). Cancer stem cells make great targets for therapeutics due to their resistance to treatment and their role in metastatic disease.

2.1.5. Extracellular Matrix

The extracellular matrix within a tumor is a variety of macromolecules such as collagen (I, II, III, and IV), laminin, fibronectin, biglycan, entactins, and other matricellular proteins (Insua-Rodriguez & Oskarsson, 2016). These proteins interact with the various other cell types within the tumor microenvironment. Stromal cells such as CAFs and immune cells facilitate the biochemical changes within the ECM. Providing the structure needed for cancer progression (Bhowmick, Neilson, & Moses, 2004; Orimo et al., 2005). Abnormal ECM plays a large role in many of the hallmarks of cancer. Abnormal ECM contributes to angiogenesis by having a large amount of collagen IV within the tumor microenvironment. Collagen IV and XVIII break down into a variety of smaller proteins such as endostatin, tumstatin, canstatin, and hexstatin which aid in the formation or inhibition of new blood vessels (Mott & Werb, 2004). The ECM also aids in the branching process of angiogenesis by guiding and aiding in endothelial cell survival (Bignon et al., 2011). The ECM also plays a vital role in inhibiting and promoting various leukocytes. The ECM inhibits a variety of immune cells from interacting with the primary tumor by creating physical barriers which cells cannot pass (S. Wang et al., 2006). Laminin binds to integrin receptors on the surface of neutrophils. Neutrophils stay trapped within the binding region between the basement membrane and the endothelium (Dangerfield, Larbi, Huang, Dewar, & Nourshargh, 2002). The ECM

provides small scale interactions with all types of immune cells within the tumor microenvironment.

The ECM also provides structural rigidity which promotes tumor invasiveness. The degradation of the ECM increases invadopodia activity which is directly linked to tumor cell invasiveness (Parekh & Weaver, 2009). *In vivo* tumor cells must overcome a variety of physical barriers in order to metastasize to other areas of the body. ECM presence is required for tumor cells to phenotypically change into aggressive metastatic cells. The rate of tumor progression is directly related to the ability of tumor cells to interact with the supporting ECM (Weaver, 2006). ECM components interact with tumor cells, fibroblasts, leukocytes, angiogenic cells, and cancer stem cells. Interaction between these components is what is known as the tumor microenvironment.

2.2. Two-Dimensional Modeling

A typical bench top research study always involves some form of two-dimensional cell culture analysis. As the limitations of two-dimensional cell culture are constantly brought to light, researchers merely use this method to save time and funds (Edmondson, Broglie, Adcock, & Yang, 2014). Finding basic phenotypical expressions of cancer cells and scientific principles unrelated to interactions with the environment is the extent of data these studies can provide. Typically, a more robust animal or three-dimensional model is required for increased reliability when it comes to therapeutic research. When dealing with the progression of cancer, most changes are due to more

than just the cancer cell itself. Progression severely depends on the recruitment of a variety of cells and interaction with the extracellular matrix. Two-dimensional studies fail to address the complex process that cancer goes through. Once cells have progressed through a majority of oncogenesis they are considerably resistant to many types of treatment. Thus, therapeutic analysis on a two-dimensional level yields incredibly inaccurate results compared to the realistic nature occurred in more complex systems.

2.3. Three-Dimensional Modeling

Two-dimensional modeling has been the most widely used modality for therapeutic testing. However there has been a recent shift in the utilization of three-dimensional models. Two-dimensional models fail to incorporate a variety of factors seen in *in vivo* tumor models. Three-dimensional models have shown increased drug resistance, higher proliferation rates, and phenotypical changes (Knowlton, Onal, Yu, Zhao, & Tasoglu, 2015). There is a large variety of research paradigms that use three-dimensional modeling prior to animal modeling. These three-dimensional models include various scaffolding techniques, the hanging drop model, and transwell-based modeling. Of these models, the hanging drop is widely used in industry due to the ease with which it is carried out. Tumor engineering focuses around a complex concept focusing on mimicking the natural environment in which tumor cells reside. Biopsies have been a model for the various synthetic materials and spacing needed in order to mimic the natural environment in which tumors grow. There are a variety of synthetic scaffolding techniques each with a unique set of properties. Techniques vary in polymer type and

spacing, which influence cell line compatibility. Table 3 outlines different scaffolding techniques and the cell lines associated with a variety of methods. Tumor engineering focuses on complex oncogenic issues seen from a variety clinical cases. Research on the complex microenvironment and clinical data have significantly altered the way tumor engineers approach creating environments that are habitable for tumors.

Table 3. List of synthetic production techniques and the polymer composition associated with compatible cells lines for each (Bolgen, 2016).

Scaffold Type/ Production Technique	Polymer	Tumor	Cell Line
Microsphere	Dextran, Sephadex G-50	Colon	HCT-116 and HepG2
Microsphere	Polystyrene	Breast	MCF-7
Microsphere	PLGA/PLA	Breast	MCF-7
Electrospinning	PCL	Ewing Sarcoma	TC-71
Electrospinning	PGA-TMC, Gelatin	Pancreas	CD24+, CD44+
Solvent-casting and particulate leaching	PLGA	Oral	OSCC-3
Freeze Drying	Chitosan, Alginate	Brain	U-87MG, U-118MG
Freeze Drying	Chitosan	Breast	MCF-7
Gas foaming and particulate-leaching	PLGA	Breast	MCF-7
Three-Dimensional Printing	Polystyrene	Lymphoma	HBL2, Z138

Materials and spacing are the key components that are involved in tumor engineering. Cells do not naturally migrate within the three-dimensional structure. This leads to difficulties in seeding scaffolds no matter how well the natural environment is mimicked. Production techniques have a variety of pros and cons. However, due to the infancy of tumor engineering, researchers utlize a trial and error methodology. Once the production method isolates a suitable scaffold for a specific cell type then alterations and small changes can be made in order to further mimic the tumor environment.

2.3.1. Electrospinning

Electrospinning is a process that uses given polymer and creates a fine mat-like mesh of fibers. The key luxury of electrospinning is the control of variables such as fiber size and polymer type. Polymer is housed in a syringe type apparatus which is released onto a collecting structure. An applied electric field allows for charge to build between the plate and the collecting device. Voltage is applied to the polymer and eventually adhesion forces holding the polymer together are overcome and a thin fiber is collected on the other side. Electrospinning has been around for many decades but has only recently been used in tumor engineering applications. Electrospun scaffolds have housed a variety of cell types including breast cancer, Ewing sarcoma, and pancreatic cancer. Pancreatic studies have shown that cells can be grown with electrospun PGA-TCM. These cells show anti-tumorigenesis mechanisms involved in chemotherapeutics (He et al., 2013). Triple negative breast cancer studies have shown increased representation of the original niche of breast cancer stem cell populations (Palomeras et al., 2016).

Increasing the natural environment of tumor cells not only provides an increase in growth but changes the internal expressions within a cell. Modeling conducted with Ewing sarcoma cells have shown to drastically increase expression in IGF-1 when compared to its two-dimensional counterpart (Fong et al., 2013). Electrospinning can be used as a method for therapeutic research within a variety of cells types. The most notable quality for electrospun scaffold is the ability to alter fiber density and a wide range of polymer availability.

2.3.2. Solvent-casting and Particulate-leaching

Solvent casting and particulate leaching utilizes the chemical nature of polymers and porogens in order to create a porous scaffold. The production method for this scaffold starts with a polymer solution with a uniform distribution of porogens with a desired volume. The solvent is extracted leaving a hard polymer and porogen mix. Since the porogens are non-soluble in the polymer solution they can be leached out by dissolving them in water. Figure 7 shows the relative technique that solvent casting and particulate leaching follow (Bolgen, 2016).

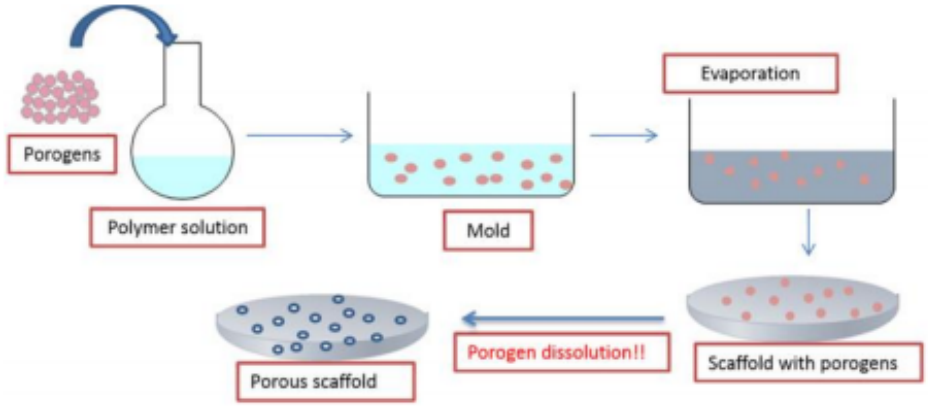

Figure 7. Step by step procedure of solvent-casting and particulate-leaching. Solvent casting and particulate-leaching is a three-dimensional scaffolding technique that utilizes chemical properties of polymers and porogens to create hard porous structure made out of synthetic materials (Bolgen, 2016).

2.3.3. Freeze Drying

Researchers typically seek out the least complicated production technique for scaffolds. Freeze drying utilizes sublimation as a way to easily and effectively create porous scaffolds. Choosing polymers and solvents with drastically different sublimation temperatures yields homogenous pores within a scaffold. After initial mixing of the polymer and solvent the resulting solution is frozen creating ice crystals within the polymer mix. A low-pressure system, partial vacuum, extracts the ice crystals resulting in the desired scaffold. A chitosan-HA freeze-dried scaffold has been used to proliferate U-118 MG human GBM in a multidrug chemotherapeutic study. Ultimately, leading to an increase within malignant cultures that possessed greater invasiveness and drug resistance (Florczyk et al., 2013). Typical specifications for scaffolds made via freeze-drying are: pore diameter between 55-243 μm; porosity between 33-68%; and low

incorporation of vascular structures (T. Lu, Li, & Chen, 2013). Low incorporation of vasculature hinders the use of such scaffolds when trying to mimic the natural environment.

2.3.4. Three-Dimensional Printing

Three-dimensional printing has become one of the most exciting biomedical advancements in recent years. Three-dimensional printing techniques have the ability to replicate much of the structure found in native tumors. Over the last decade three-dimensional printing has attempt to create functional organs and revitalize damaged tissue. Recently advancements in the machinery and techniques behind 3D printing utilize computer-generated models in order to design and mimic the complexity seen within a variety of tissue types (Stanton, Samitier, & Sanchez, 2015). Three-dimensional printing gives engineers the ability to control variables easily such as spacing between structures, use of biocompatible materials, and implementation of ECM components (Charbe, McCarron, & Tambuwala, 2017). With improvements in CAD and bioinks, complex structures such as vasculature have been incorporated into tumor models. Three-dimensional tumor models have the ability to interact with the ECM, embed necessary growth factors, and contain supportive stromal cells (Samavedi & Joy, 2017). Three-dimensional printers aim to properly incorporate cells within bioinks to print structures containing cells. Imbedding cells within a printed structure eliminates the need for seeding scaffolds after fabrication, which is a complex process that often causes unwanted variability. MCF-7 breast cancer cells have been used in 3D-printed spheroid

studies, showing uniform distribution of cells within the printed structure. MCF-7 cells were combined with in a gelatin-based mixture and used as the bioink for tumor spheroid production (Ling et al., 2015). SU3 glioma stem cells have been printed with a mixture of gelatin and sodium alginate in order to provide a drug resistant testing modality. SU3 and U87 printed models have shown increased resistance to TMZ compared to the two-dimensional counterpart (Dai, Ma, Lan, & Xu, 2016). Printed models have been used to show increases in phenotypes that mimic migratory cells and can simulate metastatic processes (T. Q. Huang, Qu, Liu, & Chen, 2014; Soman et al., 2012). Many other *in vivo* tumor characteristics have been modeled using three-dimensional printing these include metastasis, interactions with auxiliary cell types, and increased therapeutic resistance (Samavedi & Joy, 2017).

2.3.5. Decellularized Scaffolds

Decellularized scaffolds have been used by tissue engineers as a method for exact replication of the natural environment seen in tissues. Decellularized tissue is tissue that has been removed from an animal and cleared of all nuclear material from the previous host. Detergent-based removal of the nucleated cells will leave the extracellular matrix and small growth factors which are vital for recellularization. The decellularized models are a great basis for recreating a tumor outside an *in vivo* host. These recreated tumors have almost all the non-cellular components and factors that one will see within a clinical tumor. The decellularization process is difficult to characterize and conduct uniformly however once a process has been perfected, it can be commercialized for use

within synthetic systems. Successful decellularized tissue has been used in recent years as a means for tissue engineering. Decellularized tumors have been used as a scaffold for recellularization of MCF-7 breast cancer cells, SW-480 colorectal adenocarcinoma cells, and KYSE-510 esophageal squamous cell carcinoma cells. Not all cell types mentioned repopulated well in decellularized tissue (W. D. Lu et al., 2014). Decellularized tissues have complex processes that still need to be perfected before commercialized use can begin.

2.3.6. Hydrogel

As cancer modeling continues to show the importance of the tumor microenvironment, testing modalities attempt to further replicate the ECM. Tumor cells need the ECM in order to further oncogenesis. Natural gels are biocompatible materials such as collagen, fibrin, chitosan, and hyaluronic acid that are used as basic scaffolding material (Butcher, Arulpragasam, & Minchin, 2004). However, these components lead to variabilities due to a variety of unknown factors present such as growth factors (Tibbitt & Anseth, 2009). Hydrogels are commercially made synthetic materials that mimic many of the natural ECM components. Many hydrogels also include purified forms of ECM components such as laminin or collagen. Hydrogels provide a solid 3D structure for cells to grow in while taking into consideration variables such as biocompatibility, biodegradation, porosity, and surface chemistry.

Matrigel®, a form of hydrogel, scaffolds have been used to mimic the natural tumor microenvironment for MCF-7 breast cancer cells. The *in vitro* breast cancer model showed high replicability of the tumor niche. The model successfully replicated cluster organization and cellular morphology of *in vivo* breast cancer cells (Cavo et al., 2016). Matrigel® has been used in a variety of cell types as a basis for replication of the natural tumor microenvironment. Matrigel® has been used with A253 epidermoid carcinoma and B16F10 melanoma lines in order to enhance growth rate of injected tumor cells (Asghar et al., 2015; Webber, Bello, Kleinman, & Hoffman, 1997). Matrigel® scaffolds have also been used in co-culture situations to provide necessary stromal cells involved in oncogenesis. Hydrogels have been widely used in tumor engineering as a solid tool in replicating the tumor microenvironment and establishing the tumor niche.

2.4. Research Model

This research aims to create a three-dimensional model which includes native tumor components. A three-dimensional model was created using a 96 well plate with a conical bottom to help induce spheroid formation. The native tumor environment was replicated by coating spheroids with Corning® Matrigel® BM matrix. This matrix allowed spheroids to interact with components that mimic the native tumor extracellular matrix. Radiation was given to this model to identify similarities observed in clinical settings. Osteosarcoma (SJSA) and breast cancer (SKBR3) were the available cell lines used in the creation of the tumor spheroids.

CHAPTER III

MATERIALS AND METHODS

3.1. Spheroid Formation

SJSA and SKBR3 tumor spheroids were formed using 4 Corning® 96 Well spheroid microplates. These plates contain an ultra-low attachment surface and geometric properties that allow spheroid formation to occur easily and directly in the center of the well. SKBR3 cells were passaged 3 times and plated at 20k cells/well. SJSA cells were passage 10 times and were plated at 20k cells/well. Cells were taken from a 20 mL sample which contained $2x10^5$ cells/mL and seeded with a volume of 100 μL/well. Plates were separated into four categories: (1) SKBR3 High-Dose, (2) SKBR3 Low-Dose, (3) SJSA High-Dose, and (4) SJSA Low-Dose. Every testing condition was replicated a total of four times to maintain proper redundancies and account for small variabilities.

3.2. Matrigel® Preparation

Corning® Matrigel® BM matrix is a unique extract of EHS mouse tumor. Corning® Matrigel® BM matrix forms a gel at room temperature. Tumor ECM is generally composed of a variety of collagens, laminin, fibronectin, SPARC, and entactin (Giussani, Merlino, Cappelletti, Tagliabue, & Daidone, 2015). Matrigel® is primarily composed of laminin (60%), collagen (30%), entactin, and a variety of growth factors.

High concentration Corning® Matrigel® BM matrix was placed overnight in a 4°C freezer to thaw. Since Matrigel® forms a gel above 10°C, pre-cooled pipet tips were used to avoid unwanted gel formation. High concentration Corning® Matrigel® BM matrix was placed on ice once out of the 4°C environment. Once thawed, 2 mL of Matrigel® was pipetted in 8ml chilled DMEM media, creating a 20% concentration of Matrigel®. The 10 mL vial was then labeled and placed within -20°C storage. After approximately five minutes, the vial was taken out and vortexed gently to mix Matrigel®, creating a less viscous solution.

A similar process was conducted with the creation of 40% concentration of Matrigel®. 4 mL of Matrigel® was pipetted in 6 mL DMEM media. The 10 mL vial was labeled and place within -20°C storage. After approximately five minutes, the vial was taken out and vortexed gently in order to mix Matrigel®, creating a less viscous solution. Both solutions were then placed on ice.

3.3. Generation of Matrigel® Coated Spheroids and Media Replacement

To create Matrigel® coated spheroids, media must first be carefully extracted from each well on the day following initial plate seeding (Day 2). Media extraction from the Corning® 96 Well spheroid microplates was done using a 3 mL syringe and a 26G needle. Corning® 96 Well spheroid microplates were tilted at a 45° angle while media was carefully extracted for each well. Approximately, 80 μL/well was extracted; an ideal

extraction should not move the spheroid from the center of well after completion. Once all media was extracted, 80μL/well of varying Matrigel® concentrations were put back in. 0% Matrigel® concentration simply used 80 μL/well of DMEM. Other Matrigel® concentrations used 80 μL/well of the desired concentration. All Matrigel® culture was done using chilled tips to avoid gel formation. Media was inserted carefully in order to avoid disrupting the spheroid

The same extraction process was utilized to replace the media. Media extraction from the Corning® 96 Well spheroid microplates was done using a 3 mL syringe and a 26G needle. Corning® 96 Well spheroid microplates were tilted at a 45° angle while media was carefully extracted for each well. Spheroids coated in Matrigel® did not have an exact amount of media to extract due to the gel formation within the well. Media was extracted until spheroid started to migrate toward the edge of the well. Approximately, 50 μL/well was extracted and then replaced with 50 μL/well in order to provide fresh media. Media changes were done on Day 2 (80 μL/well), Day 12 (50 μL/well), and Day 22 (50 μL/well).

3.4. Radiation Treatment of Tumor Spheroids

Radiation treatment was carried out on a clinical helical TomoTherapy unit maintained within the College of Veterinary Medicine & biomedical Sciences at Texas A&M University. The helical TomoTherapy platform combines IMRT delivery with helical CT image guidance. Helical TomoTherapy is a unique form of radiation therapy that

delivers radiation 360 degress around the patient as the patient translates through the gantry. Helical TomoTherapy generates complex dose distributions allowing for aggressive tumor management while minimizing normal tissue toxicity.

A custom 3D printed phantom containing two 96 well plates stacked directly on top of each other were simulated on a Siemens Somatom Definition AS CT simulator with a 0.6 mm slice thickness. Two sets of contours were constructed, one for the low dose plates (2 Gy, 1.5 Gy, 1Gy) and one for the high dose plates (10.0 Gy, 8.0 Gy, 6.0 Gy, and 4.0 Gy) using VelocityAI. Each set contained a contour representing each dose level separated by a contour representing the dose gradient between the two. Both sets of contours were transferred to the helical tomotherapy planning station and two plans were made, one with the low dose plate contours and one with the high dose plate contours. Treatment planning for the two plans were conducted using beamlet mode with a Normal dose grid (0.184 cm X 0.184 cm). A jaw width of 1.05 cm and a nominal modulation factor of 3.2 were used for both optimization. Pitch, defined as distance of couch travel per gantry rotation relative to beam width, was set at 0.215 for both plans. All plans were run using Tomo H™ System Planning Station build 5.1.2.12.

TomoH PlanningStation was used to create an initial IMRT Plan Report. The planning station utilizes a CT image taken prior to treatment and creates dose profiles given a variety of input. Specific conditions can be given an importance value to indicate where dose should and should not be given. Figure 8 shows expected dose levels given to the low dose plates from sagittal, transverse, and coronal views.

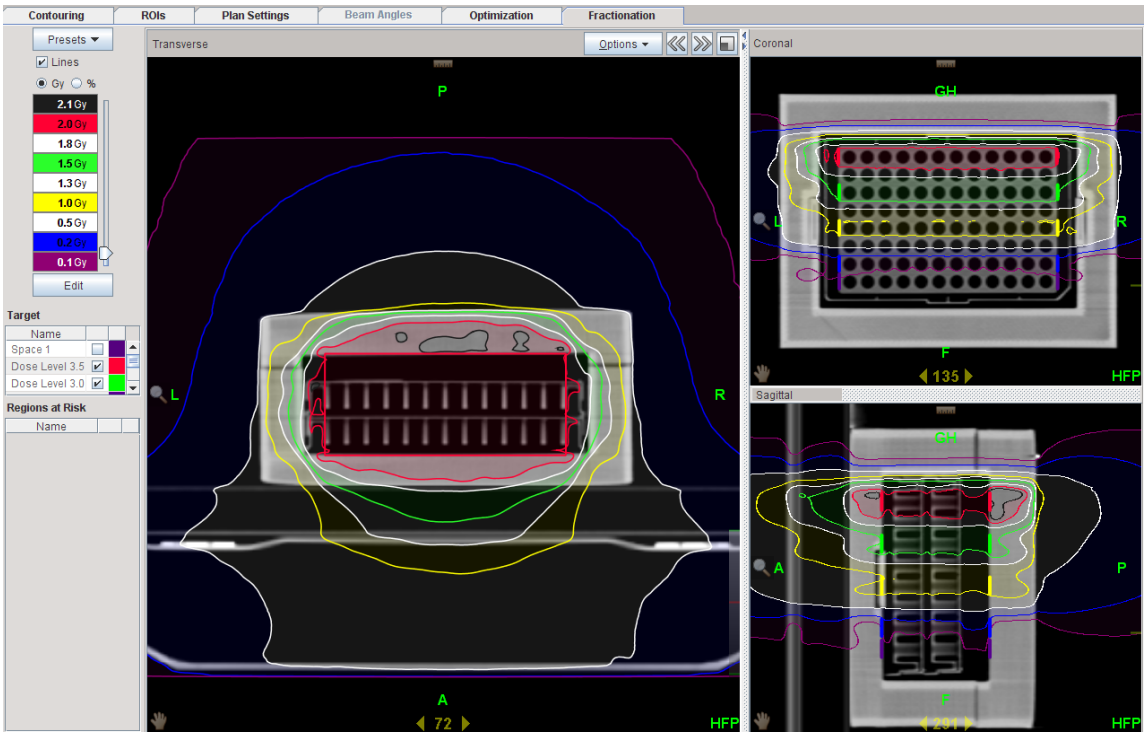

Figure 8. Optimization views of delivered dose for low dose plates calculated from the TomoH PlanningStation. Low dose plates contained controls and dose fractionations of 2 Gy, 1.5 Gy, and 1 Gy.

Figure 9 shows expected dose levels given to the high dose plates from sagittal, transverse, and coronal views. Beam on time for high dose plates lasted approximately 30 minutes and low dose plates ran for approximately 10 minutes. SJSA and SKBR3 plates were placed on top of each other during the radiation treatment which can be seen in Figure 8 and Figure 9.

Plans were carried out in three distinct time periods. Day 8, Day 13, and Day 14 were the three radiation times for each plan. On all three of those days the treatment plan was

carried out in the same manner. Total doses for the low dose plates were (6 Gy, 4.5 Gy, 3 Gy) and for the high dose plates (30.0 Gy, 24.0 Gy, 18.0 Gy, and 12.0 Gy)

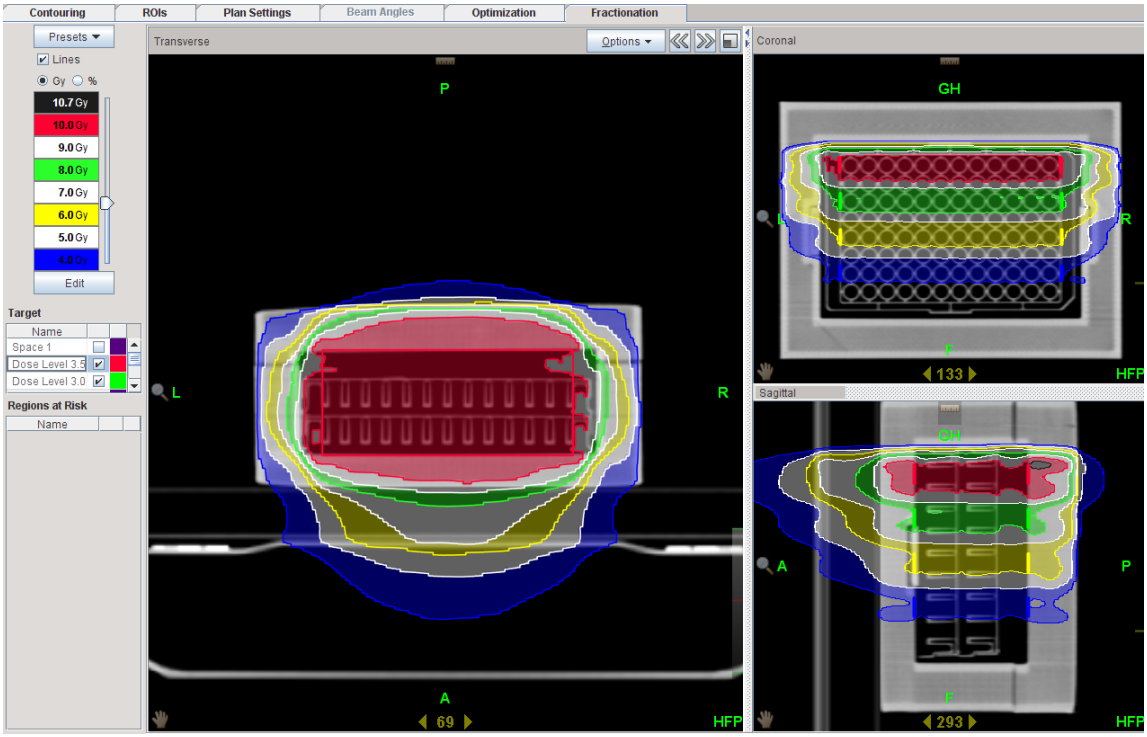

Figure 9. Optimization views of delivered dose for high dose plates calculated from the TomoH PlanningStation. High dose plates contained dose fractionations of 4 Gy, 6 Gy, 8 Gy and 10 Gy.

3.5. Live/Dead Characterization

Live/Dead analysis was conducted on Day 24 to verify pockets of live cells and necrotic regions within the tumor. Live staining was conducted using Calcein-AM and dead staining using Propidium Iodine solutions. Plates were stained individually and then

imaged prior to the start of the next plate. Staining solution for each plate was created by combining 40 μL of Propidium Iodine, 10 μL of Calcein-AM, and 10 mL of PBS. At these concentrations 100 μL staining solution was added per well. Incubation lasted for approximately 40 minutes, and then plates were imaged. Confocal imaging sliced tumor spheroids into approximately 30 slices. Then, these images were stacked and analyzed for live regions within individual tumor spheroids.

3.6. NFkB Characterization

An InstantOne® ELISA was used to quantify NF-κB levels within tumor spheroids. ELISA is a detecting assay used in situations with low target protein content, as it provides a wide range of sensitivity. InstantOne® ELISA plates utilize the sandwich antibody method. However, capture antibodies and detection antibodies can be combined at the same time. As the capture antibody binds to the plate and specific antigen (NF-κB), the detection antibody also binds to the antigen. This method allows for less time-consuming steps and easier protocols to follow.

At day 24 50 μL of media was removed per well by the same protocol mentioned above. Corning® 96 Well spheroid microplates were placed in -80°C storage to promote ice crystal formation within tumor spheroids. Ice crystals within a sample penetrates cell membranes and helps break apart tumor spheroids. The low temperature also reverses some bond formation within the Matrigel® coating. Both of these aspects are essential in order to create proper cell lysates prior to use of the ELISA. After a 24h period, cells

were thawed and 100 μL of cell Lysis mix was added per well. Plates were placed on a microplate shaker (400 rpm) at room temperature for 10 minutes. Plates were then incubated at 37°C for 90 minutes. Once incubation time was completed, the plates were placed back on to the microplate shaker (400 rpm) for 10 minutes. The samples were then ready for an antibody cocktail which contained both capture antibody and detection antibody. 50 μL of cell lysate and 50μL of antibody cocktail was added to ELISA strips. The strips were placed on a plastic microplate holder which was then foiled and left for incubation. Incubation was conducted on a microplate shaker (300 rpm) at room temperature for an hour. Once incubation of antibodies and cell lysates completed, wells were washed via plate washer. The plate washer aspirated all fluid from the wells and then dispensed 200 μL of wash buffer. This process was conducted three times until plates were considered thoroughly washed. After the final wash, strips were gently tapped upside down to remove any remaining wash solution. One hundred microliters of detection reagent was added to each well. The plate was then foiled and left to incubate on the plate shaker (300 rpm) at room temperature for 30 mins. After incubation, 100μl of stop solution was added to each well. Plates were placed in a spectrophotometric plate reader set at 450 nm to measure fluorescence of each well. Measured fluorescence is directly related to the amount of NF-κB present in each sample.

The ELISA plate used two spheroids sets for every treatment condition as redundancies. A total of seven different dose fractionations, three different Matrigel® concentrations,

and two different cell lines occupied 84 wells within the 96 well ELISA. The remaining wells were used to establish controls.

3.7. EMT Phenotype Assessment

A human E Cadherin EIA kit was used to establish the number of cells expressing EMT phenotypes. The human E-cadherin EIA Kit by ThermoFisher Scientific quantitatively determines the amount of soluble E cadherin present in the lysates created from tumor spheroids. The ELISA utilizes a sandwich method similar to the InstantOne™ NF-κB ELISA. However, the EIA kits use a two-step procedure rather than combining capture antibodies with detection antibodies. Each well within EIA kits contain immobilized antibodies which binds desired antigens (E cadherin). Labeled antibody, which is anti-human E cadherin labeled with peroxidase, creates a sandwich effect. This binds E cadherin from one side while immobilized antibodies bind it to the plate. Finally, substrate is added and reacts with anti-human E cadherin to create a yellow color. The hue is proportionate to the amount of E cadherin present.

On day 24, 50 μL of media was removed per well using the same protocol mentioned above. Corning® 96 Well spheroid microplates were placed in -80°C storage to promote ice crystal formation within tumor spheroids. Ice crystals within a sample penetrate cell membranes and help break apart tumor spheroids. The low temperature also reverses some bond formation within the Matrigel® coating. Both of these aspects are essential in order to create proper cell lysates prior to use of the EIA. After a 24 hour period, cells

were thawed and 100 μL of cell Lysis mix was added per well. Plates were placed on a microplate shaker (400 rpm) at room temperature for 10 minutes. Plates were then incubated at 37°C for 90 minutes. Once incubation time was completed plates were placed back on to the microplate shaker (400 rpm) for 10 minutes. Samples and controls were then ready to be added to the EIA plate. One hundred microliters of cell lysate was added to the EIA plate and left for incubation. Plates were sealed with foil prior to incubation, which lasted 120 minutes at 37°C. Once primary incubation was completed, wells were washed via a plate washer. The plate washer aspirated all fluid from the wells and then dispensed 400 μL of wash buffer. This process was conducted three times until plates were considered thoroughly washed. After the final wash, strips were gently tapped upside down to remove any remaining wash solution. 100 μL of anti-human E cadherin, labeled with peroxidase, was then added to each well. Plates were foiled and left to incubate at 37°C for 60 mins. Once secondary incubation completed, wells were washed via a plate washer. The plate washer aspirated all fluid from the wells then dispensed 400μl of wash buffer. This process was conducted four times until plates were considered thoroughly washed. After final wash, strips were gently tapped upside to remove any remaining wash solution. 100 μL of substrate was added to each well. Plates were foiled and left to incubate at room temperature for 15 minutes. 100 μL of substrate was added to each well. Plates were then placed on a microplate shaker (400 rpm) in room temperature for 10 minutes. Once all steps were completed, plates were placed within a spectrophotometric plate reader. This was set at 450nm to measure the

fluorescence of each well. Measured fluorescence is directly related to the amount of E cadherin present in each sample.

The EIA plate used two spheroids sets for every treatment condition as redundancies. A total of seven different dose fractionations, three different Matrigel® concentrations, and two different cell lines occupied 84 wells within the 96 well ELISA. The remaining wells were used to establish controls. E cadherin sample was given to establish controls, that had concentrations of 2700 ng/mL, 1350 ng/mL, 675 ng/mL, 338 ng/mL, 169 ng/mL, and 84 ng/mL.

CHAPTER IV

RESULTS

4.1. Control Growth

The Corning® 96 well spheroid microplate supported continual growth for both SJSA and SKBR3 cell lines. However, due to the non-adherent nature of the SKBR3 cell line, tumor spheroids were not produced. SKBR3 breast cancer cells could not proliferate into a three-dimensional shape. Figure 10 shows an image focusing only on the outer most cells of the well. As the depth microscope is adjusted the image becomes sharper and the inner most cells can be seen with clarity. This observation indicates that the cells are aligned along bottom of the U-shaped well rather than stacked on top each other. Therefore, growth was modeled as a flat two-dimensional surface. SKBR3 cells have been shown to exhibit grape-like morphology. Grape-like cells have less cell-to-cell adhesion and form poor colonies (G. Y. Lee, Kenny, Lee, & Bissell, 2007). For this reason, SKBR3 cells form poor three-dimensional structures and cannot be used as a model for tumor spheroid analysis.

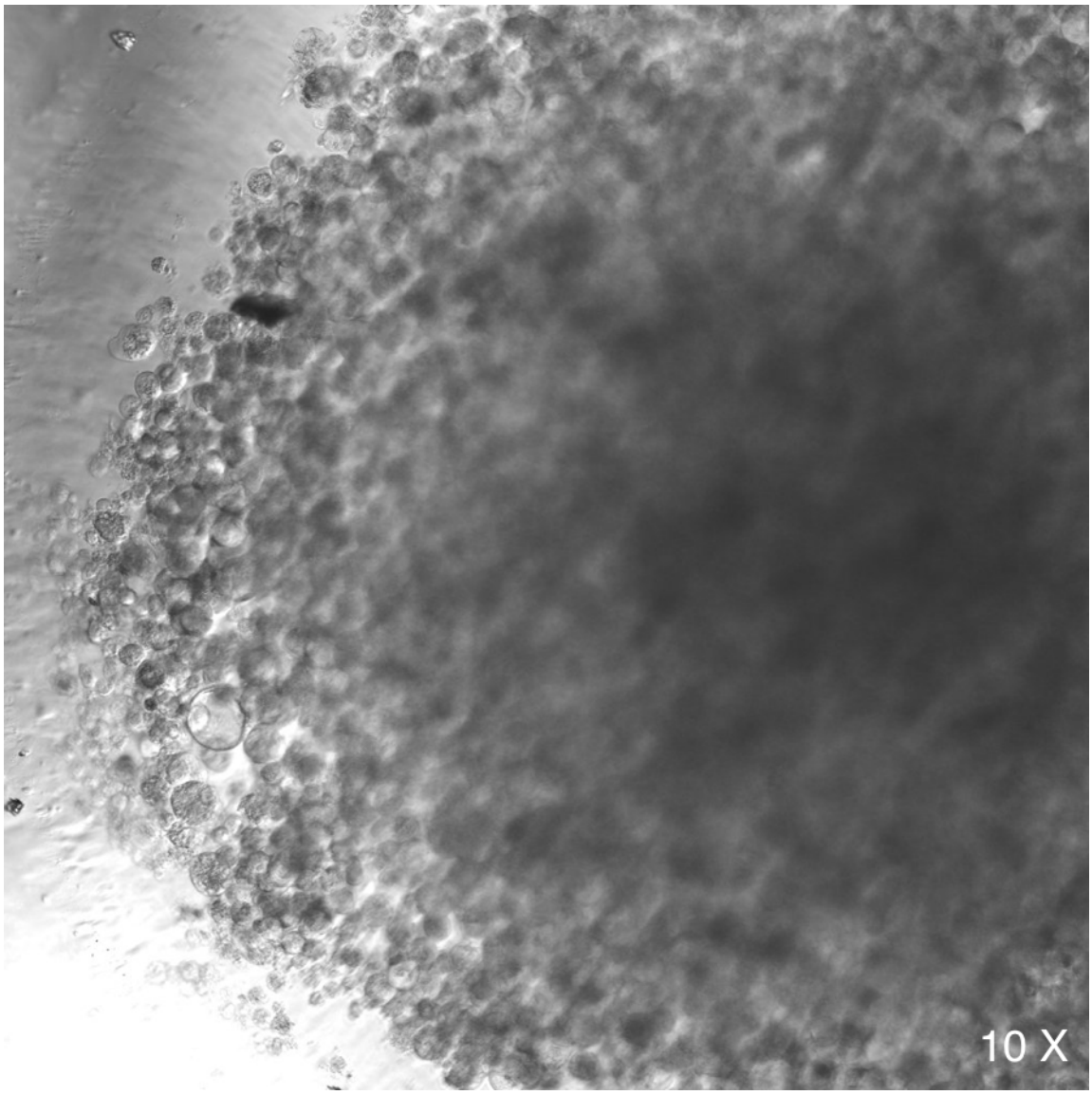

Figure 10. Confocal image of SKBR3 cells seeded into a 96 well spherical plate. Growth can be seen as a non-three-dimensional structure as the cells have highly adhered to the bottom of the well and slightly to adherent to adjacent cells.

Growth studies that involved SJSA osteosarcoma cells showed similar stacking properties, which are seen in *in vivo* studies. Figure 11 shows the drastic difference between SJSA osteosarcoma cells and SKBR3 breast cancer cells.

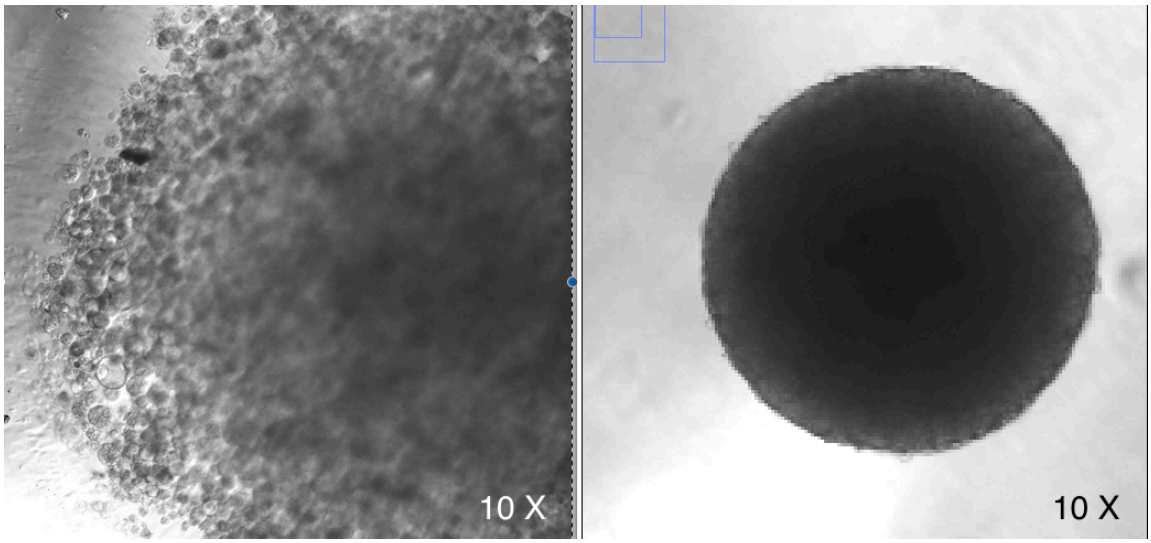

Figure 11. Images taken of SKBR3 cells (left) compared to the SJSA osteosarcoma cells (right). Distinct differences can be seen in the cell-to-cell adherence between the tightly bound SJSA cells compared to the spread out SKBR3 cells.

4.1.1. Spheroid Formation Without Matrigel®

Controls were used primarily as a base line for comparison against radiation and ECM effects. Control samples display typical tumor spheroid growth patterns. Figure 12 shows the growth of SJSA cells over the course of 24 days.

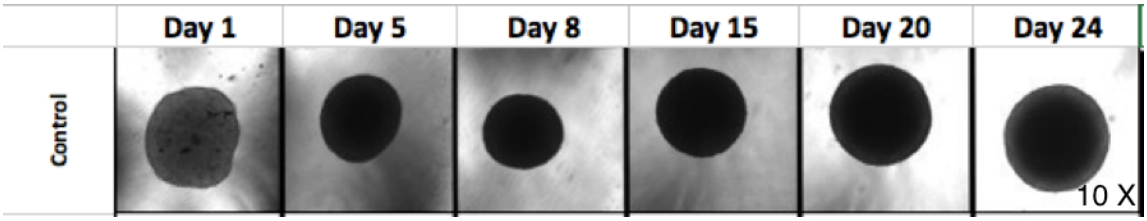

Figure 12. Growth for the SJSA cells over 24-day period. Distinct shrinkage can be seen from Day 1 to Day 8, followed by a visible growth of the tumor spheroid.

4.1.1.1. Cellular Density and Growth

SJSA cells within the 96 well spherical microplate were initially seeded with an initial concentration of 2.0 x 10^4 cells per well. These cells spread out over the bottom layer of the plate before converging toward each other. The relative size of the spheroid initially shrinks and as time progresses, it starts to upregulate adherent junctions and increases cellular density. This is seen by observing the opaqueness of the control spheroid on Day 1 versus the distinct darkness on Day 8 in Figure 12. The spheroid starts to increase its volume around Day 8 which is why an 8-day cell cycle is considered for the SJSA cells. The average growth per day, in respect to volume, can be seen in Figure 13 over the entire 24-day period.

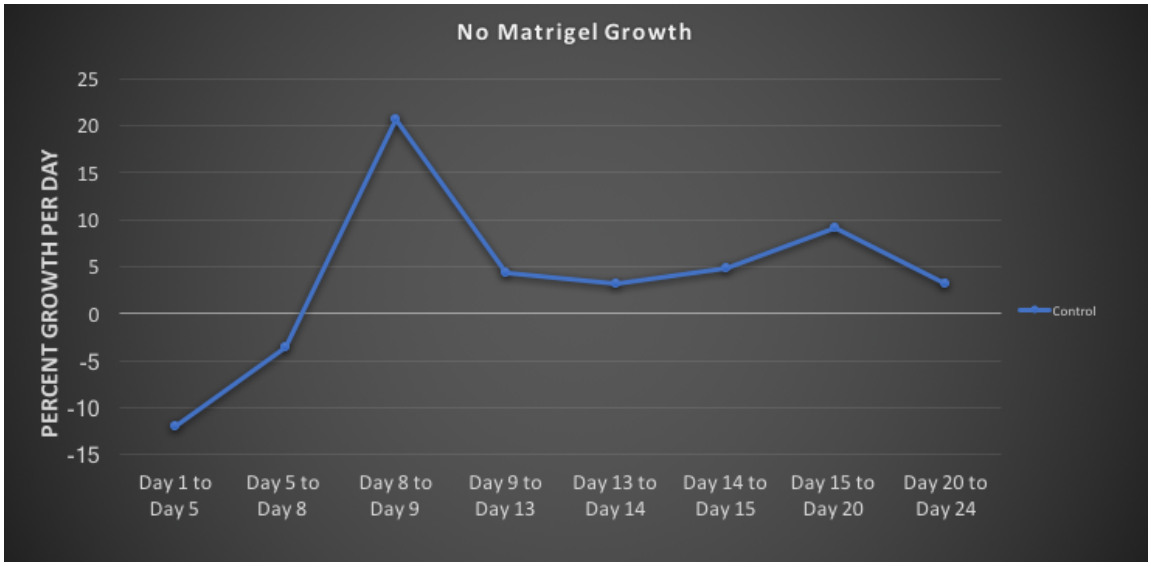

Figure 13. The average growth with respect to volume per day that the control spheroid exhibited. Negative growth indicates shrinkage of the tumor spheroid. Shrinkage can be observed from Day 1 to Day 5 with an average reduction in volume of 12 percent per day.

4.1.1.2. Invasiveness

Invasiveness is exhibited as cells start to alter their phenotype and progress through oncogenesis. Control spheroids without the presence of Matrigel® do not have the ability to change their phenotype due to the lack of initial ECM presence.

4.1.2. Spheroid Formation with Matrigel®

Spheroids were coated with Matrigel® on Day 2. Cells were allowed to grow into and utilize the ECM as a tool to alter cellular expression. Distinct visual difference can be seen in spheroids grown in Matrigel®. The most notable visual effect is the extension of invadopodia into the ECM. Figure 14 distinctly shows the presence of invadopodia within the Matrigel® coated spheroids in comparison to controls.

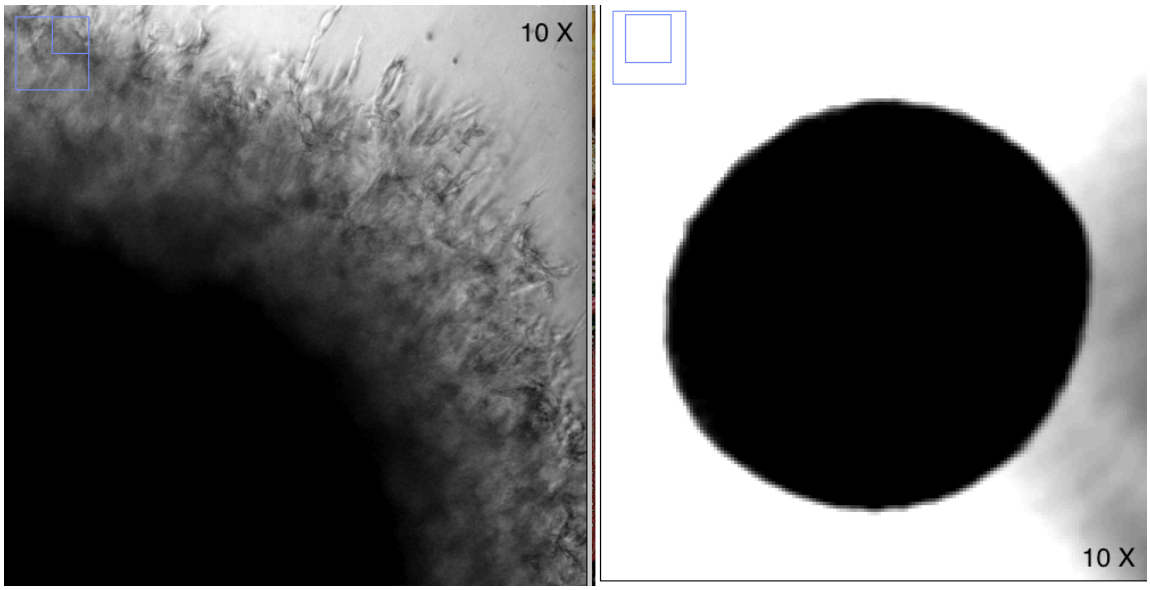

Figure 14. Tumor spheroid grown in Matrigel® (left) has a distinct presence of invadopodia by Day 5 of growth. Compared to control samples (right) that present no extension beyond the outer edges of the spheroid.

4.1.2.1. Cellular Density and Growth

SJSA cells were seeded with an initial concentration of 2.0 x 10^4 cells per well and spread out over the bottom layer of the plate. Due to the presence of ECM factors, Matrigel® coated spheroids do not shrink. Due to the presence of ECM components, the cells no longer seek each other and increase adherent junctions. The cells spread into the Matrigel® and continued to grow without decreasing in size. Two concentrations of Matrigel® were used to assess the approximate impact of Matrigel® within the system. The growth with respect to volume can be seen in Figure 15 over a 20-day period for both 20% and 40% Matrigel® concentrations. After 20 days, many of the spheroids grew

out of the visual range of the microscope. Consequently, images were not taken past that point.

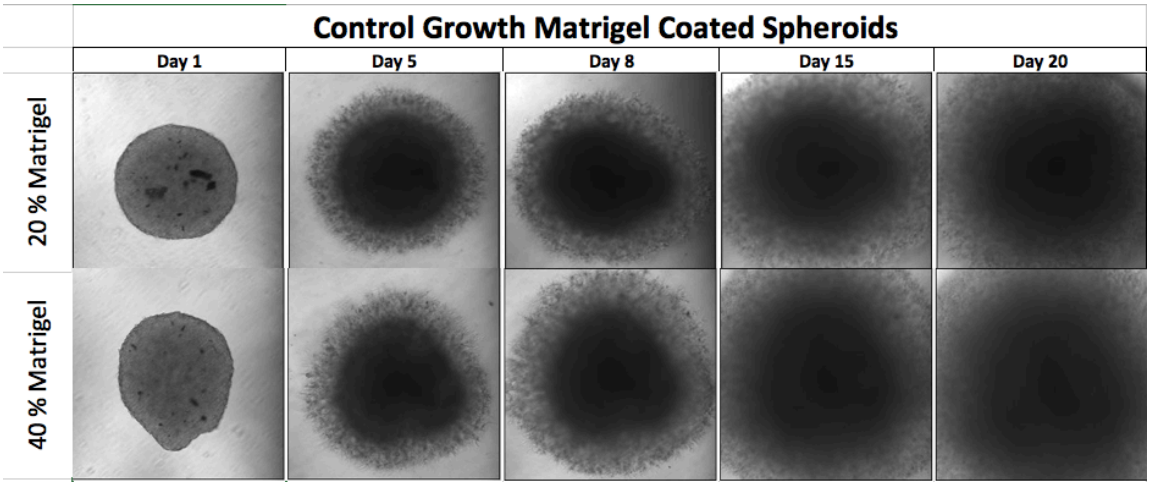

Figure 15. Growth of spheroids coated in Matrigel® over a 20-day time period. Constant growth can be seen from both samples without clear distinction between 20% Matrigel® concentrations and 40% Matrigel® concentrations.

Spheroid volume for Matrigel® controls continuously increase over the experiment interval. However, there is no distinct difference in growth between the 20% concentration and the 40% concentration. The tumor volume seems to be unaffected by the amount of Matrigel® past 20%, which appears to be enough to saturate the tumor. Figure 16 shows the difference between controls and Matrigel® coated spheroids on growth rate. There is a distinct difference in the initial growth rate of Matrigel® coated spheroids.

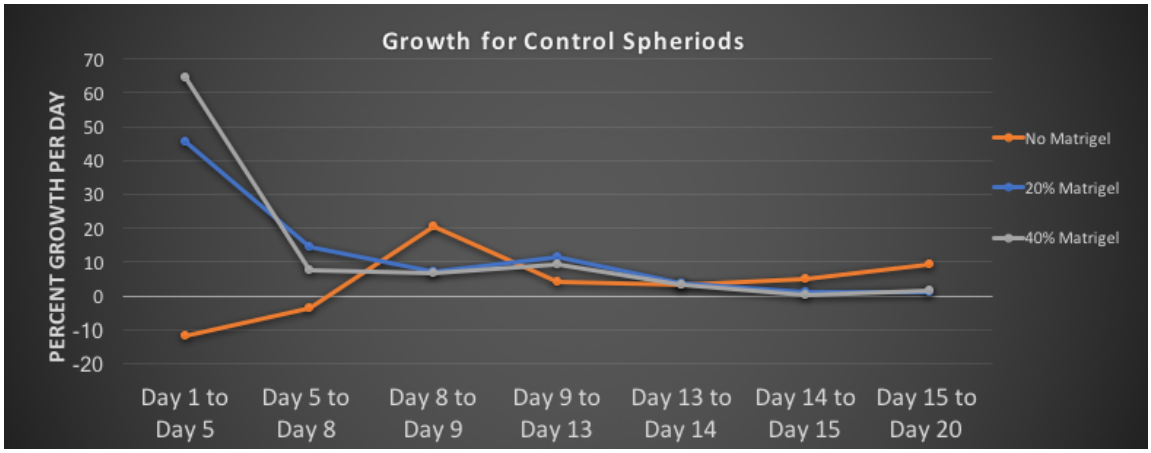

Figure 16. Growth comparison per day of initial control samples with and without Matrigel®. Both 20 and 40 percent concentrations are similar in growth per day and drastically differ from no Matrigel® spheroids.

Spheroids without Matrigel® exhibit distinct growth properties in the beginning and show some similarities by Day 20. However, due to the initial differences in growth, the presence of Matrigel® drastically changes the size of the tumor spheroid by Day 20.

4.1.2.2. Invasiveness

Spheroids interact with the Matrigel® in order to alter their phenotype and demonstrate progression through oncogenesis. One phenotypically alteration is the morphological changes seen within the spheroids. Figure 17 shows the presence of invadopodia in spheroids containing 20% Matrigel® and 40% Matrigel®.

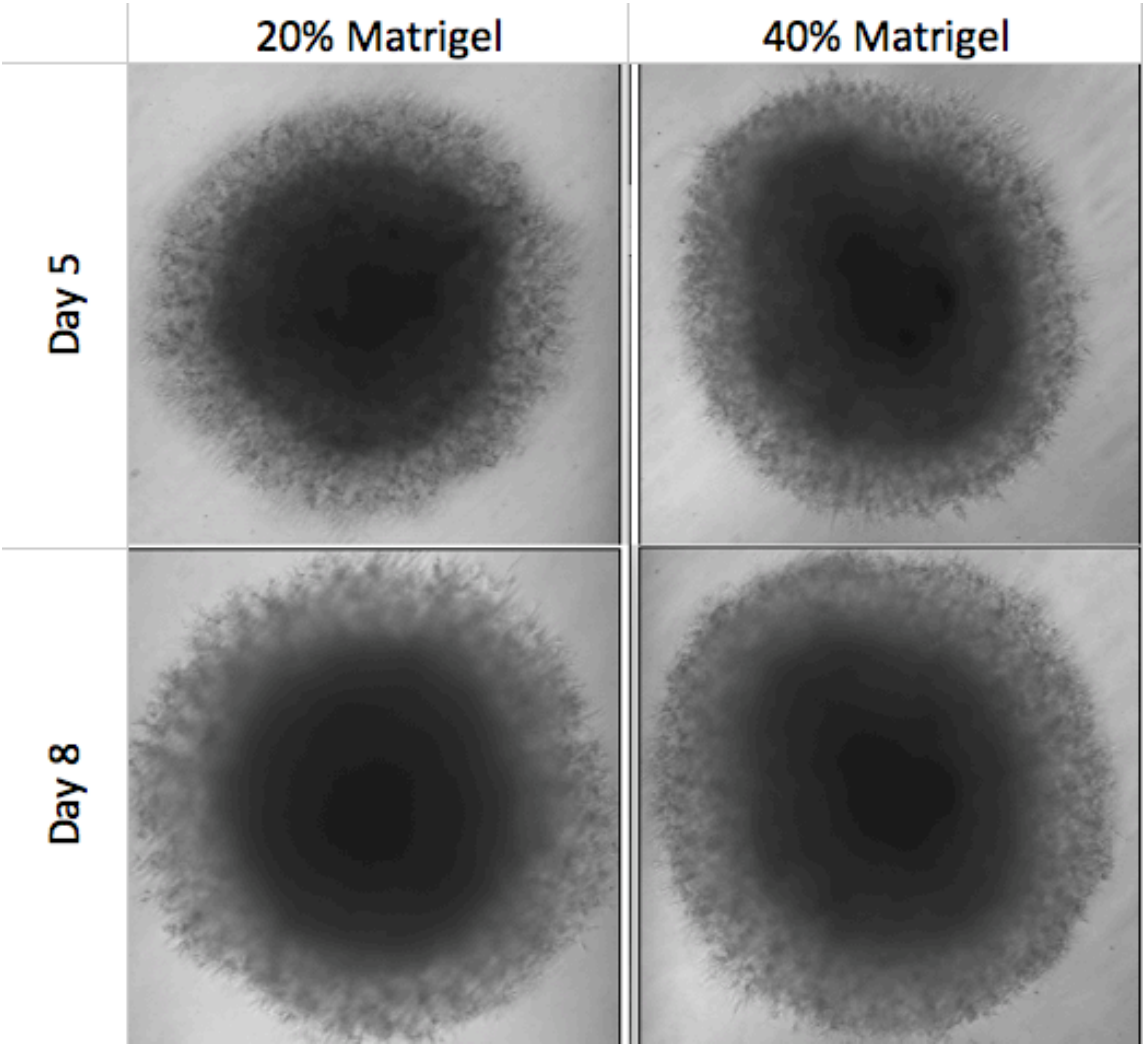

Figure 17. Progression of spheroid coated in Matrigel® at different concentrations. There are no distinct visual differences in invadopodia between 20% and 40% concentrations of Matrigel®.

Tumor spheroids coated in Matrigel® can be broken down into two distinct regions. The first region is primarily a solid dense area in the center and the second region includes surrounding cells that have interactions with Matrigel® through invadopodia. Figure 18

demonstrates the growth exhibited by the dense area in the center of the spheroid, with varying concentrations of Matrigel®.

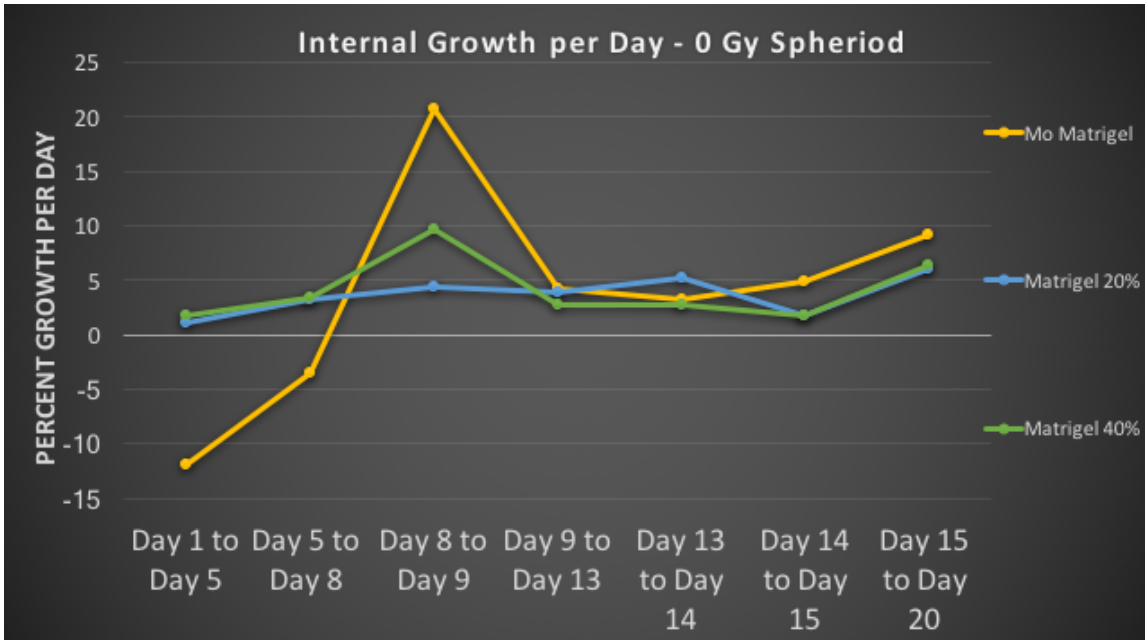

Figure 18. Growth progression of dense area within SJSA spheroids over 20-day period. Spheroids with both 20% and 40% Matrigel® concentrations show similar internal growth patterns.

The dense region within a spheroid exhibits similar growth patterns regardless of the initial Matrigel® concentration, with the exception of the first 8 days. With Matrigel® present, cells have the ability to attach to the ECM provided rather than attaching to themselves as seen in controls. Due to the interactions with Matrigel®, the spheroids no longer condense in the first eight days. Once Day 8 is reached, the internal region within spheroids demonstrate similar growth patterns with or without Matrigel®. As seen in

Figure 15, spheroids grow much larger than the field of view making it hard for the microscope to image well.

As a result, the full growth rate of the invadopodia becomes difficult to calculate past Day 8. Figure 17 shows consistent growth between Day 5 and Day 8 of the invadopodia. Past Day 8, growth cannot be seen but is assumed to continue. Invadopodia growth is indicative of invasive characteristics present within *in vivo* tumors.

4.2. Radiation Growth

The radioresistant properties that the ECM provides tumors *in vivo* is incredibly difficult to replicate in an *in vitro* environment. Utilizing Matrigel® as a tool to replicate the interactions between cells and the ECM enhances the ability to bridge the gap between *in vivo* studies and *in vitro* studies. Similarly, radiation has been seen as a tool to drastically reduce tumor sizes more effectively than some chemotherapy drugs. However, the adverse effects of radiation therapy are well known and certain dose levels progress oncogenesis. Growth studies on SJSA cells indicate radiation fractionations that can be suitable as a treatment mechanism.

4.2.1 Spheroid Formation Without Matrigel®

Radiation therapy conducted on SJSA osteosarcoma cells without the presence of Matrigel® has revealed the extreme radioresistance of the cell line. Even at extremely high dose levels, SJSA osteosarcoma cells have continued to survive in a minimal

capacity. Reduction in tumor volume is apparently at 10 Gy dose fractionations (total 30 Gy) and stoppage in growth is facilitated by 4 Gy dose fractionation (total 12 Gy). Figure 19 is a visual representation of the tumor spheroids over time at various dose levels. Dose levels can be split into three distinct categories: low, mid, and high dose fractionations. Table 4 outlines the dose fractionations by category and the total dose received by each spheroid in the respective category.

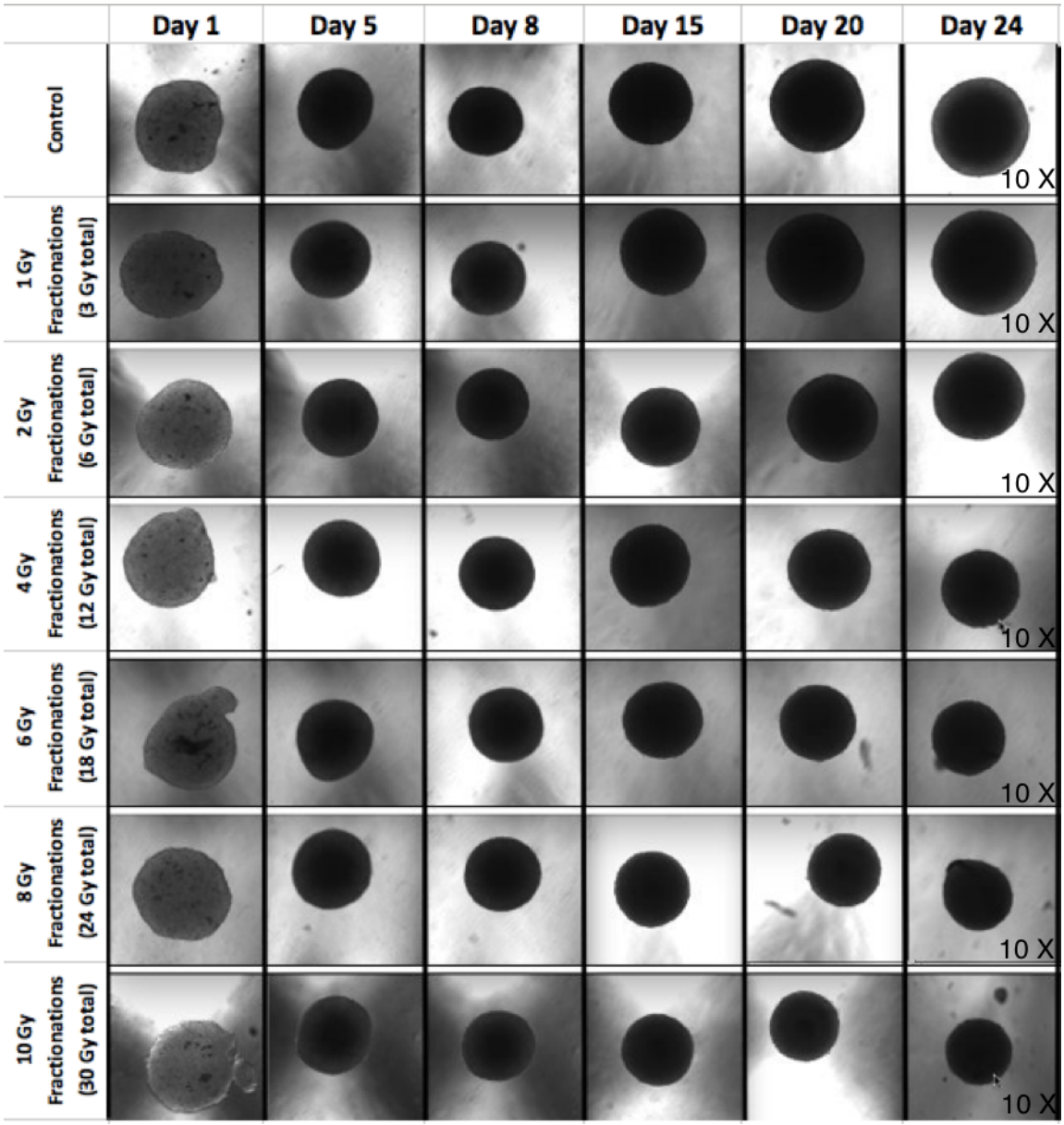

Figure 19. SJSA spheroids growth over time at different total doses and dose per fractionations. Reduction in tumor size is apparent as dose level increases. Spheroids were irradiated after Day 8 and received a total of three fractions.

Table 4. Radiation ranges, fractionations, and total dose values given to SJSA osteosarcoma cells.

Dose Range	Low	Mid	High
Dose per Fractionation (Gy)	**0-2**	**4**	**6-10**
Total Dose (Gy)	**0-6**	**12**	**18-30**

4.2.1.1. Cellular Density and Growth

Radiation can be seen to directly impact the growth of SJSA osteosarcoma cells in a variety of ways. In the low-dose category, controls grow at a normal expected rate. Dose fractions of 1 Gy have an adverse impact on growth, rather than impeding growth the dose enhances growth. Dose fractions of 2 Gy demonstrate growth reduction compared to controls. However, growth continues at a slower rate and almost doubles in size by Day 24. The mid-range dose level, 4 Gy fractionations, demonstrated a relative stoppage in growth by Day 24. At high dose levels, spheroids hovered around the same volume for a few days followed by a decrease in size most notably by the 10 Gy fractionation. Figure 20 shows the normalized growth patterns for each radiation condition. Spheroids were normalized to Day 8 due to the predicted 8-day cell cycle seen in the control group.

Figure 20. SJSA spheroids normalized size over time at different dose fractionations. Spheroids were normalized to the size seen on Day 8 due to the cell cycle duration. Spheroids were irradiated on Day 8, 13, and 14. Size decrease are observed in the 6, 8, and 10 dose fractionations.

A total size comparison of non-Matrigel® spheroids for each dose level is demonstrated in Figure 21. Spheroids took approximately 5 days after the first irradiation to show a size reduction.

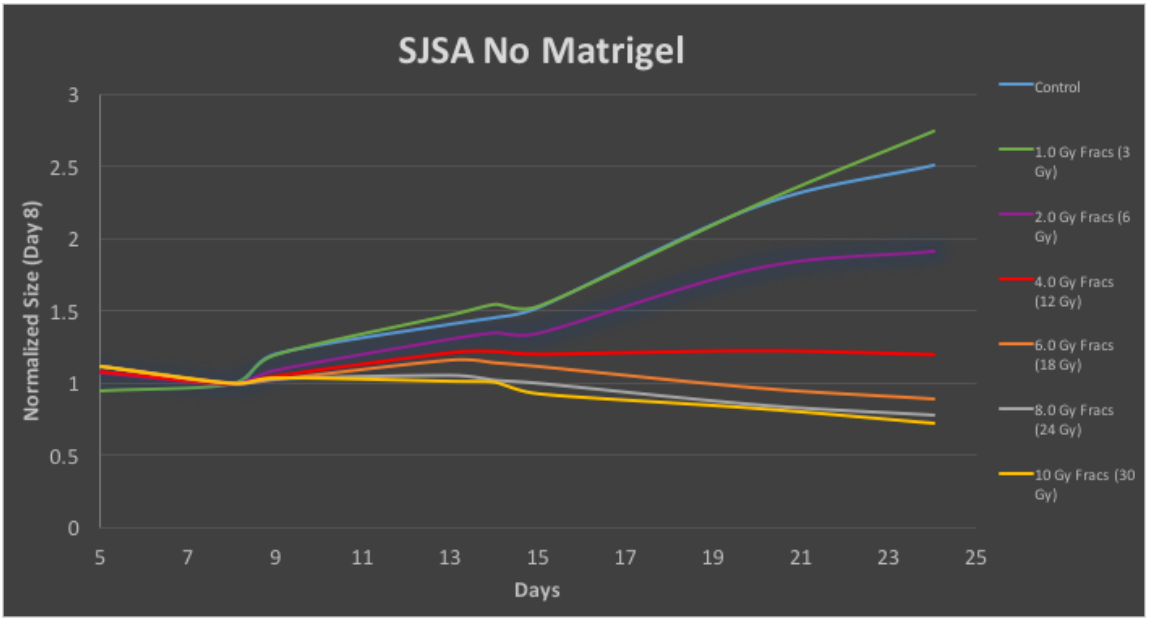

Figure 21. Total comparison of tumor spheroids (without Matrigel®) shows the impact that radiation has on growth. Tumor volumes were normalized to Day 8 due to cell cycle considerations.

The final sizes for many of the conditions drastically differ and it is unknown how much of the bulk tumor still remains alive post radiation. Live/Dead analysis indicated the amount of the SJSA cells that were still alive within the tumor spheroid as well as cells that had gone through necrosis. Figure 22 shows the relative number of live cells within the tumor spheroids for each radiation condition.

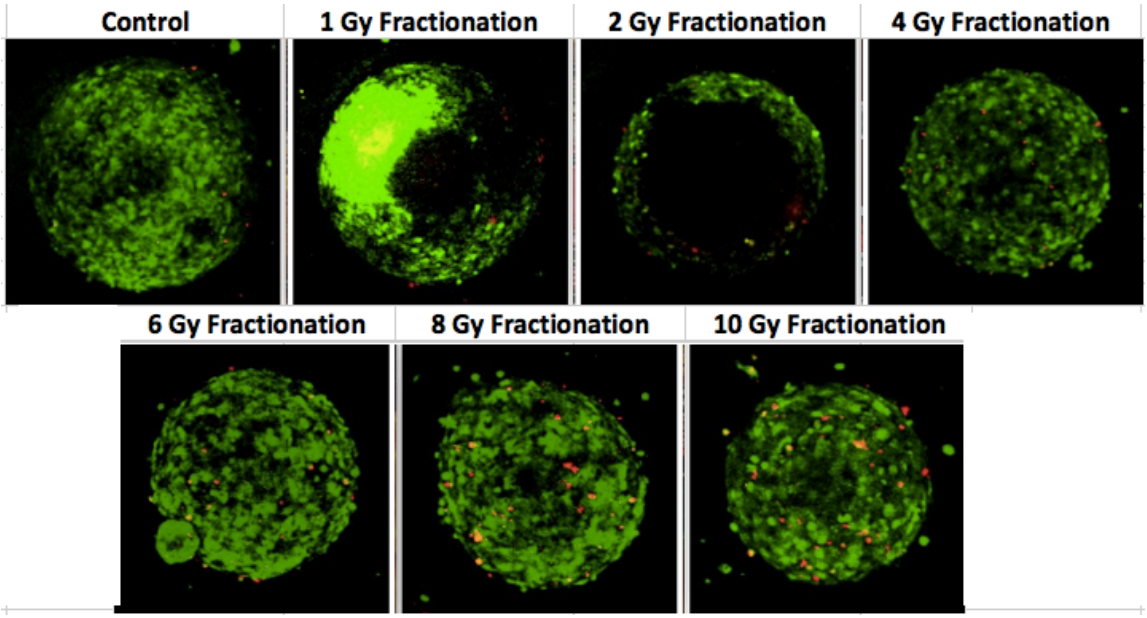

Figure 22. Live/Dead imaging of SJSA tumor spheroids post irradiation at different total absorbed doses. Live cells (green) are present throughout most of the tumor spheroid. An increase in dead cells (red) can be seen in higher dose levels. Spheroids were adjusted to display similar sizes.

Tumor spheroids did not display a fully observable necrotic region. However, stains may have not reached the center of the spheroid. Stains within the 1 Gy and 2 Gy fractionations had difficulty reaching the center of the spheroid. However, cell death can be observed clearly at higher absorbed doses. Spheroids shown in Figure 22 seem to be similar in size, however, they are adjusted to appear that way for clarity purposes. As the dose received by the spheroid increases the number of dead cells increases as well, establishing a correlation between increased dose and number of dead cells.

4.2.2. Spheroid Formation with Matrigel®

SJSA spheroids were grown in Matrigel® as a representation of the natural tumor microenvironment which increases the radioresistance of the spheroid. Tumor spheroids coated with Matrigel® were given the same radiation fractionations as the spheroids without Matrigel®. Compared to spheroids lacking Matrigel®, the spheroids with both 20% and 40% Matrigel® show increases in final volume and very radioresistant tendencies. Figure 23 shows the growth comparison of Matrigel® coated spheroids compared to non-Matrigel® spheroids.

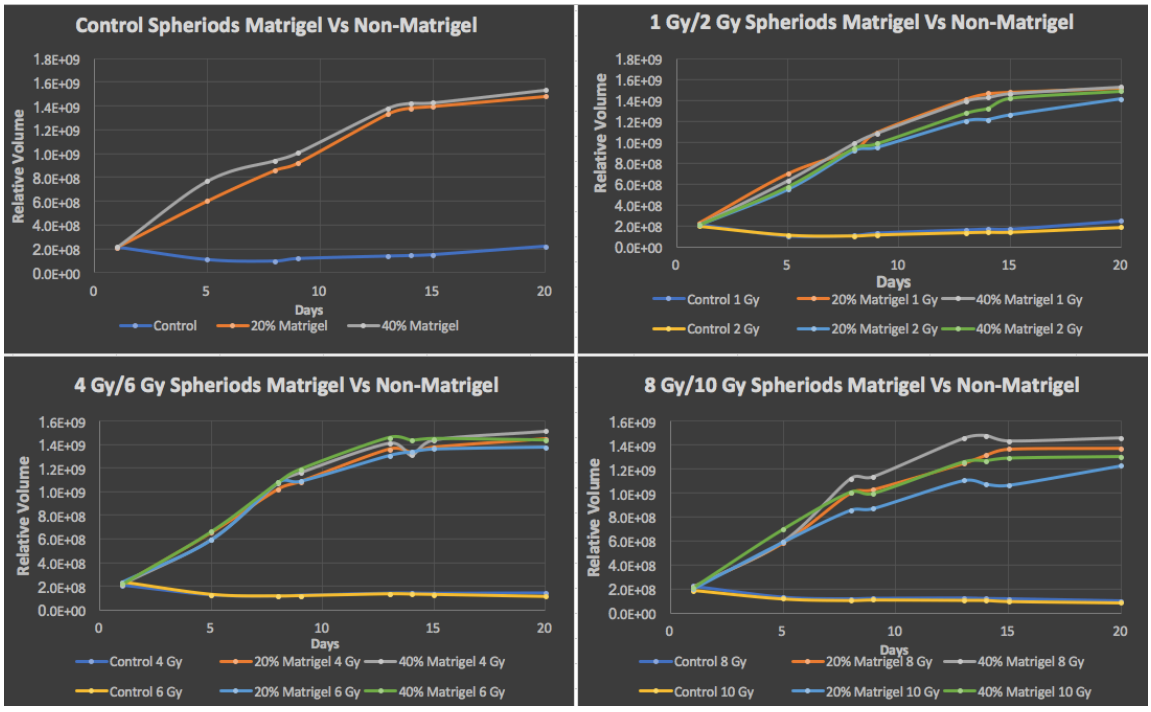

Figure 23. SJSA growth comparison of different radiation fractionations and Matrigel® concentrations (0%, 20%, and 40%). Cells within Matrigel® coated spheroids grew well past the size of spheroids without and Matrigel® (Control) regardless of the amount of radiation applied.

Growth rate was clearly altered by the presence of Matrigel® regardless of the concentration. There is clear radioresistance in spheroids grown in the presence of Matrigel®. High doses of radiation tend to limit growth of the spheroid. Growth of the dense center and invadopodia regions of the spheroid can be seen in Figure 24 and Figure 25.

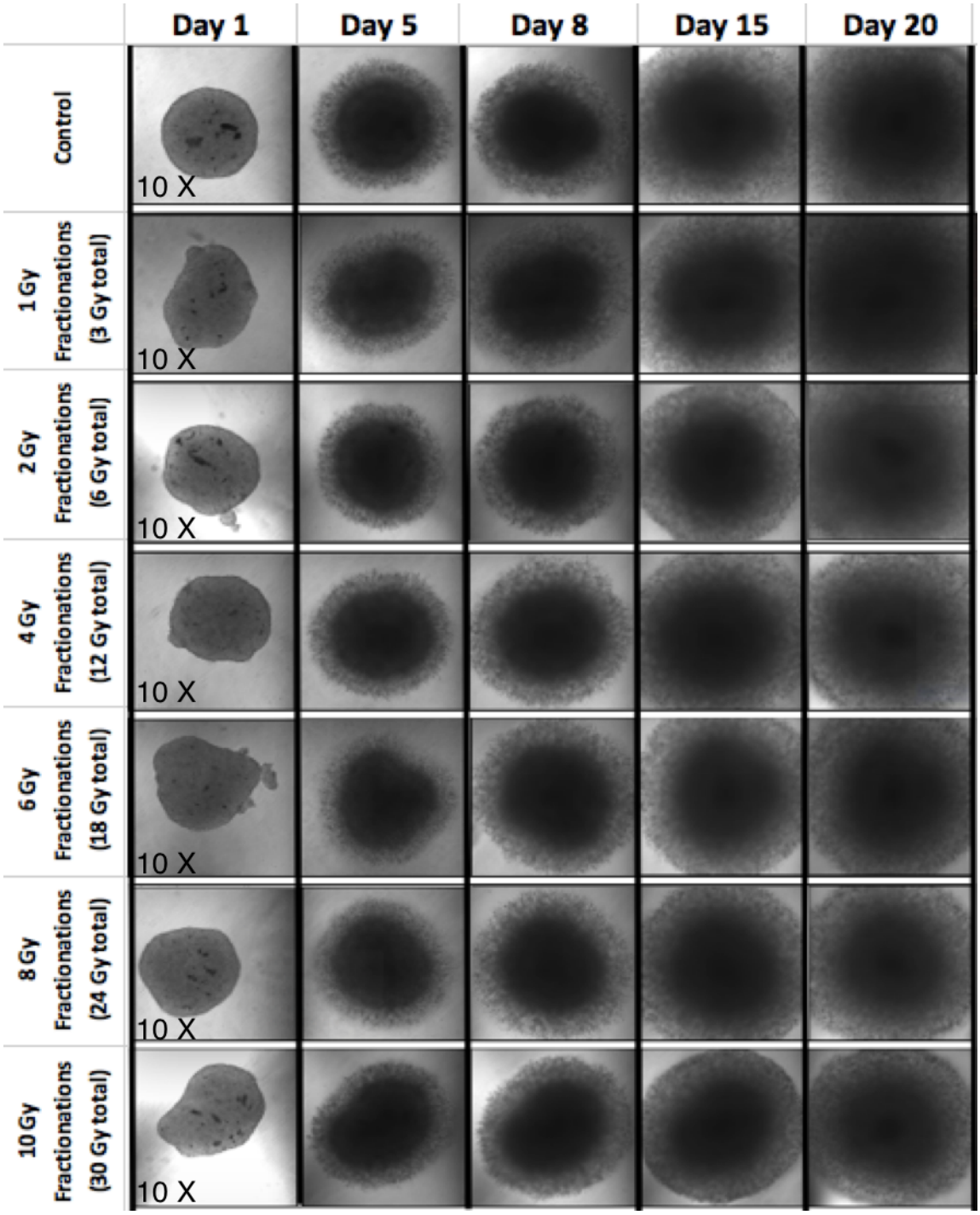

Figure 24. The growth associated with tumor spheroids coated in 20% Matrigel®. Spheroids received radiation treatments in varying dose fractionations. The microscope's field of view inhibits the ability to accurately quantify the total volume of a few spheroids.

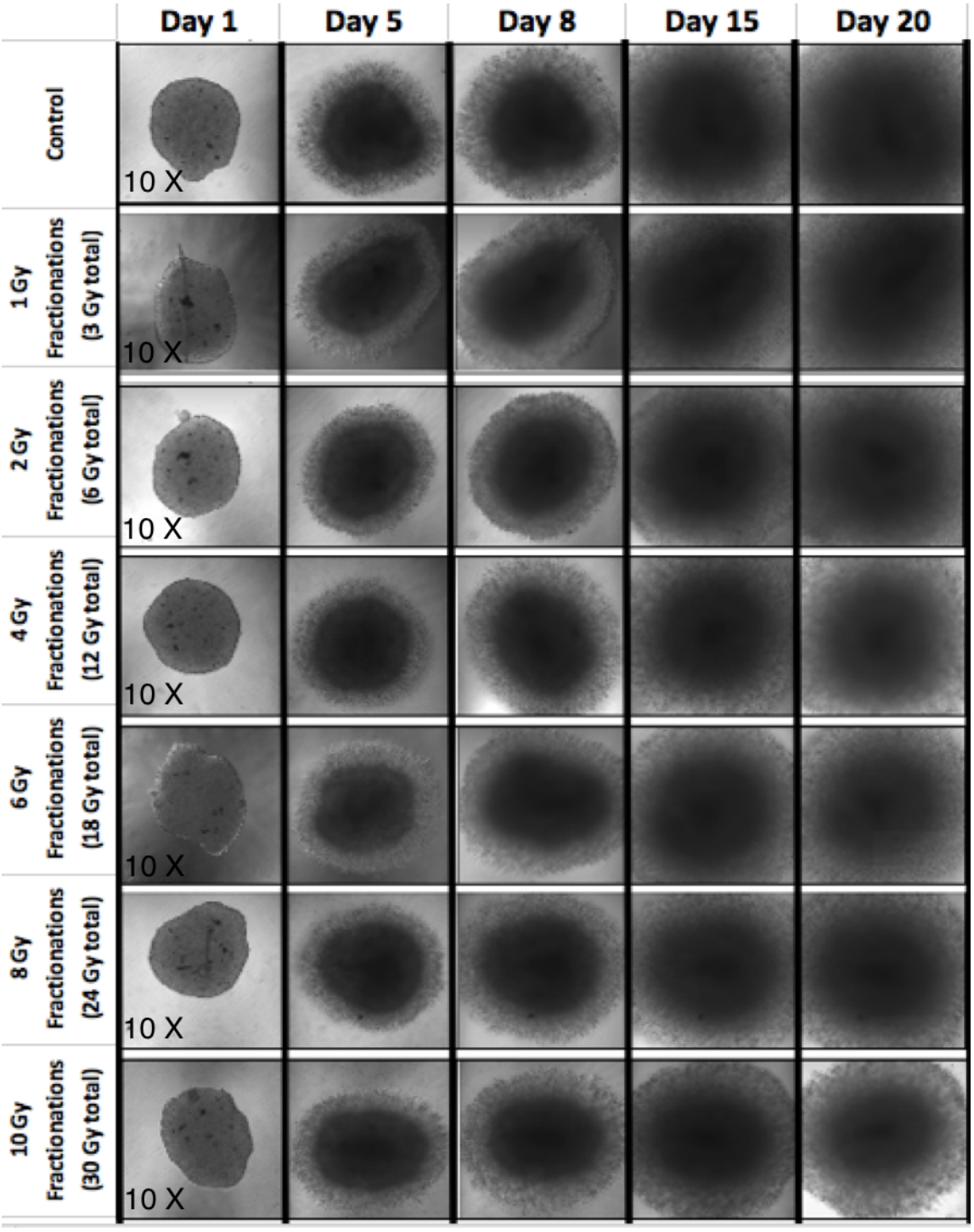

Figure 25. The growth associated with tumor spheroids coated in 20% Matrigel®. Spheroids received radiation treatments in varying dose fractionations. The microscope's field of view inhibits the ability to accurately quantify the total volume of a few spheroids.

4.2.2.1. Cellular Density and Growth

Spheroid growth becomes difficult to process once the cells grows out of visual acuity. However, clear patterns can be observed within each radiation condition. Figure 26 shows the relative volume within each radiation condition.

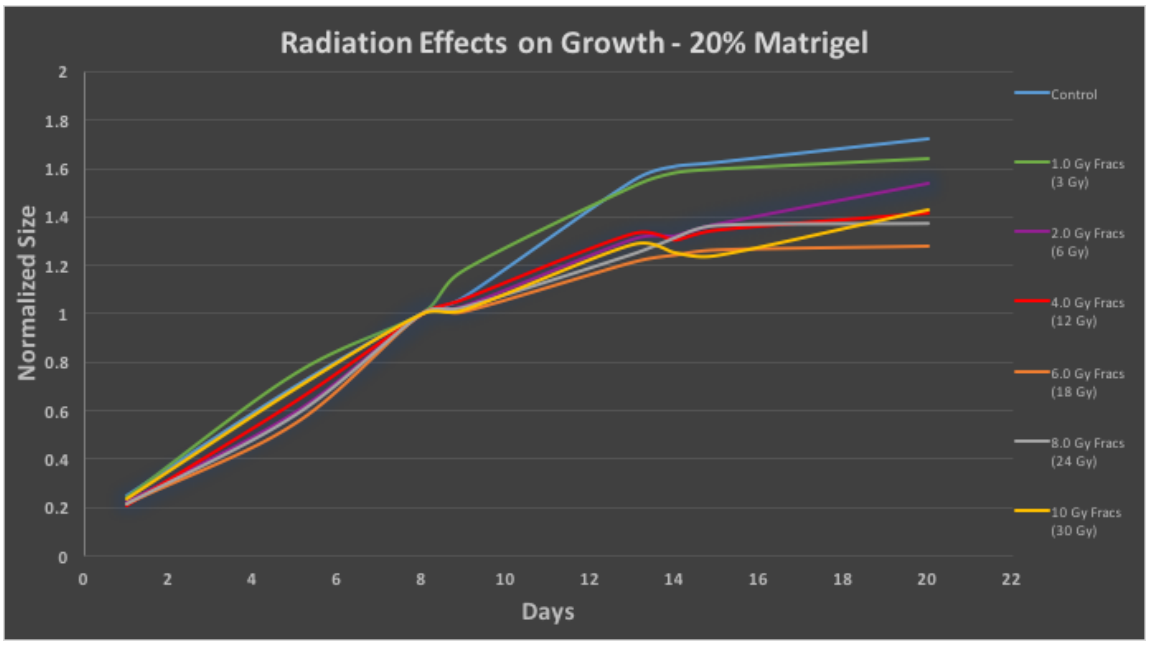

Figure 26. The total growth of SJSA spheroids containing 20% Matrigel® and varying dose fractionation. Growth is normalized to the start of irradiation (day 8). Spheroids tend to decrease in size as the fractionation dose increases.

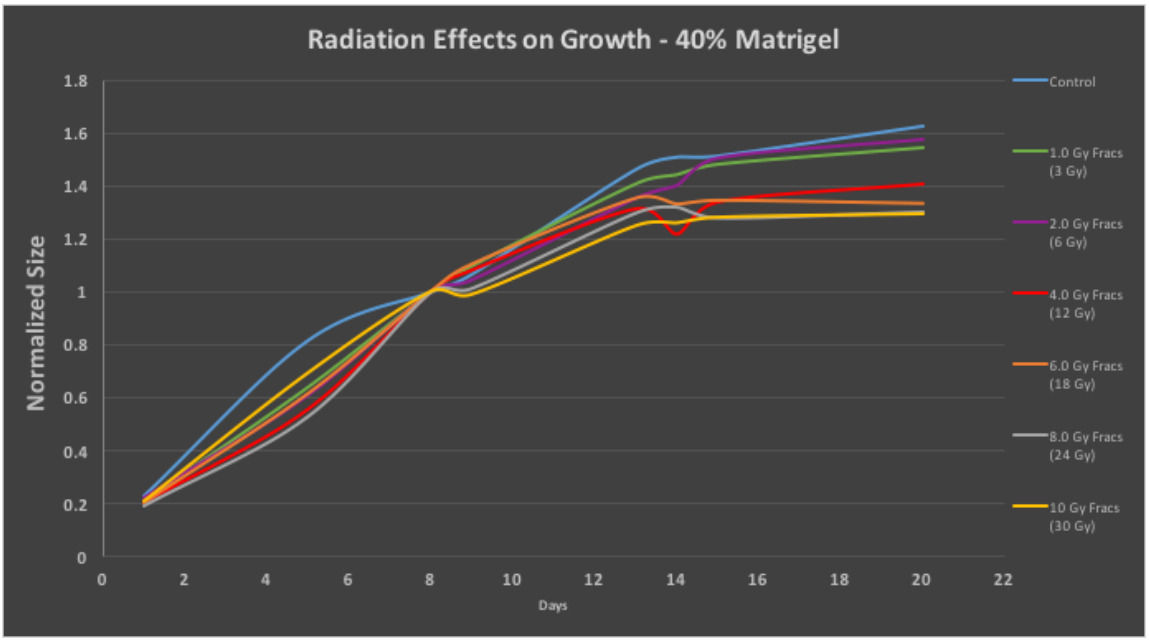

Figure 27. The total growth of SJSA spheroids containing 40% Matrigel® and varying dose fractionation. Growth is normalized to the start of irradiation (Day 8). Spheroids exhibit a gradient in which the final volume of the spheroid decreases as the amount of dose applied to the spheroid increases.

Matrigel® has a clear impact on the final volume and appearance of the spheroid. However, the concentration of Matrigel® does not play a factor in changing the radioresistance spheroids exhibit.

Spheroids coated in Matrigel® possess distinct increases in density at the center of the spheroid which can be seen in Figure 24 and Figure 25. These dense areas would not have much interaction with Matrigel®. Dense areas within spheroids follow similar growth patterns as control spheroids when subjected to radiation treatment. Figure 28-

Figure 31 outline the growth similarities between spheroids without Matrigel® and the inner dense region of spheroids which were coated in Matrigel®.

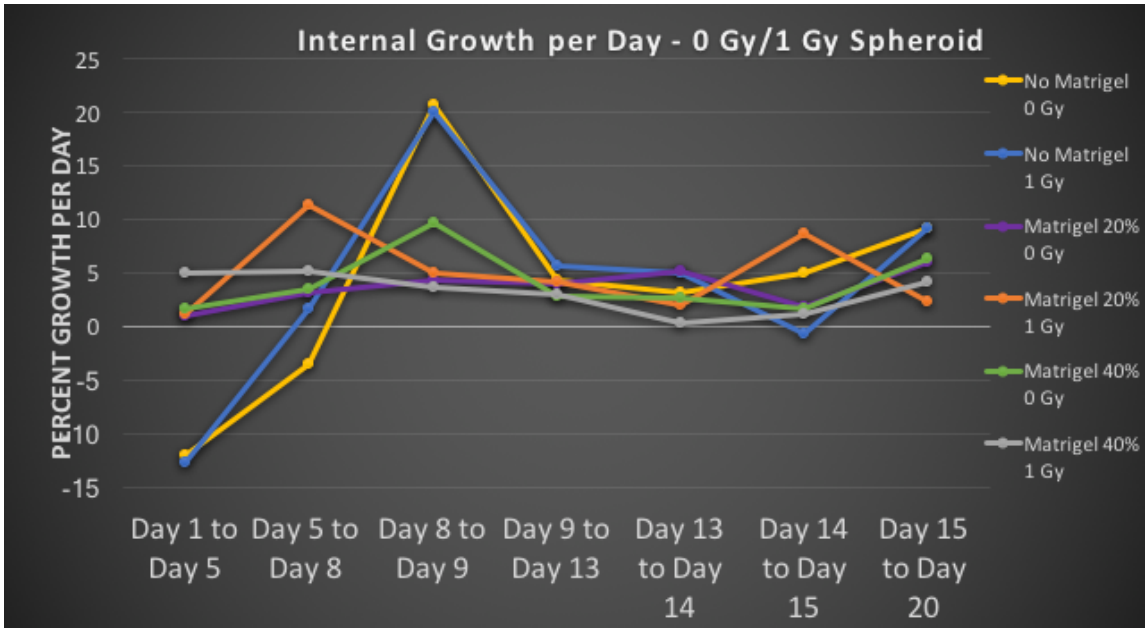

Figure 28. Radiation effects on growth between control spheroids without Matrigel® and the inner dense regions of spheroids coated in Matrigel®. Spheroids were irradiated with 0 Gy and 1 Gy fractionations.

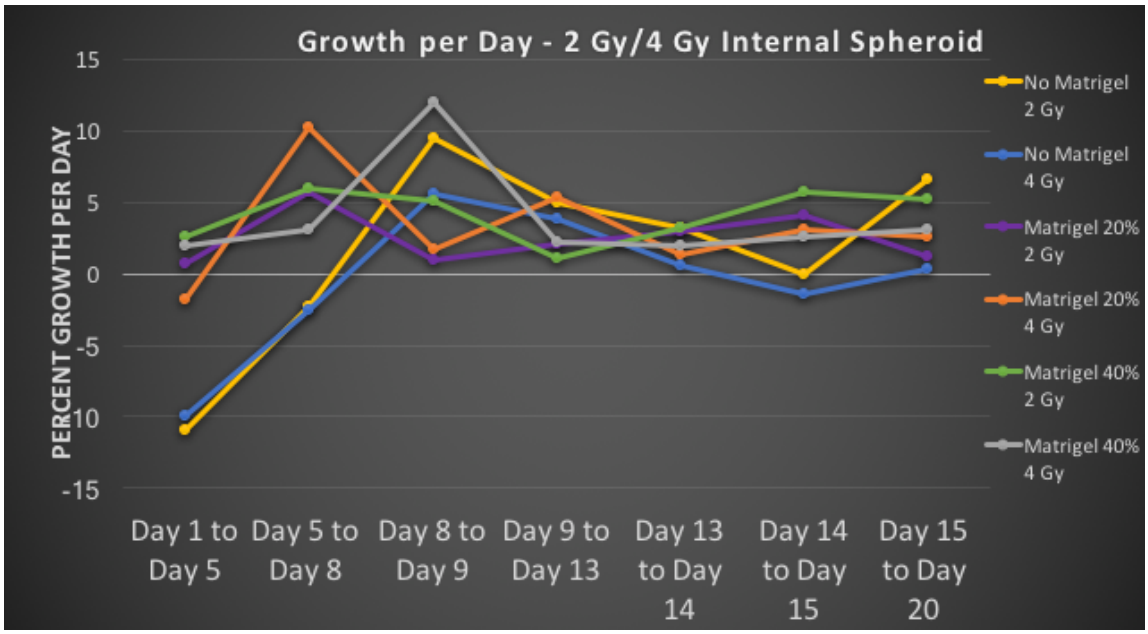

Figure 29. Radiation effects on growth between control spheroids without Matrigel® and the inner dense regions of spheroids coated in Matrigel®. Spheroids were irradiated with 2 Gy and 4 Gy fractionations.

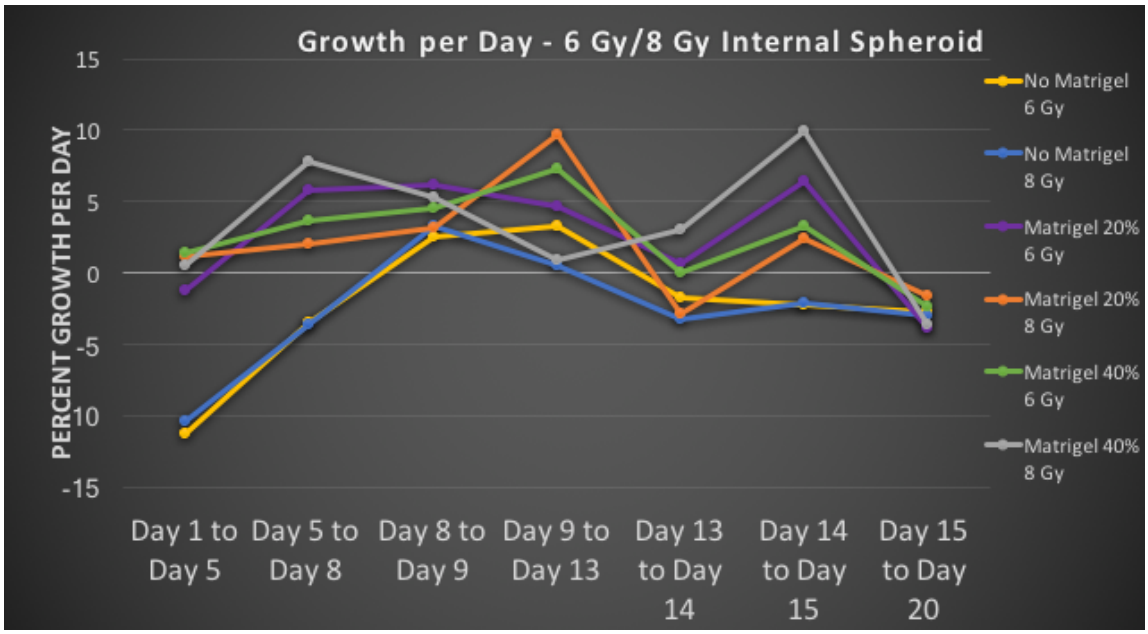

Figure 30. Radiation effects on growth between control spheroids without Matrigel® and the inner dense regions of spheroids coated in Matrigel®. Spheroids were irradiated with 6 Gy and 8 Gy fractionations.

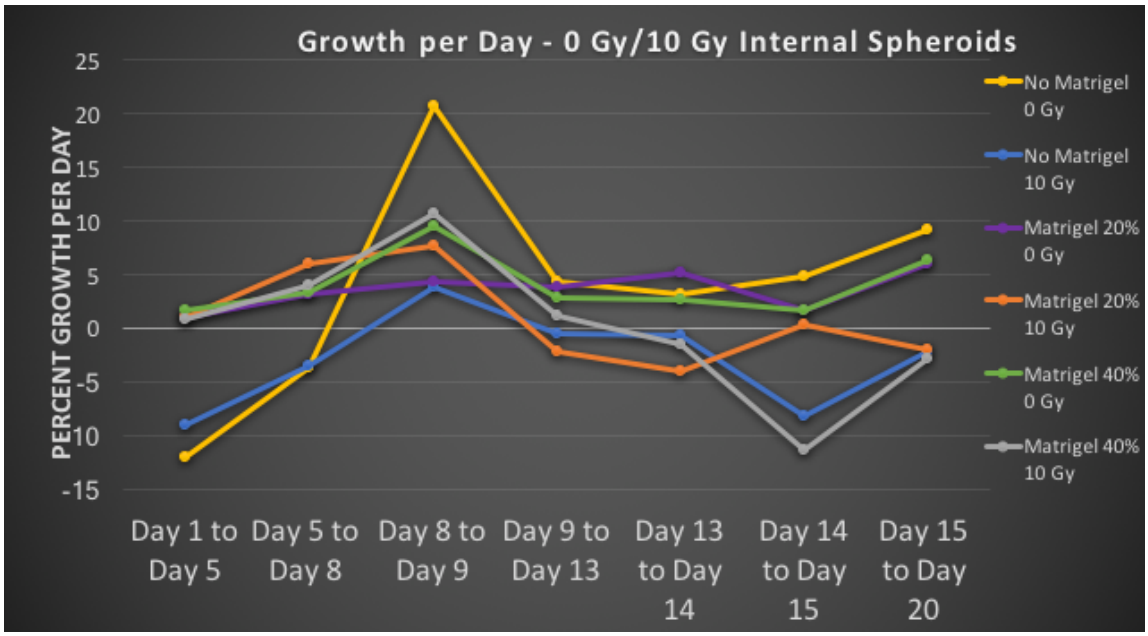

Figure 31. Radiation effects on growth between control spheroids without Matrigel® and the inner dense regions of spheroids coated in Matrigel®. Spheroids were irradiated with 0 Gy and 10 Gy fractionations.

Inner regions within spheroids coated in Matrigel® have similar growth patterns as control spheroids. Figure 28 - Figure 31 replicate the same growth patterns within the same radiation conditions as controls. Inner regions within spheroids coated in Matrigel® reduce in size as dose levels increase, similar to control spheroids. Table 5 shows the comparison of normalized sizes at day 20 between control spheroids and dense regions within Matrigel® coated spheroids.

Table 5. Comparison between normalized sizes of dense regions within Matrigel® coated spheroids compared to control spheroids lacking Matrigel®. Volumes were normalized to the day irradiation initiated (Day 8). Three fractionations occurred (Days 8, 13, and 14)

Normalized Size (Day 20)			
Fractionation Dose (Gy)	**No Matrigel®**	**20% Matrigel®**	**40% Matrigel®**
0	223%	166%	168%
1	153%	151%	142%
2	135%	125%	151%
4	120%	145%	147%
6	97%	109%	123%
8	85%	131%	102%
10	82%	85%	87%

As radiation levels increase the size of control spheroids clearly starts to decrease by day 20. Matrigel® coated spheroids demonstrate more radioresistant properties, decreases in volume only happen as the fractionation dose becomes quite large. Interactions with Matrigel® has a clear impact within the center of the tumor as well. Interactions may be morphologically noticeable only on the outside but paracrine signaling clearly increases radioresistance within the center of the tumor spheroid as well.

4.2.2.2. Invasiveness

The invasiveness of spheroids containing Matrigel® is directly linked to the amount of invadopodia growth observed. Spheroids were irradiated with total dose between 0 – 30 Gy at different dose fractionations. Figure 24 and Figure 25 demonstrate the inability to see invadopodia growth past day 8. The only expectation is growth associated with 10 Gy fractionations. Most of the invadopodia growth can still be seen due to the reduction

in volume of the dense center within the tumor. Invadopodia growth is difficult to access in images where the dense center has significantly positive growth. Positive growth within the center of the spheroid is associated with 0 Gy – 8 Gy fractionation conditions. Figure 32 and Figure 33 show progression of the invadopodia radii at various radiation levels. However, only 10 Gy conditions should be taken into account as the entire image could not be taken and various parts of the invadopodia cannot be measured.

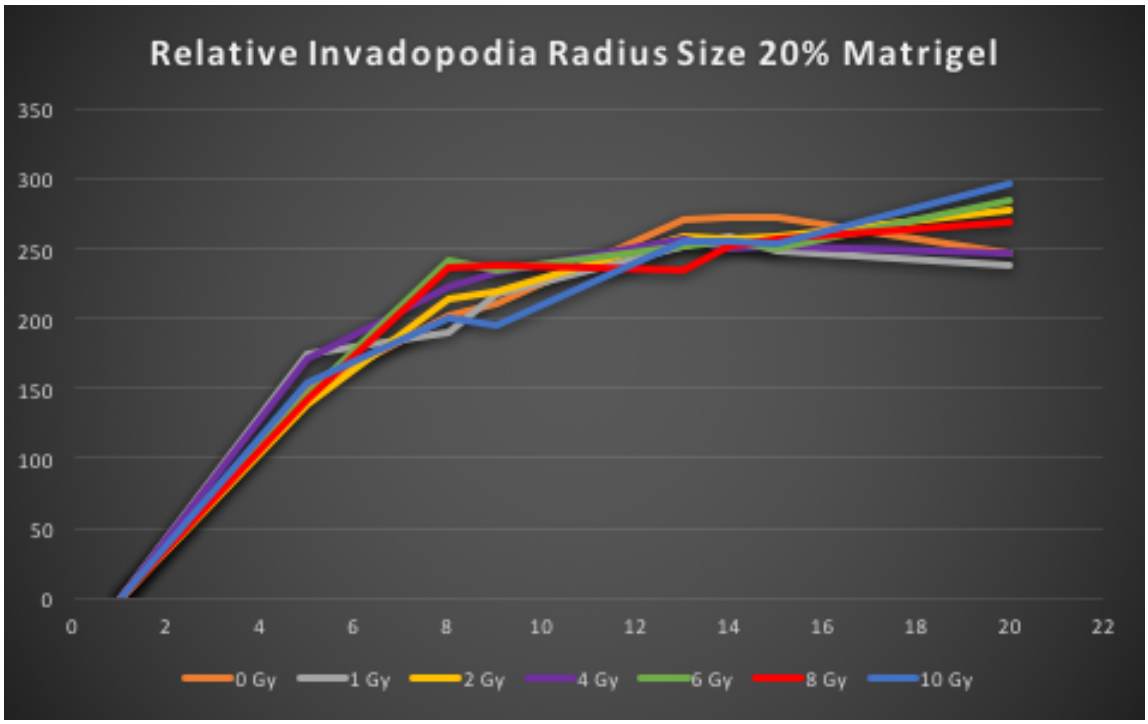

Figure 32. Shows invadopodia radii growth as a function of time for various radiation levels for spheroids coated in 20% Matrigel®. 0 Gy – 8 Gy radiation levels are slightly in accurate as the field of view for the microscope fails to capture all of the image.

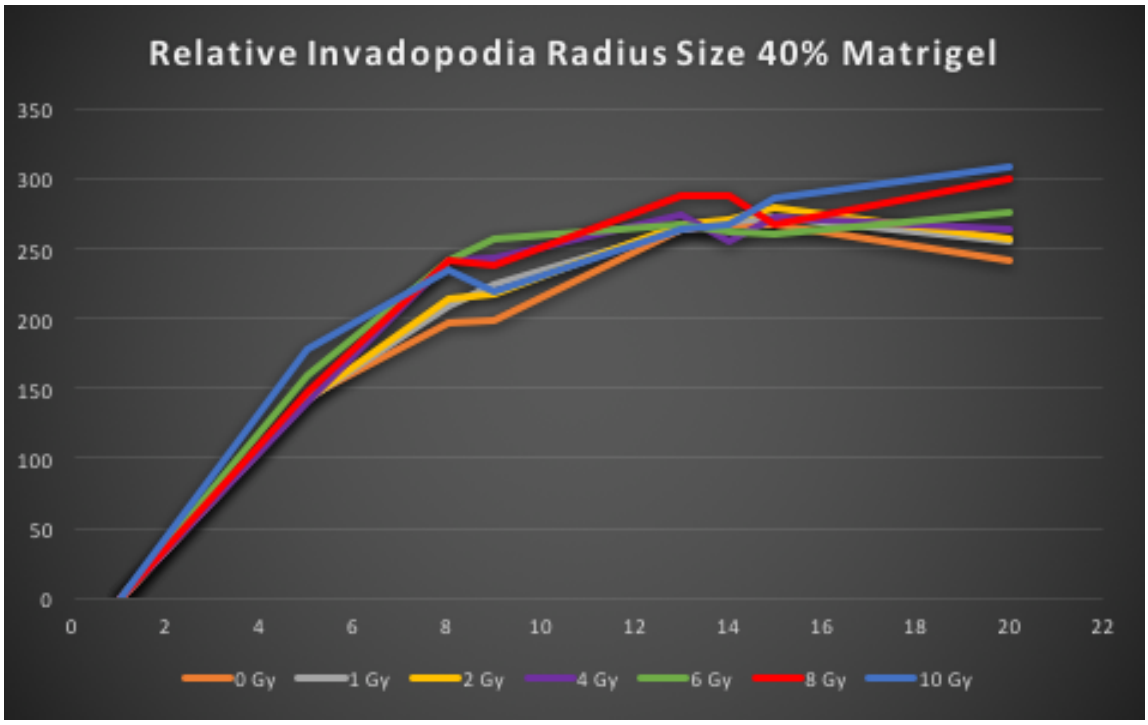

Figure 33. Shows invadopodia radii growth as a function of time for various radiation levels for spheroids coated in 40% Matrigel®. 0 Gy – 8 Gy radiation levels are slightly in accurate as the field of view for the microscope fails to capture all of the image.

The highest radiation fraction given to the tumor spheroids was 10 Gy and has shown to reduce growth in control spheroids as well as the dense center of Matrigel® coated spheroids. However, invadopodia growth remains steady in 10 Gy fractionation spheroids. This is a reflection of the radioresistant aspect of tumor spheroids coated in Matrigel®. Cells that have increased invadopodia have clearly progressed further in the oncogenic process than most. Increased resistance to treatment and morphological changes are associated with cells that are going through EMT. The addition of Matrigel®

to spheroids furthers cells down the oncogenic process by demonstrating morphological changes as well as internal changes related to increased resistant to treatment.

4.3. Protein Analysis

Spheroids coated in Matrigel® have increased resistance to treatment compared to tumor spheroids without Matrigel®. These spheroids also appear significantly further along the oncogenic process by demonstrating EMT type characteristics. Increases in resistance and EMT characteristics can be measured by a variety of protein expression. NF-κB and E-cadherin are possible proteins that demonstrate how much resistance a tumor spheroid has and how far along the oncogenic process it is.

4.3.1. NF-κB Protein Levels

NF-κB protein content is utilized for measuring pathways associated with interactions between cells and β1 integrin. Matrigel® provides a variety of ECM components including laminin which binds to integrin receptors located on the periphery of cells. In turn, upregulation of integrin receptors due to the presence of laminin creates downstream effects for NF-κB. Post irradiation NF-κB content yields indications for proteins possibly responsible for radioresistance within tumor spheroids.

4.3.1.1. Standards and Controls

Controls for NF-κB were established by samples provided within the ELISA kit. Relative quantities for NF-κB protein presence were analyzed to establish a relationship

between radioresistance and protein quantity. Control spheroids without Matrigel® were used to establish standard levels of NF-κB present within the tumor spheroid at day 24. Figure 34 outlines the differences in NF-κB levels at day 24 for various dose fractionation within tumor spheroids.

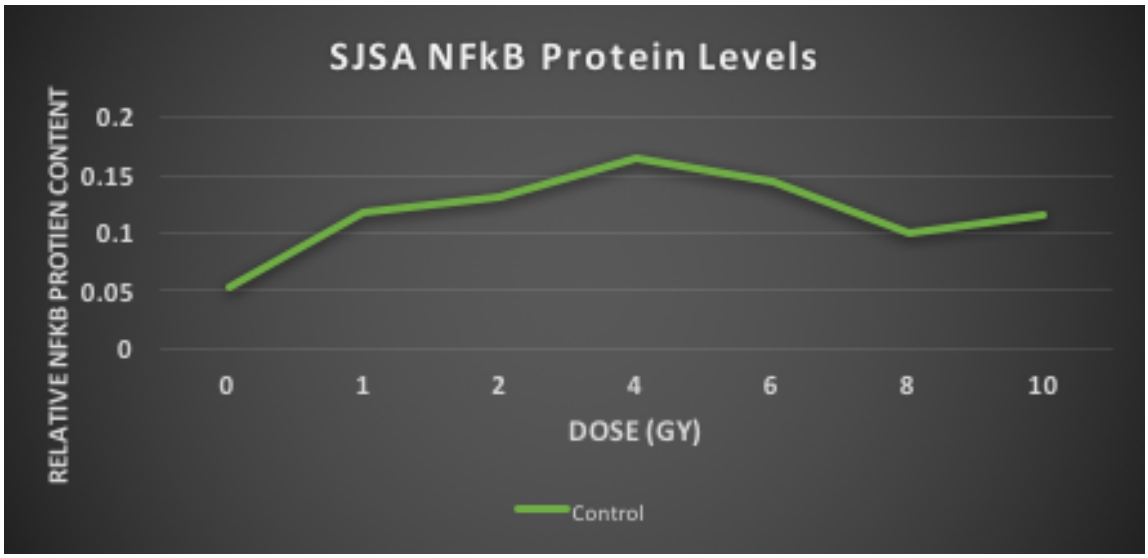

Figure 34. NF-κB protein levels within control tumor spheroids at day 24 for each dose fractionation given. Control spheroids lack Matrigel®. Increases in NF-κB protein content can be seen as the dose level increases.

Control spheroids lack Matrigel® and have little radioresistance compared to spheroids coated in Matrigel®. Control spheroids have increased NF-κB levels as the total dose given to the spheroid increased. This is primarily due to the survival pathways associated with radiation treatment.

4.3.1.2. NF-κB Levels Post Radiation

NF-κB levels present within tumor spheroids coated in Matrigel® were expected to differ drastically from control spheroids. However, Figure 35 shows only slightly elevated levels of NF-κB in Matrigel® coated spheroids. Increases were observed in 40% Matrigel® coated spheroids which indicates slight radioresistance within tumor spheroids.

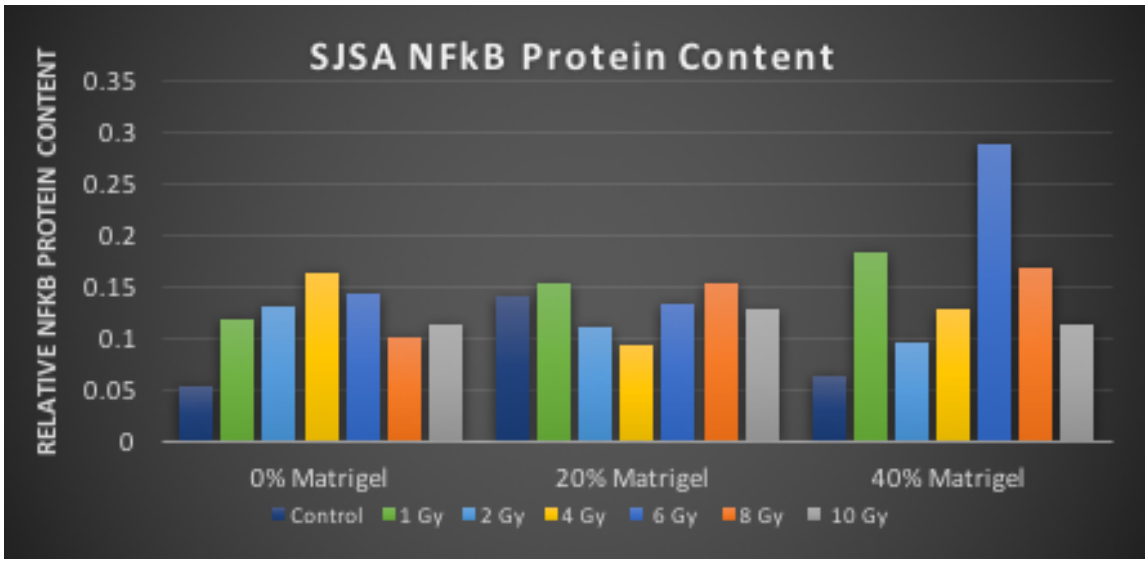

Figure 35. NF-κB levels associated with all tumor spheroids at day 24. Relative protein content associated with various dose levels and Matrigel® concentrations can be observed. Slight increases in NF-κB can be seen in 40% Matrigel® concentration.

NF-κB levels do not increase drastically as spheroids increase in radioresistance. NF-κB levels do not fluctuate with dose levels and are seemingly uncorrelated. NF-κB levels for control spheroids increase as dose fractionations approach 4 Gy then decrease as higher fractionation occur. NF-κB levels in spheroids coated in Matrigel® are highest at 1Gy, 6 Gy, and 8 Gy fractionations. High NF-κB levels at mid-range dose fractionations were expected but only seen in 1 Gy fractionation treatments. Increases in NF-κB is not likely the primary protein associated radioresistance observed in tumor spheroids with heavy ECM interactions. However, there is some indication that increased levels of NF-κB can indicate slight radioresistance as seen in spheroids with higher Matrigel® concentrations.

NF-κB levels were also measured for plates containing SKBR3 breast cancer cells. Spheroid growth analysis and E cadherin levels were not reported for SKBR3. This was due to the inability of SKBR3 cells to make spheroids and the lack of interaction between SKBR3 cells and Matrigel®. However, increases in NF-κB after treatment have been observed in breast cancer cells (Ahmed, Zhang, & Park, 2013). Figure 36 shows elevated NF-κB levels for higher dose fractionations.

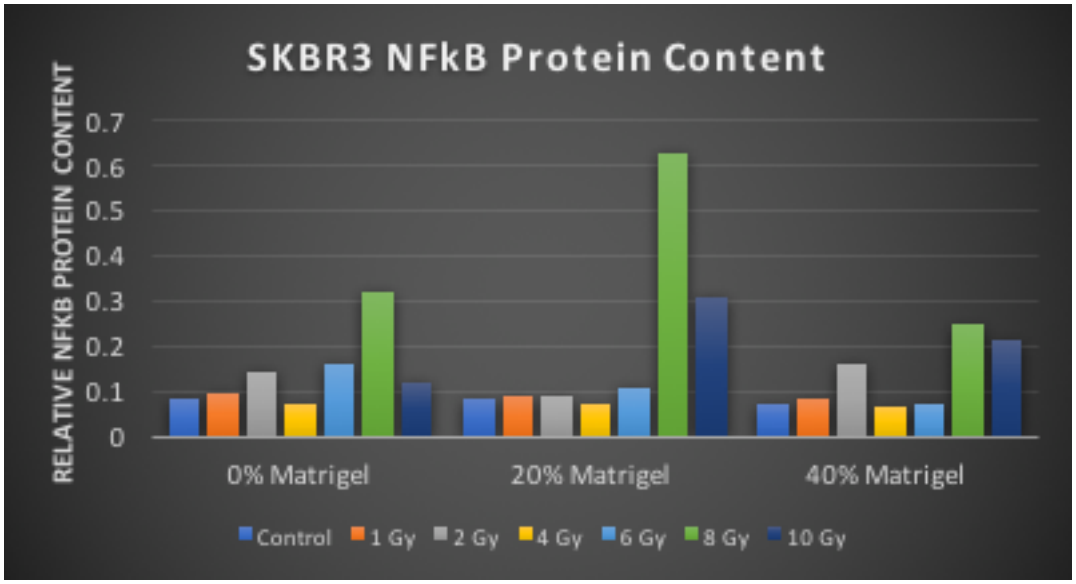

Figure 36. NF-κB levels associated with SKBR3 tumor spheroids at day 24. Relative protein content associated with various dose levels and Matrigel® concentrations can be observed. Increases in NF-κB can be seen at higher dose levels.

4.3.2. E-Cadherin Protein Presence

E-cadherin content in tumors is heavily associated with the EMT transition. Spheroids coated in Matrigel® are visually undergoing the EMT process. However, loss of E-cadherin is the main component of the EMT phenotype.

4.3.2.1. Standards and Controls

Soluble E cadherin is present only in samples that do not express an EMT phenotype. Controls were established from the ELISA kit in order to quantify E cadherin levels in tumor spheroids.

An ELISA standard curve for E cadherin can be seen in Figure 37. Seven known dilutions of E Cadherin were measured to create a standard curve. A polynomial fit was applied to obtain an equation that correlates measured florescence to E cadherin content. The final equation obtained is as follows:

$$E\ Cadherin = 5 * (\sqrt{5} * \sqrt{40000 * Florescence - 2019} - 25)$$

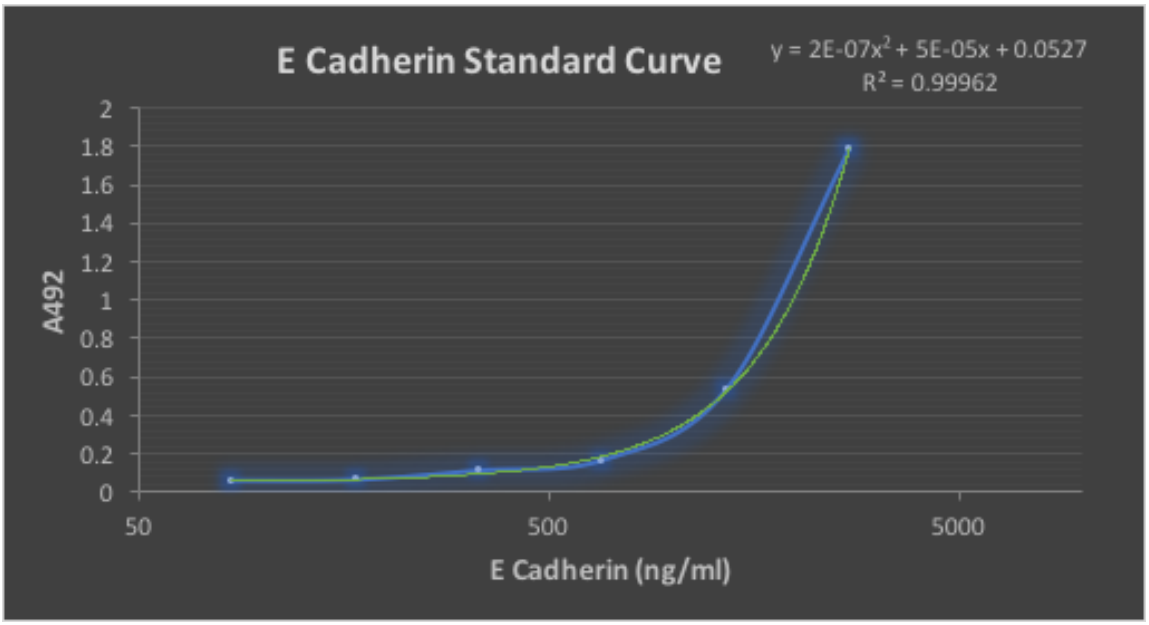

Figure 37. Standard curve for E cadherin ELISA kits. Standards were diluted to reflect a variety of measurable E-cadherin levels (2700 ng, 1350 ng, 675 ng, 338 ng, 169 ng, and 84 ng) as well as a negative control.

4.3.2.2. E-Cadherin Levels Post Radiation

E cadherin content was measured against dose levels and Matrigel® content. Figure 38 shows the E cadherin content at day 24 for all conditions. Increased E Cadherin levels

are seen in spheroids without Matrigel®. Non-Matrigel® spheroids also have decreased E cadherin content at high dose levels. Loss of E cadherin symbolizes the transition toward the EMT phenotype. Cells that express the EMT phenotype are also radioresistant. Growth studies confirm that spheroids coated in Matrigel® are more radioresistant than non-Matrigel® spheroids. Loss of E cadherin positively correlates with radioresistance in tumor spheroids.

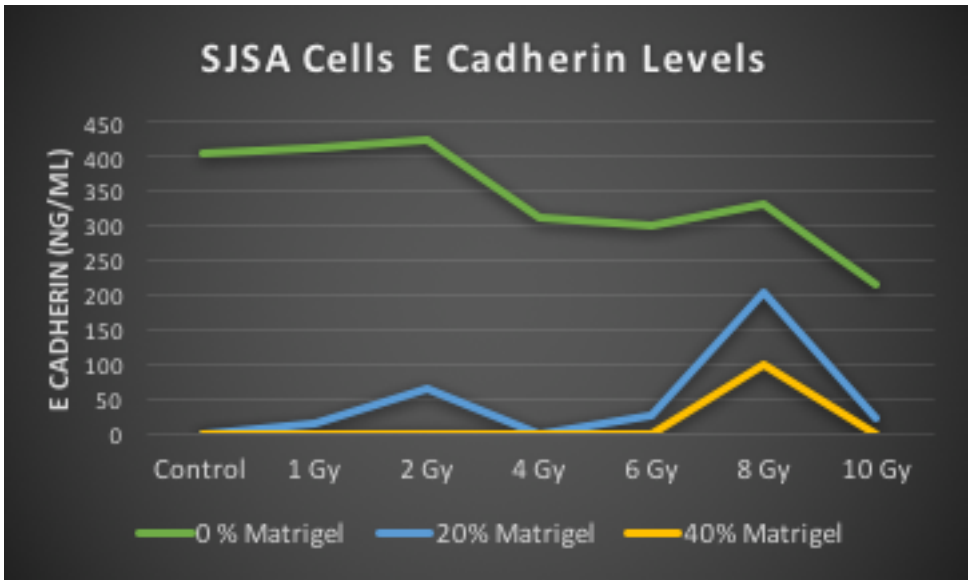

Figure 38. E Cadherin content (ng/mL) at day 24 of tumor spheroids with and without Matrigel® after radiation treatment. Clear increases in E cadherin content can be seen by non-Matrigel® spheroids.

E cadherin levels shown in Figure 38 indicate that Matrigel® coated spheroids have less E cadherin present on the surface compared to non-Matrigel® spheroids. Matrigel®

coated spheroids also exhibit a spike in E cadherin content around 8 Gy. These measurements have a substantial range and are not considered to be accurate. Figure 39, 40, and Figure 41 show the typical errors associated with each measurement in non-Matrigel® and Matrigel® spheroids for each treatment condition.

Figure 39. Error associated with E-cadherin content in non-Matrigel® spheroids given various radiation treatments. Errors are consistent throughout each fractionation level given.

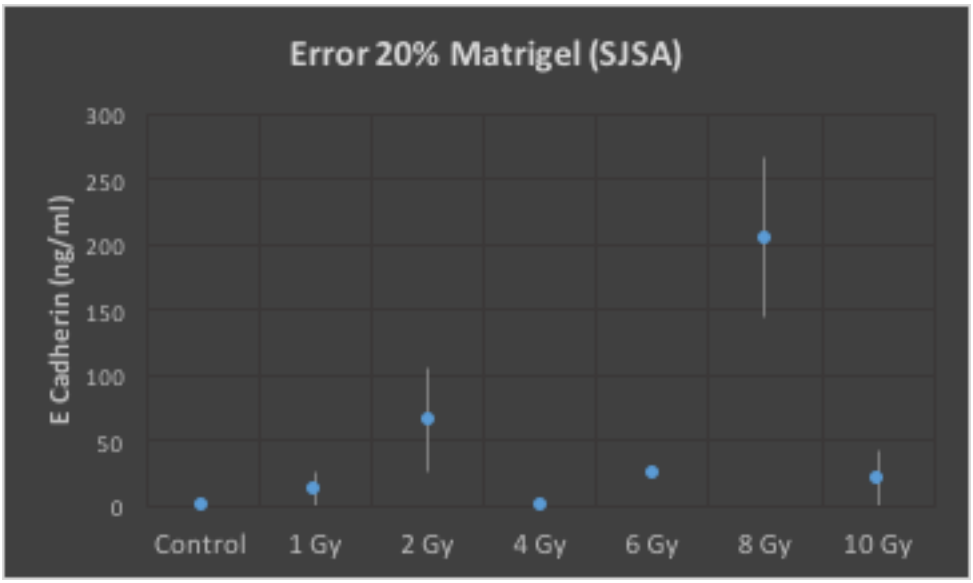

Figure 40. Error associated with E-cadherin content in spheroids coated with 20% Matrigel®. Errors are separated by the radiation fractionations given. Errors are consistent throughout each fractionation with the exception of a large error at 8 Gy.

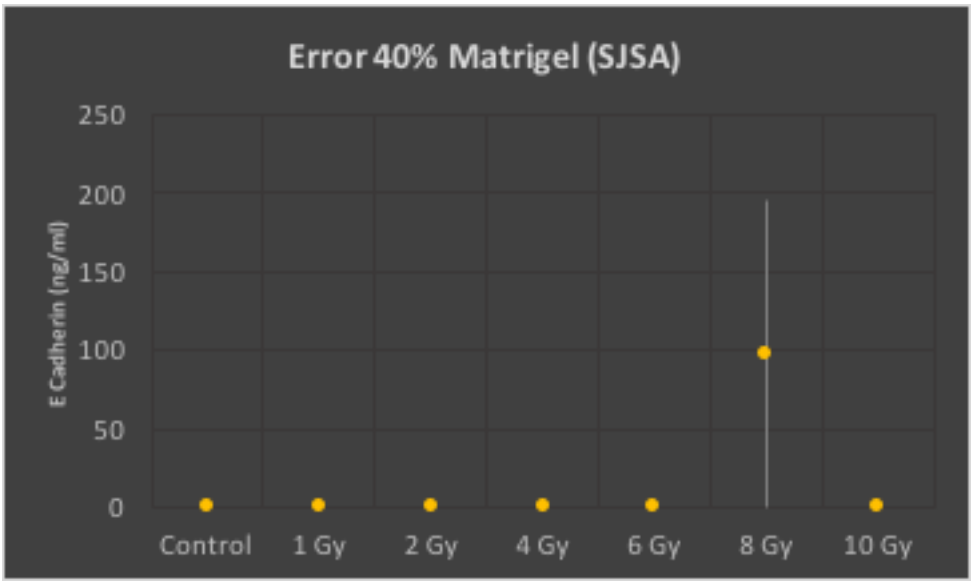

Figure 41. Error associated with E-cadherin content in spheroids coated with 20% Matrigel®. Errors are separated by the radiation fractionations given. Errors are consistent throughout each fractionation with the exception of a large error at 8 Gy.

E cadherin content ranged within 200-400 ng/mL in non-Matrigel® samples, while E cadherin content in Matrigel® coated spheroids ranged from 0-200 ng/ml. Errors bars associated with Matrigel® spheroids span over 200 ng/mL and clearly indicate the 8 Gy measurements are statistically insignificant. ELISA assays are accurate however, many procedural errors often occur. That is why samples are recommended to be done in duplicates. Overall, E cadherin content has a positive inverse correlation with radioresistance and EMT phenotype expression.

CHAPTER V

DISCUSSION

The purpose of this dissertation was to create a tumor model that replicated an environment similar to what is seen *in vivo*. A model that provides oncogenic progression through the presence of the extracellular matrix and three-dimensional structuring. This goal was to create effective and accurate testing models for cancer therapeutics. These models will identify biomarkers that can be used to help isolate and target treatment resistance cell types. These testing models enhance the efficacy of research done at the pre-clinical stage.

The goal of enhanced pre-clinical models is to replicate *in vivo* characteristics of tumors outside the host environment. The biggest concern for therapeutic testing using *in vitro* modeling is high sensitivity to all forms of treatment. *In vitro* modeling lacks a wide variety of survival pathways typically expressed in most cancers. The model proposed here reduced radiation sensitivity by the inclusion of the extracellular matrix found within tumors.

Matrigel® coated spheroids were found to be more resistant to radiation treatment than spheroids lacking Matrigel®. Matrigel® enhanced the expression of the EMT phenotype seen in late primary tumor cells. Cancer progression is directly linked to the EMT

phenotype and is not seen in spheroids where no Matrigel® is present. The EMT phenotype is associated with the morphological changes seen in tumor spheroids. The presence of invadopodia helps establish a phenotype consistent with tumor cells that are further along in oncogenesis. Tumor cells use invadopodia to break down the surrounding extracellular matrix and extend drastically past the initial spheroid boundary. These invasive characteristics are expressions based on the EMT of tumor cells. Once cells express the EMT phenotype other cellular pathways associated with EMT are active as well. This research established radiation resistance and the EMT phenotype in SJSA tumor cells by the use of Matrigel®. The presence of extracellular matrix components clearly enhances radioresistance of tumor cells by activating pathways associated with EMT.

Clinical biomarkers are currently in use for identifying cell types in a tumor that may be unaffected by radiation treatment. Some of these biomarkers include androgen receptors, NF-κB, AHSG, PAI-2, NOMO2, KLC4, YAP-1, and c-MET. Increased androgen receptor expression in patients with triple negative breast cancer was highly linked with reoccurrence after radiation treatment (Speers et al., 2017). AHSG is a potential biomarker for radioresistance seen in prostate cancer (Chang et al., 2017). PAI-2, NOMO2, and KLC4 are used in identification of radioresistant cells in lung cancer (Yun et al., 2016). NF-κB was identified as a biomarker/target for silencing to reduce radioresistance in osteosarcoma cells (Zuch et al., 2012). Combination of YAP-1 and c-MET are used to identify squamous cell carcinoma (head and neck) (Akervall et al.,

2014). Generalized biomarkers, that apply to most cancer to identify radioresistance have been theorized, these include TGF-β and IL-6 (Centurione & Aiello, 2016).

NF-κB has been established as a biomarker for radioresistance in osteosarcoma cells (Eliseev et al., 2005). NF-κB has also been used as a biomarker as an indicator of radioresistance in laryngeal cancer (Yoshida et al., 2010). The relation of NF-κB levels and radioresistance is well documented in specific cancer types. This research did not observe a strong correlation between increases in NF-κB levels as absorbed dose increased in SJSA cell lines. However, there were some indications that increased levels of NF-κB were present after radiation was given. NF-κB levels in spheroids without Matrigel® are lowest without IR. Once irradiated NF-κB levels in spheroids without Matrigel® are slightly elevated at all dose levels. Resistance to treatment is seen in conditions where Matrigel® is coated around the spheroid. With the exception of 4 Gy fractionations (12 Gy total), NF-κB levels are generally higher in spheroids coated in Matrigel®. This research observed that in SKBR3 cell lines, NF-κB levels were drastically increased at higher radiation doses. This researched confirm that NF-κB could be used as a biomarker to indicate resistance to radiation. However, from this research data suggests that NF-κB levels as an indicator of radioresistance heavily depend on cell type. The suggestion that the tumor ECM contributes to greater activation of NF-κB levels does not correlate with the data recorded. This suggests that NF-κB

levels are kept high once cellular stress signals have been received by the cell regardless of interactions from the extracellular matrix.

E cadherin levels have been studied alongside radioresistance in the form of cellular transformation. E cadherin loss is widely used as a measure of oncogenic progression and EMT. E cadherin as a biomarker for radioresistance has been utilized for patients with cervical cancer and esophageal squamous cell carcinoma (Da, Wu, Liu, Wang, & Li, 2017; Kilic, Cracchiolo, Gabel, Haffty, & Mahmoud, 2015; Zhang, Liu, Zhao, Hou, & Huang, 2014). However, many studies regarding biomarkers are conducted in a clinical setting. Finding from this research indicate that the inclusion of Matrigel® in three-dimensional spheroids allows for phenotypical changes associated with EMT and radioresistance. This research also indicates that spheroids coated in Matrigel® are significantly more radioresistant. These spheroids have little to no levels of E cadherin. An analysis of Matrigel® coated spheroids found that E cadherin loss correlates with radioresistance in spheroids. E cadherin loss was guided by the presence of Matrigel®, therefore ECM contributions to radioresistance through E cadherin seem significant. Therefore, E cadherin levels become a prime candidate for indications of radioresistance prior to and post radiation treatment.

The goal of this research was to apply therapeutic analysis on testing a modality that simulated the complexity seen in *in vivo* tumors. A correlation between resistance and known biomarkers such as NF-κB and E cadherin, confirmed the use of 3D spheroids

coated in Matrigel® as a strong testing modality. Future research should build upon the inclusion of the ECM and mimic more components of the natural tumor environment. Inclusion of components such as fibroblast many increase the resistance to treatment seen in heterogeneous tumors. These studies will shed light on the mechanisms guiding treatment resistance that is seen *in vivo*. Other promising routes for this testing modality will be the use of patient derived tumor cells to populate tumor growth *ex vivo*. The added components of the tumor microenvironment will help facilitate growth and model tumor response to treatment. This application in the field of personalized medicine has the potential for direct clinical applicability. Patient derived tumor spheroid models should be used as a prerequisite for more advanced treatment models such as patient derived xenographs.

This research model aimed to encompass many cell types. However, the data presented here shows that the inclusion of the extracellular matrix does not assist some cell types in forming spheroids. The nature of some cell lines is such that they do not form spheroids in culture often. This research model aimed to help provide structural extracellular matrix support and help induce spheroid formation. Cell lines such as SKBR3 have not formed spheroids in other culture systems (Manuel Iglesias et al., 2013). The necessary support provided by the extracellular matrix did not help formation of SKBR3 tumor spheroids. This cell line was used to see the applicability of this research model across various cell lines and confirmed that SKBR3 cells do not form spheroids even with extracellular matrix support. The research model presented

here works for a limited number of cell types. Future work may establish a list of cell types that spheroids formation will occur in. Future work should reduce the seeding concentration of each well to approximately 1k cells/well. This adjustment will ensure that the growth of each spheroid will not pass the field of view for a 10x microscope. Lower cell concentrations will also result in higher impacts associated with treatment response. Lastly, this model can be used in conjunction with three-dimensional assays which monitor cell growth over time. This quantitative measurement can be used with volumetric data to help establish tumor growth with a high efficacy. This model has the potential for inclusion of various components of the tumor microenvironment. This model should eventually include cancer associated fibroblast to determine their impact on treatment resistance.

CHAPTER VI

CONCLUSIONS

There is great potential for the application of three-dimensional modeling involving all the components of the tumor microenvironment. Current culture systems simply lack the ability to accurately reflect and incorporate the necessary aspects of oncogenesis. A variety of aspects influence tumor progression and have the ability to increase efficacy of *in vitro* studies.

This research aimed to establish a testing modality that integrated the tumor extracellular matrix into spheroid culture with ease. The testing modality aimed to confirmed the protein levels of well-known biomarkers, NF-κB and E cadherin, as a tool to verify phenotypical changes associated with radioresistance. This was accomplished by coating spheroids with Matrigel® and exposing spheroids to radiation therapy. These studies confirm results seen in clinical studies relating loss of E cadherin and the EMT phenotype to radioresistance. Although results for NF-κB levels in SJSA osteosarcoma cells did not follow many correlations seen in osteosarcoma patients, NF-κB levels for SKBR3 breast cancer cells mimicked clinical studies. The successful inclusion of the extracellular matrix in therapeutic studies yielded radiation responses similar to those seen in clinical studies.

REFERENCES

Ahmed, K. M., Zhang, H., & Park, C. C. (2013). NF-kappaB regulates radioresistance mediated by beta1-integrin in three-dimensional culture of breast cancer cells. *Cancer Res, 73*(12), 3737-3748. doi:10.1158/0008-5472.CAN-12-3537

AJCC cancer staging manual. (2016). New York, NY: Springer Science+Business Media.

Akervall, J., Nandalur, S., Zhang, J., Qian, C. N., Goldstein, N., Gyllerup, P., . . . Teh, B. (2014). A novel panel of biomarkers predicts radioresistance in patients with squamous cell carcinoma of the head and neck. *Eur J Cancer, 50*(3), 570-581. doi:10.1016/j.ejca.2013.11.007

Allan, A. L. (2011). *Cancer stem cells in solid tumors*. New York: Humana Press.

Allavena, P., Sica, A., Solinas, G., Porta, C., & Mantovani, A. (2008). The inflammatory micro-environment in tumor progression: the role of tumor-associated macrophages. *Crit Rev Oncol Hematol, 66*(1), 1-9. doi:10.1016/j.critrevonc.2007.07.004

Asghar, W., El Assal, R., Shafiee, H., Pitteri, S., Paulmurugan, R., & Demirci, U. (2015). Engineering cancer microenvironments for in vitro 3-D tumor models. *Mater Today (Kidlington), 18*(10), 539-553. doi:10.1016/j.mattod.2015.05.002

Bao, S., Wu, Q., McLendon, R. E., Hao, Y., Shi, Q., Hjelmeland, A. B., . . . Rich, J. N. (2006). Glioma stem cells promote radioresistance by preferential activation of the DNA damage response. *Nature, 444*(7120), 756-760. doi:10.1038/nature05236

Barkan, D., Green, J. E., & Chambers, A. F. (2010). Extracellular matrix: a gatekeeper in the transition from dormancy to metastatic growth. *Eur J Cancer, 46*(7), 1181-1188. doi:10.1016/j.ejca.2010.02.027

Behrens, J., Mareel, M. M., Van Roy, F. M., & Birchmeier, W. (1989). Dissecting tumor cell invasion: epithelial cells acquire invasive properties after the loss of uvomorulin-mediated cell-cell adhesion. *J Cell Biol, 108*(6), 2435-2447.

Bhowmick, N. A., Neilson, E. G., & Moses, H. L. (2004). Stromal fibroblasts in cancer initiation and progression. *Nature, 432*(7015), 332-337. doi:10.1038/nature03096

Bignon, M., Pichol-Thievend, C., Hardouin, J., Malbouyres, M., Brechot, N., Nasciutti, L., . . . Germain, S. (2011). Lysyl oxidase-like protein-2 regulates sprouting angiogenesis and type IV collagen assembly in the endothelial basement membrane. *Blood, 118*(14), 3979-3989. doi:10.1182/blood-2010-10-313296

Blonska, M., You, Y., Geleziunas, R., & Lin, X. (2004). Restoration of NF-kappaB activation by tumor necrosis factor alpha receptor complex-targeted MEKK3 in receptor-interacting protein-deficient cells. *Mol Cell Biol, 24*(24), 10757-10765. doi:10.1128/MCB.24.24.10757-10765.2004

Bolgen, S. C. a. N. (2016). A review in three dimensional scaffolds for tumor engineeing *Biomaterials and Biomechanics in Bioengineering, 3*(3), 141-155.

Bonnans, C., Chou, J., & Werb, Z. (2014). Remodelling the extracellular matrix in development and disease. *Nat Rev Mol Cell Biol, 15*(12), 786-801. doi:10.1038/nrm3904

Brach, M. A., Hass, R., Sherman, M. L., Gunji, H., Weichselbaum, R., & Kufe, D. (1991). Ionizing radiation induces expression and binding activity of the nuclear factor kappa B. *J Clin Invest, 88*(2), 691-695. doi:10.1172/JCI115354

Buck, E., Eyzaguirre, A., Barr, S., Thompson, S., Sennello, R., Young, D., . . . Haley, J. D. (2007). Loss of homotypic cell adhesion by epithelial-mesenchymal transition or mutation limits sensitivity to epidermal growth factor receptor inhibition. *Mol Cancer Ther, 6*(2), 532-541. doi:10.1158/1535-7163.MCT-06-0462

Bunt, S. K., Clements, V. K., Hanson, E. M., Sinha, P., & Ostrand-Rosenberg, S. (2009). Inflammation enhances myeloid-derived suppressor cell cross-talk by signaling through Toll-like receptor 4. *J Leukoc Biol, 85*(6), 996-1004. doi:10.1189/jlb.0708446

Butcher, N. J., Arulpragasam, A., & Minchin, R. F. (2004). Proteasomal degradation of N-acetyltransferase 1 is prevented by acetylation of the active site cysteine: a mechanism for the slow acetylator phenotype and substrate-dependent down-regulation. *J Biol Chem, 279*(21), 22131-22137. doi:10.1074/jbc.M312858200

Cavo, M., Fato, M., Penuela, L., Beltrame, F., Raiteri, R., & Scaglione, S. (2016). Microenvironment complexity and matrix stiffness regulate breast cancer cell activity in a 3D in vitro model. *Sci Rep, 6*, 35367. doi:10.1038/srep35367

Centurione, L., & Aiello, F. B. (2016). DNA Repair and Cytokines: TGF-beta, IL-6, and Thrombopoietin as Different Biomarkers of Radioresistance. *Front Oncol, 6*, 175. doi:10.3389/fonc.2016.00175

Chang, L., Ni, J., Beretov, J., Wasinger, V. C., Hao, J., Bucci, J., . . . Li, Y. (2017). Identification of protein biomarkers and signaling pathways associated with prostate cancer radioresistance using label-free LC-MS/MS proteomic approach. *Sci Rep, 7*, 41834. doi:10.1038/srep41834

Charbe, N., McCarron, P. A., & Tambuwala, M. M. (2017). Three-dimensional bio-printing: A new frontier in oncology research. *World J Clin Oncol, 8*(1), 21-36. doi:10.5306/wjco.v8.i1.21

Chiang, S. P., Cabrera, R. M., & Segall, J. E. (2016). Tumor cell intravasation. *Am J Physiol Cell Physiol, 311*(1), C1-C14. doi:10.1152/ajpcell.00238.2015

Cho, R. W., & Clarke, M. F. (2008). Recent advances in cancer stem cells. *Curr Opin Genet Dev, 18*(1), 48-53. doi:10.1016/j.gde.2008.01.017

Da, C., Wu, L., Liu, Y., Wang, R., & Li, R. (2017). Effects of irradiation on radioresistance, HOTAIR and epithelial-mesenchymal transition/cancer stem cell marker expression in esophageal squamous cell carcinoma. *Oncology Letters, 13*(4), 2751-2757. doi:10.3892/ol.2017.5774

Dai, X., Ma, C., Lan, Q., & Xu, T. (2016). 3D bioprinted glioma stem cells for brain tumor model and applications of drug susceptibility. *Biofabrication, 8*(4), 045005. doi:10.1088/1758-5090/8/4/045005

Dangerfield, J., Larbi, K. Y., Huang, M. T., Dewar, A., & Nourshargh, S. (2002). PECAM-1 (CD31) homophilic interaction up-regulates alpha6beta1 on transmigrated neutrophils in vivo and plays a functional role in the ability of alpha6 integrins to mediate leukocyte migration through the perivascular basement membrane. *J Exp Med, 196*(9), 1201-1211.

De Palma, M., & Hanahan, D. (2012). The biology of personalized cancer medicine: facing individual complexities underlying hallmark capabilities. *Mol Oncol, 6*(2), 111-127. doi:10.1016/j.molonc.2012.01.011

de Visser, K. E., & Coussens, L. M. (2006). The inflammatory tumor microenvironment and its impact on cancer development. *Contrib Microbiol, 13*, 118-137. doi:10.1159/000092969

Deonarain, M. P., Kousparou, C. A., & Epenetos, A. A. (2009). Antibodies targeting cancer stem cells: a new paradigm in immunotherapy? *MAbs, 1*(1), 12-25.

Dick, J. E., Bhatia, M., Gan, O., Kapp, U., & Wang, J. C. (1997). Assay of human stem cells by repopulation of NOD/SCID mice. *Stem Cells, 15 Suppl 1*, 199-203; discussion 204-197. doi:10.1002/stem.5530150826

Edmondson, R., Broglie, J. J., Adcock, A. F., & Yang, L. (2014). Three-dimensional cell culture systems and their applications in drug discovery and cell-based biosensors. *Assay Drug Dev Technol, 12*(4), 207-218. doi:10.1089/adt.2014.573

Egeblad, M., Nakasone, E. S., & Werb, Z. (2010). Tumors as organs: complex tissues that interface with the entire organism. *Dev Cell, 18*(6), 884-901. doi:10.1016/j.devcel.2010.05.012

Eliseev, R. A., Zuscik, M. J., Schwarz, E. M., O'Keefe, R. J., Drissi, H., & Rosier, R. N. (2005). Increased radiation-induced apoptosis of Saos2 cells via inhibition of NFkappaB: a role for c-Jun N-terminal kinase. *J Cell Biochem, 96*(6), 1262-1273. doi:10.1002/jcb.20607

Erez, N., Truitt, M., Olson, P., Arron, S. T., & Hanahan, D. (2010). Cancer-Associated Fibroblasts Are Activated in Incipient Neoplasia to Orchestrate Tumor-Promoting Inflammation in an NF-kappaB-Dependent Manner. *Cancer Cell, 17*(2), 135-147. doi:10.1016/j.ccr.2009.12.041

Fernandez-Medarde, A., & Santos, E. (2011). Ras in cancer and developmental diseases. *Genes Cancer, 2*(3), 344-358. doi:10.1177/1947601911411084

Ferrara, N. (2010). Pathways mediating VEGF-independent tumor angiogenesis. *Cytokine Growth Factor Rev, 21*(1), 21-26. doi:10.1016/j.cytogfr.2009.11.003

Florczyk, S. J., Wang, K., Jana, S., Wood, D. L., Sytsma, S. K., Sham, J., . . . Zhang, M. (2013). Porous chitosan-hyaluronic acid scaffolds as a mimic of glioblastoma microenvironment ECM. *Biomaterials, 34*(38), 10143-10150. doi:10.1016/j.biomaterials.2013.09.034

Fong, E. L., Lamhamedi-Cherradi, S. E., Burdett, E., Ramamoorthy, V., Lazar, A. J., Kasper, F. K., . . . Ludwig, J. A. (2013). Modeling Ewing sarcoma tumors in vitro with 3D scaffolds. *Proc Natl Acad Sci U S A, 110*(16), 6500-6505. doi:10.1073/pnas.1221403110

Giacinti, C., & Giordano, A. (2006). RB and cell cycle progression. *Oncogene, 25*(38), 5220-5227. doi:10.1038/sj.onc.1209615

Giussani, M., Merlino, G., Cappelletti, V., Tagliabue, E., & Daidone, M. G. (2015). Tumor-extracellular matrix interactions: Identification of tools associated with breast cancer progression. *Semin Cancer Biol, 35*, 3-10. doi:10.1016/j.semcancer.2015.09.012

Gottlieb, T. M., & Oren, M. (1996). p53 in growth control and neoplasia. *Biochim Biophys Acta, 1287*(2-3), 77-102.

Gupta, G. P., Minn, A. J., Kang, Y., Siegel, P. M., Serganova, I., Cordon-Cardo, C., . . . Massague, J. (2005). Identifying site-specific metastasis genes and functions. *Cold Spring Harb Symp Quant Biol, 70*, 149-158. doi:10.1101/sqb.2005.70.018

Gupta, P. B., Onder, T. T., Jiang, G., Tao, K., Kuperwasser, C., Weinberg, R. A., & Lander, E. S. (2009). Identification of selective inhibitors of cancer stem cells by high-throughput screening. *Cell, 138*(4), 645-659. doi:10.1016/j.cell.2009.06.034

Hanahan, D., & Folkman, J. (1996). Patterns and emerging mechanisms of the angiogenic switch during tumorigenesis. *Cell, 86*(3), 353-364.

Hanahan, D., & Weinberg, R. A. (2011). Hallmarks of cancer: the next generation. *Cell, 144*(5), 646-674. doi:10.1016/j.cell.2011.02.013

He, Q., Wang, X., Zhang, X., Han, H., Han, B., Xu, J., . . . Yin, H. (2013). A tissue-engineered subcutaneous pancreatic cancer model for antitumor drug evaluation. *Int J Nanomedicine, 8*, 1167-1176. doi:10.2147/IJN.S42464

Hermann, P. C., Huber, S. L., Herrler, T., Aicher, A., Ellwart, J. W., Guba, M., . . . Heeschen, C. (2007). Distinct populations of cancer stem cells determine tumor growth and metastatic activity in human pancreatic cancer. *Cell Stem Cell, 1*(3), 313-323. doi:10.1016/j.stem.2007.06.002

Hielscher, A., & Gerecht, S. (2015). Hypoxia and free radicals: role in tumor progression and the use of engineering-based platforms to address these relationships. *Free Radic Biol Med, 79*, 281-291. doi:10.1016/j.freeradbiomed.2014.09.015

Hollstein, M., Sidransky, D., Vogelstein, B., & Harris, C. C. (1991). p53 mutations in human cancers. *Science, 253*(5015), 49-53.

Huang, T. Q., Qu, X., Liu, J., & Chen, S. (2014). 3D printing of biomimetic microstructures for cancer cell migration. *Biomed Microdevices, 16*(1), 127-132. doi:10.1007/s10544-013-9812-6

Huang, Z., & Bao, S. D. (2004). Roles of main pro- and anti-angiogenic factors in tumor angiogenesis. *World J Gastroenterol, 10*(4), 463-470.

Insua-Rodriguez, J., & Oskarsson, T. (2016). The extracellular matrix in breast cancer. *Adv Drug Deliv Rev, 97*, 41-55. doi:10.1016/j.addr.2015.12.017

Jones, P. A., & Baylin, S. B. (2002). The fundamental role of epigenetic events in cancer. *Nat Rev Genet, 3*(6), 415-428. doi:10.1038/nrg816

Joyce, J. A., & Pollard, J. W. (2009). Microenvironmental regulation of metastasis. *Nat Rev Cancer, 9*(4), 239-252. doi:10.1038/nrc2618

Kalluri, R., & Weinberg, R. A. (2009). The basics of epithelial-mesenchymal transition. *J Clin Invest, 119*(6), 1420-1428. doi:10.1172/JCI39104

Kalluri, R., & Zeisberg, M. (2006). Fibroblasts in cancer. *Nat Rev Cancer, 6*(5), 392-401. doi:10.1038/nrc1877

Kandalaft, L. E., Motz, G. T., Duraiswamy, J., & Coukos, G. (2011). Tumor immune surveillance and ovarian cancer: lessons on immune mediated tumor rejection or tolerance. *Cancer Metastasis Rev, 30*(1), 141-151. doi:10.1007/s10555-011-9289-9

Kang, Y., & Pantel, K. (2013). Tumor cell dissemination: emerging biological insights from animal models and cancer patients. *Cancer Cell, 23*(5), 573-581. doi:10.1016/j.ccr.2013.04.017

Kilic, S., Cracchiolo, B., Gabel, M., Haffty, B., & Mahmoud, O. (2015). The relevance of molecular biomarkers in cervical cancer patients treated with radiotherapy. *Ann Transl Med, 3*(18), 261. doi:10.3978/j.issn.2305-5839.2015.10.18

Knowlton, S., Onal, S., Yu, C. H., Zhao, J. J., & Tasoglu, S. (2015). Bioprinting for cancer research. *Trends Biotechnol, 33*(9), 504-513. doi:10.1016/j.tibtech.2015.06.007

Korkaya, H., Liu, S., & Wicha, M. S. (2011). Breast cancer stem cells, cytokine networks, and the tumor microenvironment. *J Clin Invest, 121*(10), 3804-3809. doi:10.1172/JCI57099

Kyjacova, L., Hubackova, S., Krejcikova, K., Strauss, R., Hanzlikova, H., Dzijak, R., . . . Hodny, Z. (2015). Radiotherapy-induced plasticity of prostate cancer mobilizes stem-like non-adherent, Erk signaling-dependent cells. *Cell Death Differ, 22*(6), 898-911. doi:10.1038/cdd.2014.97

Lee, G. Y., Kenny, P. A., Lee, E. H., & Bissell, M. J. (2007). Three-dimensional culture models of normal and malignant breast epithelial cells. *Nat Methods, 4*(4), 359-365. doi:10.1038/nmeth1015

Lee, S. Y., Lee, S. Y., & Choi, Y. (1997). TRAF-interacting protein (TRIP): a novel component of the tumor necrosis factor receptor (TNFR)- and CD30-TRAF signaling complexes that inhibits TRAF2-mediated NF-kappaB activation. *J Exp Med, 185*(7), 1275-1285.

Li, F., & Sethi, G. (2010). Targeting transcription factor NF-kappaB to overcome chemoresistance and radioresistance in cancer therapy. *Biochim Biophys Acta, 1805*(2), 167-180. doi:10.1016/j.bbcan.2010.01.002

Ling, K., Huang, G., Liu, J., Zhang, X., Ma, Y., Lu, T., & Xu, F. (2015). *Bioprinting-Based High-Throughput Fabrication of Three-Dimensional MCF-7 Human Breast Cancer Cellular Spheroids* (Vol. 1).

Liu, J. A., Wu, M. H., Yan, C. H., Chau, B. K., So, H., Ng, A., . . . Cheung, M. (2013). Phosphorylation of Sox9 is required for neural crest delamination and is regulated downstream of BMP and canonical Wnt signaling. *Proc Natl Acad Sci U S A, 110*(8), 2882-2887. doi:10.1073/pnas.1211747110

Lotfi, R., Kaltenmeier, C., Lotze, M. T., & Bergmann, C. (2016). Until Death Do Us Part: Necrosis and Oxidation Promote the Tumor Microenvironment. *Transfus Med Hemother, 43*(2), 120-132. doi:10.1159/000444941

Loupakis, F., Bocci, G., Pasqualetti, G., Fornaro, L., Salvatore, L., Cremolini, C., . . . Falcone, A. (2010). Targeting vascular endothelial growth factor pathway in first-line treatment of metastatic colorectal cancer: state-of-the-art and future perspectives in clinical and molecular selection of patients. *Curr Cancer Drug Targets, 10*(1), 37-45.

Lu, P., Weaver, V. M., & Werb, Z. (2012). The extracellular matrix: a dynamic niche in cancer progression. *J Cell Biol, 196*(4), 395-406. doi:10.1083/jcb.201102147

Lu, T., Li, Y., & Chen, T. (2013). Techniques for fabrication and construction of three-dimensional scaffolds for tissue engineering. *Int J Nanomedicine, 8*, 337-350. doi:10.2147/IJN.S38635

Lu, W. D., Zhang, L., Wu, C. L., Liu, Z. G., Lei, G. Y., Liu, J., . . . Hu, Y. R. (2014). Development of an acellular tumor extracellular matrix as a three-dimensional

scaffold for tumor engineering. *PLoS One, 9*(7), e103672. doi:10.1371/journal.pone.0103672

Mak, I. W., Evaniew, N., & Ghert, M. (2014). Lost in translation: animal models and clinical trials in cancer treatment. *Am J Transl Res, 6*(2), 114-118.

Manuel Iglesias, J., Beloqui, I., Garcia-Garcia, F., Leis, O., Vazquez-Martin, A., Eguiara, A., . . . Martin, A. G. (2013). Mammosphere formation in breast carcinoma cell lines depends upon expression of E-cadherin. *PLoS One, 8*(10), e77281. doi:10.1371/journal.pone.0077281

McDonald, D. M., & Baluk, P. (2005). Imaging of angiogenesis in inflamed airways and tumors: newly formed blood vessels are not alike and may be wildly abnormal: Parker B. Francis lecture. *Chest, 128*(6 Suppl), 602S-608S. doi:10.1378/chest.128.6_suppl.602S-a

Moncharmont, C., Levy, A., Gilormini, M., Bertrand, G., Chargari, C., Alphonse, G., . . . Magne, N. (2012). Targeting a cornerstone of radiation resistance: cancer stem cell. *Cancer Lett, 322*(2), 139-147. doi:10.1016/j.canlet.2012.03.024

Mott, J. D., & Werb, Z. (2004). Regulation of matrix biology by matrix metalloproteinases. *Curr Opin Cell Biol, 16*(5), 558-564. doi:10.1016/j.ceb.2004.07.010

Olive, K. P., Jacobetz, M. A., Davidson, C. J., Gopinathan, A., McIntyre, D., Honess, D., . . . Tuveson, D. A. (2009). Inhibition of Hedgehog signaling enhances delivery of chemotherapy in a mouse model of pancreatic cancer. *Science, 324*(5933), 1457-1461. doi:10.1126/science.1171362

Orimo, A., Gupta, P. B., Sgroi, D. C., Arenzana-Seisdedos, F., Delaunay, T., Naeem, R., . . . Weinberg, R. A. (2005). Stromal fibroblasts present in invasive human breast carcinomas promote tumor growth and angiogenesis through elevated SDF-1/CXCL12 secretion. *Cell, 121*(3), 335-348. doi:10.1016/j.cell.2005.02.034

Orlowski, R. Z., & Baldwin, A. S., Jr. (2002). NF-kappaB as a therapeutic target in cancer. *Trends Mol Med, 8*(8), 385-389.

Pahler, J. C., Tazzyman, S., Erez, N., Chen, Y. Y., Murdoch, C., Nozawa, H., . . . Hanahan, D. (2008). Plasticity in tumor-promoting inflammation: impairment of macrophage recruitment evokes a compensatory neutrophil response. *Neoplasia, 10*(4), 329-340.

Pajonk, F., Vlashi, E., & McBride, W. H. (2010). Radiation resistance of cancer stem cells: the 4 R's of radiobiology revisited. *Stem Cells, 28*(4), 639-648. doi:10.1002/stem.318

Palermo, C., & Joyce, J. A. (2008). Cysteine cathepsin proteases as pharmacological targets in cancer. *Trends Pharmacol Sci, 29*(1), 22-28. doi:10.1016/j.tips.2007.10.011

Palomeras, S., Rabionet, M., Ferrer, I., Sarrats, A., Garcia-Romeu, M. L., Puig, T., & Ciurana, J. (2016). Breast Cancer Stem Cell Culture and Enrichment Using Poly(epsilon-Caprolactone) Scaffolds. *Molecules, 21*(4), 537. doi:10.3390/molecules21040537

Parekh, A., & Weaver, A. M. (2009). Regulation of cancer invasiveness by the physical extracellular matrix environment. *Cell Adh Migr, 3*(3), 288-292.

Paz, H., Pathak, N., & Yang, J. (2014). Invading one step at a time: the role of invadopodia in tumor metastasis. *Oncogene, 33*(33), 4193-4202. doi:10.1038/onc.2013.393

Peggs, K. S., Quezada, S. A., & Allison, J. P. (2009). Cancer immunotherapy: co-stimulatory agonists and co-inhibitory antagonists. *Clin Exp Immunol, 157*(1), 9-19. doi:10.1111/j.1365-2249.2009.03912.x

Phillips, J. E., Petrie, T. A., Creighton, F. P., & Garcia, A. J. (2010). Human mesenchymal stem cell differentiation on self-assembled monolayers presenting different surface chemistries. *Acta Biomater, 6*(1), 12-20. doi:10.1016/j.actbio.2009.07.023

Pradella, D., Naro, C., Sette, C., & Ghigna, C. (2017). EMT and stemness: flexible processes tuned by alternative splicing in development and cancer progression. *Mol Cancer, 16*(1), 8. doi:10.1186/s12943-016-0579-2

Prasad, V. (2018). Immunotherapy: Tisagenlecleucel - the first approved CAR-T-cell therapy: implications for payers and policy makers. *Nat Rev Clin Oncol, 15*(1), 11-12. doi:10.1038/nrclinonc.2017.156

Qian, B. Z., & Pollard, J. W. (2010). Macrophage diversity enhances tumor progression and metastasis. *Cell, 141*(1), 39-51. doi:10.1016/j.cell.2010.03.014

Raynaud, C. M., Hernandez, J., Llorca, F. P., Nuciforo, P., Mathieu, M. C., Commo, F., . . . Soria, J. C. (2010). DNA damage repair and telomere length in normal breast, preneoplastic lesions, and invasive cancer. *Am J Clin Oncol, 33*(4), 341-345. doi:10.1097/COC.0b013e3181b0c4c2

Retsky, M. W., Demicheli, R., Hrushesky, W. J., Baum, M., & Gukas, I. D. (2008). Dormancy and surgery-driven escape from dormancy help explain some clinical features of breast cancer. *APMIS, 116*(7-8), 730-741. doi:10.1111/j.1600-0463.2008.00990.x

Ruffell, B., DeNardo, D. G., Affara, N. I., & Coussens, L. M. (2010). Lymphocytes in cancer development: polarization towards pro-tumor immunity. *Cytokine Growth Factor Rev, 21*(1), 3-10. doi:10.1016/j.cytogfr.2009.11.002

Samavedi, S., & Joy, N. (2017). 3D printing for the development of in vitro cancer models. *Current Opinion in Biomedical Engineering, 2*(Supplement C), 35-42. doi:https://doi.org/10.1016/j.cobme.2017.06.003

Sanders, C. L. (2017). *Radiobiology and Radiation Hormesis* (1 ed.): Springer International Publishing.

Sepulveda, A., & Buchanan, E. P. (2014). Vascular tumors. *Semin Plast Surg, 28*(2), 49-57. doi:10.1055/s-0034-1376260

Serrano-Gomez, S. J., Maziveyi, M., & Alahari, S. K. (2016). Regulation of epithelial-mesenchymal transition through epigenetic and post-translational modifications. *Mol Cancer, 15*, 18. doi:10.1186/s12943-016-0502-x

Singh, A., & Settleman, J. (2010). EMT, cancer stem cells and drug resistance: an emerging axis of evil in the war on cancer. *Oncogene, 29*(34), 4741-4751. doi:10.1038/onc.2010.215

Soman, P., Kelber, J. A., Lee, J. W., Wright, T. N., Vecchio, K. S., Klemke, R. L., & Chen, S. (2012). Cancer cell migration within 3D layer-by-layer microfabricated photocrosslinked PEG scaffolds with tunable stiffness. *Biomaterials, 33*(29), 7064-7070. doi:10.1016/j.biomaterials.2012.06.012

Speers, C., Zhao, S. G., Chandler, B., Liu, M., Wilder-Romans, K., Olsen, E., . . . Feng, F. Y. (2017). Androgen receptor as a mediator and biomarker of radioresistance in triple-negative breast cancer. *NPJ Breast Cancer, 3*, 29. doi:10.1038/s41523-017-0038-2

Stanton, M. M., Samitier, J., & Sanchez, S. (2015). Bioprinting of 3D hydrogels. *Lab Chip, 15*(15), 3111-3115. doi:10.1039/c5lc90069g

Theys, J., Jutten, B., Habets, R., Paesmans, K., Groot, A. J., Lambin, P., . . . Vooijs, M. (2011). E-Cadherin loss associated with EMT promotes radioresistance in human tumor cells. *Radiother Oncol, 99*(3), 392-397. doi:10.1016/j.radonc.2011.05.044

Thiery, J. P., Acloque, H., Huang, R. Y., & Nieto, M. A. (2009). Epithelial-mesenchymal transitions in development and disease. *Cell, 139*(5), 871-890. doi:10.1016/j.cell.2009.11.007

Tibbitt, M. W., & Anseth, K. S. (2009). Hydrogels as extracellular matrix mimics for 3D cell culture. *Biotechnol Bioeng, 103*(4), 655-663. doi:10.1002/bit.22361

van der Zee, J. A., ten Hagen, T. L., Hop, W. C., van Dekken, H., Dicheva, B. M., Seynhaeve, A. L., . . . van Eijck, C. H. (2010). Differential expression and prognostic value of HMGA1 in pancreatic head and periampullary cancer. *Eur J Cancer, 46*(18), 3393-3399. doi:10.1016/j.ejca.2010.07.024

Vaupel, P. (2004). Tumor microenvironmental physiology and its implications for radiation oncology. *Semin Radiat Oncol, 14*(3), 198-206. doi:10.1016/j.semradonc.2004.04.008

Vega, S., Morales, A. V., Ocana, O. H., Valdes, F., Fabregat, I., & Nieto, M. A. (2004). Snail blocks the cell cycle and confers resistance to cell death. *Genes Dev, 18*(10), 1131-1143. doi:10.1101/gad.294104

Vlashi, E., McBride, W. H., & Pajonk, F. (2009). Radiation responses of cancer stem cells. *J Cell Biochem, 108*(2), 339-342. doi:10.1002/jcb.22275

Wang, C. Y., Cusack, J. C., Jr., Liu, R., & Baldwin, A. S., Jr. (1999). Control of inducible chemoresistance: enhanced anti-tumor therapy through increased apoptosis by inhibition of NF-kappaB. *Nat Med, 5*(4), 412-417. doi:10.1038/7410

Wang, S., Voisin, M. B., Larbi, K. Y., Dangerfield, J., Scheiermann, C., Tran, M., . . . Nourshargh, S. (2006). Venular basement membranes contain specific matrix protein low expression regions that act as exit points for emigrating neutrophils. *J Exp Med, 203*(6), 1519-1532. doi:10.1084/jem.20051210

Wang, T., Hu, Y. C., Dong, S., Fan, M., Tamae, D., Ozeki, M., . . . Li, J. J. (2005). Co-activation of ERK, NF-kappaB, and GADD45beta in response to ionizing radiation. *J Biol Chem, 280*(13), 12593-12601. doi:10.1074/jbc.M410982200

Weaver, A. M. (2006). Invadopodia: specialized cell structures for cancer invasion. *Clin Exp Metastasis, 23*(2), 97-105. doi:10.1007/s10585-006-9014-1

Webber, M. M., Bello, D., Kleinman, H. K., & Hoffman, M. P. (1997). Acinar differentiation by non-malignant immortalized human prostatic epithelial cells and its loss by malignant cells. *Carcinogenesis, 18*(6), 1225-1231.

Weston A, H. C. (2003). *Multistage Carcinogenesis* (6th ed.). Hamilton (ON): BC Decker.

White, E., & DiPaola, R. S. (2009). The double-edged sword of autophagy modulation in cancer. *Clin Cancer Res, 15*(17), 5308-5316. doi:10.1158/1078-0432.CCR-07-5023

Wong, R. S. (2011). Apoptosis in cancer: from pathogenesis to treatment. *J Exp Clin Cancer Res, 30*, 87. doi:10.1186/1756-9966-30-87

Xia, Y., Shen, S., & Verma, I. M. (2014). NF-kappaB, an active player in human cancers. *Cancer Immunol Res, 2*(9), 823-830. doi:10.1158/2326-6066.CIR-14-0112

Yang, J. Y., Zong, C. S., Xia, W., Wei, Y., Ali-Seyed, M., Li, Z., . . . Hung, M. C. (2006). MDM2 promotes cell motility and invasiveness by regulating E-cadherin degradation. *Mol Cell Biol, 26*(19), 7269-7282. doi:10.1128/MCB.00172-06

Yoshida, K., Sasaki, R., Nishimura, H., Okamoto, Y., Suzuki, Y., Kawabe, T., . . . Sugimura, K. (2010). Nuclear factor-kappaB expression as a novel marker of radioresistance in early-stage laryngeal cancer. *Head Neck, 32*(5), 646-655. doi:10.1002/hed.21239

Yun, H. S., Baek, J. H., Yim, J. H., Um, H. D., Park, J. K., Song, J. Y., . . . Hwang, S. G. (2016). Radiotherapy diagnostic biomarkers in radioresistant human H460 lung cancer stem-like cells. *Cancer Biol Ther, 17*(2), 208-218. doi:10.1080/15384047.2016.1139232

Zhang, Y., Liu, B., Zhao, Q., Hou, T., & Huang, X. (2014). Nuclear localizaiton of beta-catenin is associated with poor survival and chemo-/radioresistance in human cervical squamous cell cancer. *Int J Clin Exp Pathol, 7*(7), 3908-3917.

Zuch, D., Giang, A. H., Shapovalov, Y., Schwarz, E., Rosier, R., O'Keefe, R., & Eliseev, R. A. (2012). Targeting radioresistant osteosarcoma cells with parthenolide. *J Cell Biochem, 113*(4), 1282-1291. doi:10.1002/jcb.24002